AN INSTRUMENTED EXPERIMENTAL STUDY OF THE BALLISTIC RESPONSE OF TEXTILE MATERIALS

by

Darlene L. Starratt

B.Eng.(Metallurgy), Technical University of Nova Scotia, 1995

A THESIS SUBMITTED IN PARTIAL FULFILMENT OF

THE REQUIREMENTS FOR THE DEGREE OF

MASTER OF APPLIED SCIENCE

in

THE FACULTY OF GRADUATE STUDIES

(Department of Metals and Materials Engineering)

We accept this thesis as conforming

to the required standard

THE UNIVERSITY OF BRITISH COLUMBIA

April, 1998

In presenting this thesis in partial fulfilment of the requirements for an advanced degree at the University of British Columbia, I agree that the Library shall make it freely available for reference and study. I further agree that permission for extensive copying of this thesis for scholarly purposes may be granted by the head of my department or by his or her representatives. It is understood that copying or publication of this thesis for financial gain shall not be allowed without my written permission.

Department of Metals and Materials Engineering

The University of British Columbia
Vancouver, Canada

Date April 28, 1998

DE-6 (2/88)

Abstract

This work describes an instrumented experimental investigation of the energy absorption of Kevlar® fabric under ballistic impact. A continuous measurement technique, the UBC Enhanced Laser Velocity System (ELVS), has been successfully used in ballistic impact experiments. The results of this measurement technique are combined with results of a discrete technique, high speed photography, yielding more detailed information about the impact event.

A combined local and global deformation response is shown to exist in fabrics when impacted ballistically. The global response involves the overall global deformation of the fabric as a pyramid, and is responsible for absorbing most of the projectile energy. The local response involves the local deformation of the material in the vicinity of the projectile tip, and dictates when local failure, i.e. perforation, of the material will occur. The maximum global response is a function of the local mechanism.

A simple mathematical model has been presented and is used to predict the total energy absorption of the target, as well as the distribution of this energy into both kinetic and strain energy components. The model is shown to be a good first approximation of the experimental results.

Table of Contents

List of Tables

List of Figures

Nomenclature

a	acceleration of projectile
A	cross-sectional area of projectile
$A_{surface}$	surface area of pyramid
b	base of deformation pyramid
c	longitudinal strain wave velocity in a yarn
c'	longitudinal strain wave velocity in a fabric
C_D	drag coefficient
d	depth (height) of deformation pyramid
d_p	diameter of projectile
E	dynamic elastic modulus for yarns in fabric
$E_{absorbed}$	energy absorbed by the target
E_{bend}	energy needed to bend projectile
E_c	the minimum impact energy at which penetration occurs
E_{global}	energy absorbed by the global deformation mechanism
E_K	kinetic energy of deformation pyramid
E_{local}	energy absorbed by the local deformation mechanism
$E_{mushroom}$	energy absorbed in deforming a projectile
E_r	residual energy of projectile
E_s	impact energy of projectile
E_{total}	total energy absorbed by two springs in series
h	height of one side of the pyramid, calculated using b and d
K_1	stiffness of primary bonds in a yarn
K_2	stiffness of secondary bonds in a yarn

l	final length of yarn after it has been strained
L	initial length of yarn in a target (equal to target size)
L_{offset}	distance between the optical sensors and the target
l_p	length of projectile
M_{bend}	fully plastic bending moment of projectile
m_p	mass of projectile
$m_{pyramid}$	mass of pyramid
r	radius of projectile
T	thickness of a target
t_{AC}	time between points A and C on the voltage-time curve
t_{BC}	time between points B and C on the voltage-time curve
U	strain energy in deformation pyramid
u	velocity of transverse wave
v	velocity of material in deformation pyramid
v_{50}	velocity at which there is a 50% probability that the projectile will perforate the target
V_A, V_B	voltage at points A and B in voltage-time curve, respectively
$V_{blocked}$	voltage at 0 % laser intensity
v_c	minimum velocity at which penetration occurs
V_{full}	voltage at 100 % laser intensity
v_{os}	velocity measured by optical sensors
v_p	velocity of projectile during penetration
V_p	volume of the deformed part of a projectile
v_r	residual velocity of projectile
v_s	impact velocity of the projectile
w	velocity of material between longitudinal and transverse wavefronts

w_{ls}	width of laser sheet in ELVS
x	position of yarn in deformation pyramid
α	Roylance's coefficient
ε	strain in the deformed fabric/yarn material
η	number of plies in a target
ρ_{air}	density of air
μ_{air}	viscosity of air
ρ_{areal}	fabric areal density
θ_{bend}	bend angle
ΔE	energy lost by the projectile during penetration
ε_p	strain in a deformed projectile
σ_y	yield strength of projectile material
ε_{yarn}	strain in a single yarn
μ_2	viscosity of yarns

Acknowledgments

"Trust in the Lord with all thine heart; and lean not unto thine own understanding. In all thy ways acknowledge Him, and He shall direct thy paths." Proverbs 3:5-6

I would like to gratefully acknowledge my supervisor, Dr. Anoush Poursartip, for his encouragement and inspiration when things were going rough, and for his genuine and enthusiastic support when all the pieces of the puzzle came together. I thank Dr. Reza Vaziri for helping a simple experimentalist gain a better understanding of the "big, bad modelling world". A very special thanks to Mr. K. Williams, who gave much help in preparing my thesis, Mr. Roger Bennett, who made the experimental tasks even more enjoyable than they already were, and Mr. E. Cepuš whose help and enthusiasm I could not have done without. Thanks to Mr. Ross McLeod, Mr. Carl Ng and Mr. Serge Milaire for their technical assistance. Much direction and support was provided by Mr. Gilles Pageau and the technical staff at the Defence Research Establishment Valcartier (DREV), for which I am very grateful. I also would like to thank every member of the UBC Composites Group for their friendship and support.

I would like to acknowledge the Defence Research Establishment Valcartier (DREV), who provided the financial aid, materials, and technical assistance for this research.

I would like to acknowledge my family and my friends for their prayers and daily support, and for lending an ear and a shoulder when needed. My gratitude for your help and encouragement I could never even begin to express in words. I thank you from the depths of my heart.

And most importantly, I thank God, my Lord and my Saviour, who willingly went to the cross at Calvary and suffered the wrath that was mine. I thank Thee Lord for bringing me through all the valleys and graciously blessing me more than I ever deserved.

Chapter One: Introduction

1.1 Background

The ballistic impact performance of woven textile armour materials is a very interesting and relatively new area of research. Prior to the 1970's, much of the work performed in this field was focused on the individual fibres and yarns used to make up the woven textile materials. Also, the majority of the research conducted on ballistic impact of textile materials was performed by military laboratories, and thus was confidential. As the need for personal body protection by law enforcement and civilian agencies increased, the number of researchers interested in the field of ballistic textile materials, outside of the military, began to grow.

The use of protective armour in the past has led a very interesting and extensive life, as shown by Figure 1.1, which gives an overview of the body armour used in Europe over a period from 650 to 1675 AD. The earliest forms of body-protective clothing consisted of a jacket of padded animal hide (650 AD), replaced in 1250 AD by a garment of interconnected steel rings, known as *chain mail.* Chain mail, used extensively for centuries, was most often worn in combination with plate armour with its introduction in 1350 AD. A full suit of plate armour was often made from certain alloys of steel, mainly manganese and chrome-nickel, and weighed anywhere from 19 to 43 kg (41 to 94 lbs). A well made suit of armour offered good resistance to the threats of the day, which included substantial blows from maces and powerful thrusts of swords and arrows. It was, however, very heavy and awkward to wear for any length of time, and by the late 16^{th} century, many officers wore their armour as little as possible. The continued use of heavy plate armour often led to a decline in the physical condition of the wearer, such that by the time they

were thirty years of age, their shoulders had already become "completely humpbacked" (Dean [1920]). This eventually led to the decline of the plate armour.

The use of soft materials in protective armour is believed to have begun even before the use of chain mail and plate armour. As shown in Figure 1.1, a jacket of animal hide was used in Europe in 650 AD. Protective armour made from silk was used as early as 600 AD by Chinese warriors, and combinations of these and other soft materials were used at length in Europe in the 14th and 15th centuries. At the start of the 20th century, during the First World War, it was found that the soft armour of the day was not economical to use due to the high cost of the material, and the substantial weight of material that was needed to offer sufficient protection. After an extensive study into the history of personal protection and the use of both hard and soft armour in early 20th century warfare, it was concluded by Dean [1920] that "the studies upon soft armour made during the present war [World War I] show convincingly that the ballistic value of this type of armour is not great enough to warrant its use." It is, therefore, very interesting that less than 80 years later, much of personal protective clothing is made from soft or semi-rigid materials, which include ballistic nylon cloth, aramid (Kevlar®), and polyethylene (Spectra®) fabrics. These materials offer excellent ballistic resistance, as well as providing the comfort of low weight and ease of maneuverability.

Kevlar® fibre, developed by DuPont de Nemours and Co. in the early 1970's, is composed of long, highly oriented molecular chains of poly-paraphenylene terephthalamide. Since its development, Kevlar® has found its use in a wide variety of applications, including sporting equipment, tires and protective clothing, and is one of the most common ballistic fibres used in soft armour applications. Another common fibre used in ballistic soft armour is Spectra®, which

was developed by Allied-Signal. Spectra® is composed of highly oriented, ultra high molecular weight chains of polyethylene. When woven into fabrics, both Kevlar® and Spectra® materials offer excellent resistance to ballistic impact.

Several standard test methods have been established to help in the characterization and testing of materials used in ballistic impact applications, and to help in the determination of ballistic resistance of new materials. These standard test methods, which include the NIJ Standard 0101.03, the NATO-STANAG-2920, and the MIL-STD-662E, have been used by law enforcement agencies and military laboratories. Most of the published experimental research conducted in the area of ballistic impact of textiles, however, does not follow a standard test strategy. The lack of consistent use of a test method in this area of research is a major disadvantage, as it is difficult to compare results of various tests and there are uncertainties as to what are the important issues to consider in this field of study.

Much of the ballistic impact results in the literature are presented in plots of impact velocity, v_s, versus residual velocity, v_r, an example of which is shown in Figure 1.2. To obtain these plots, the procedure involves performing 10 or 12 impact tests over a range of impact velocities, from velocities where the projectile does not penetrate the target, to velocities where the projectile completely perforates the target. For these tests, the velocities before and after impact are measured. The residual velocity is then plotted against the projectile impact velocity. From these plots, the critical velocity, v_c, can be determined. The data can also be plotted as impact energy, E_s, versus residual energy, E_r. Another way of presenting the ballistic performance of textiles is by the "v_{50}" value (e.g. Laible *et al* [1973]), which is the velocity at which there is a 50 % probability that a given projectile will penetrate a target. Both methods make use only of information gathered before and after the impact event, and although providing extensive

knowledge of the overall ballistic resistance of a material, they offer very little insight into what is happening in a textile material during a ballistic impact event.

One reason for using "before and after" information to determine the ballistic resistance of a textile material is the lack of measurement techniques which are able to make continuous measurements *during* the impact event. Many of the measurement systems available today, which are limited to taking discrete measurements during ballistic impact, include high speed photography (Wilde et al. [1973]), chronographs and optical sensors (Prosser [1988], Taylor and Vinson [1990]). The main drawback with discrete measurement systems is that they only provide instantaneous velocity measurements at certain points along the projectile's path rather than a continuous measurement. Some measurement systems, specifically high speed photography, are also expensive to own and operate.

A more desirable velocity measurement system is one which measures the projectile motion continuously during the impact event. Such methods available today include laser interferometry (Wu *et al.* [1994], Espinosa *et al.* [1996]), and instrumented projectiles (Delfosse *et al.* [1993]). While these techniques do provide continuous measurements during the impact event, they can be quite expensive to purchase and the data reduction can often be quite time-consuming and complex. Also, as in the case with instrumented projectiles, they may only be useful over a limited velocity range.

A more recent continuous measurement technique which is cost-effective and simple to operate is the Laser Line Velocity Sensor (LLVS). The LLVS was originally developed by Ramesh and Kelkar [1995] at Johns Hopkins University for use in flyer plate impact experiments. They have

used the LLVS system to measure the displacement of flyer plates prior to impact, and hence determine the initial plate velocity and acceleration.

1.2 Purpose and Scope of Work

The present research has involved the further investigation and the adaptation of the LLVS system for use in ballistic impact experiments. In this type of experiment, the adapted LLVS system, hereafter referred to as the UBC Enhanced Laser Velocity System, ELVS, is used to continuously measure the motion of free-flying projectiles prior to and during the impact event. From this, the velocity histories before and during impact are determined. In addition, the force versus projectile displacement plots and the energy absorbed by the target during the impact event can be generated from the measured data.

The main goal of the present research is to provide an overview of the current state of ballistic soft armour research, and to present additional detailed information about the ballistic response of textile materials. This is done by using both the ELVS and high speed photography to obtain more information about the ballistic response during the impact event, and using this information to obtain a better understanding of the behaviour of textiles to ballistic impact. To achieve this objective, the present research is organized as follows:

1. An overview of the experimental and modelling approaches taken in the literature on ballistic impact of textile armour materials is presented in Chapter Two. Investigations of ballistic behaviour of both yarns and fabrics are discussed. The specific test methods used are presented, along with the assumptions and considerations made.

2. The experimental investigation of the ballistic impact response of textile materials is described. The procedures followed for performing impact tests using a high speed video camera and the ELVS measurement technique are discussed in Chapter Three and Chapter Four, respectively.

3. The results from the two different measurement techniques are then presented and discussed in Chapter Five.

4. Conclusions drawn from the results of the ballistic impact tests are provided in Chapter Six. Finally, recommendations for further investigations are presented.

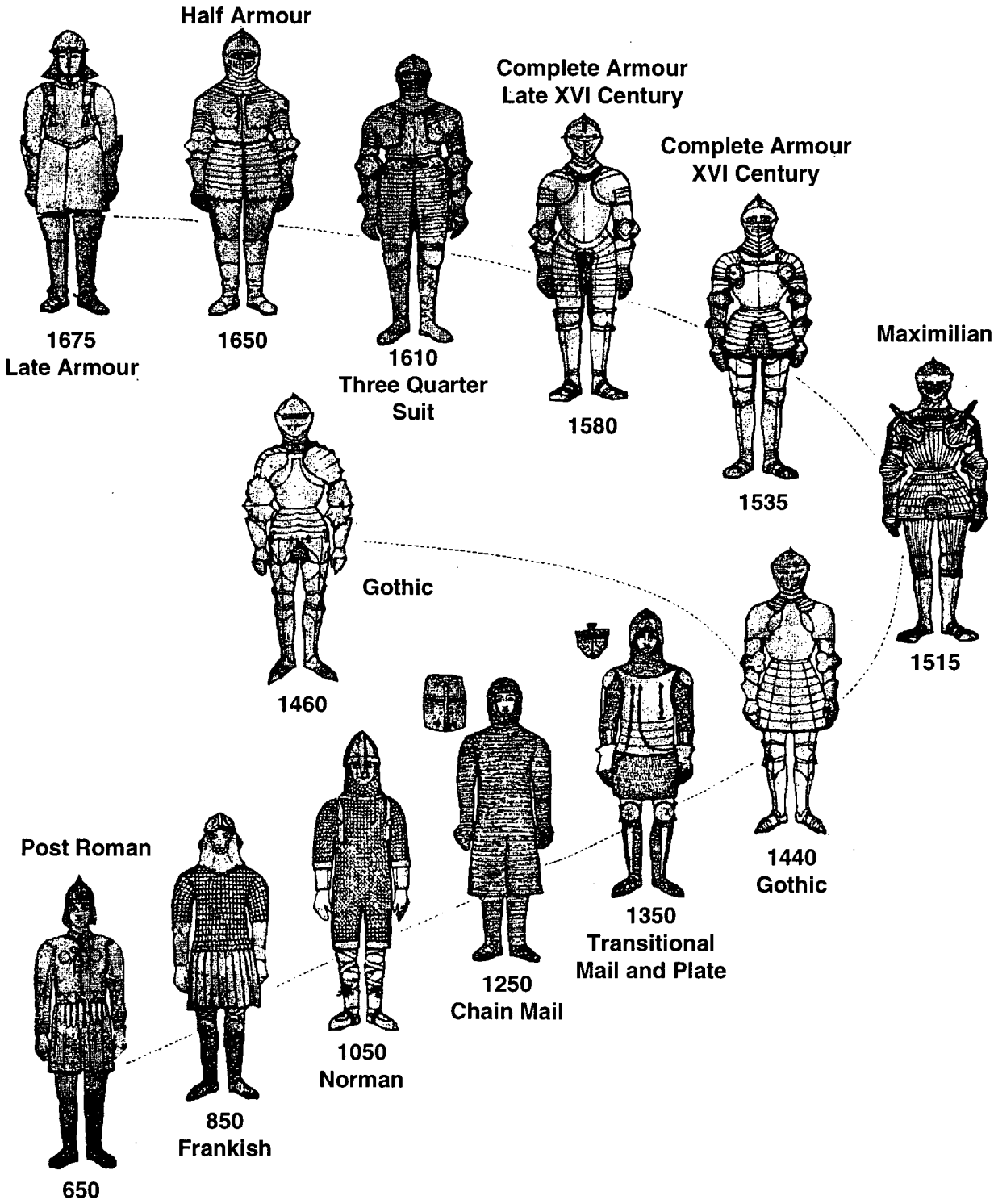

Figure 1.1: The development of European armour from 650 to 1675 AD (Dean [1920]).

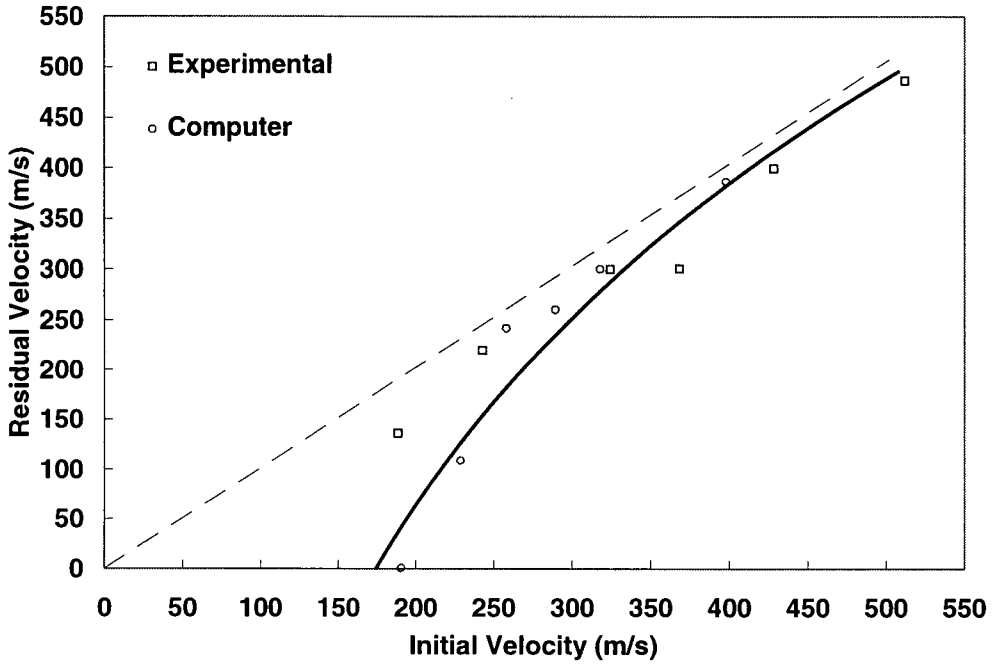

Figure 1.2: **Initial (impact) velocity versus residual velocity. (Reproduced from Roylance *et al.* [1973]).**

Chapter Two: Literature Review

2.1 Introduction

This chapter provides an overview of the experimental and modelling approaches taken in the literature on ballistic impact of textile armour materials. A foundation of knowledge of the past and present experimental work on ballistic impact response of soft textile armour systems is presented, and an attempt is made to identify any areas where significant deficiencies exist. Analytical and numerical models developed to predict ballistic response of textile materials are presented. The assumptions made in the development of these models, the main features of the models, and the model inputs and outputs are discussed.

2.2 Ballistic Impact of Yarns

When a yarn[1] is transversely impacted by a projectile traveling at a high velocity, two longitudinal strain waves are initiated at the point of impact. These strain waves propagate along the yarn away from the point of impact, with a velocity c. The material between the longitudinal wavefronts moves toward the point of impact at velocity w. At the same time, a transverse wave is also initiated at the point of impact, and propagates away from the impact point at velocity u. When the material moving in towards the impact point at velocity w meets this transverse wavefront, it is taken up into a "tent" shape, as shown in Figure 2.1. The material in this "tent" moves in the same direction and at the same velocity, v_p, as the projectile. The strain in the

[1] In this thesis, the term *yarn* will be used to describe a combination of fibres that have been twisted together.

material between the point of impact and the longitudinal wavefront is assumed to be a constant value, ε. The material in front of the longitudinal wave is not strained.

The transverse impact behaviour of infinitely long yarns was investigated by Smith *et al.* [1958]. In this work, Smith developed a theory of transverse impact in which the modulus of the yarn is assumed to remain constant during a ballistic impact event. This "rate-independent" theory was used by Smith *et al.* [1960] to develop a new method of measuring the propagation velocity of the strain waves. This method makes use of photographs of the yarn at various times during the impact event. From these photographs, the time required for the longitudinal strain wave to travel from the impact point, to the clamp and then back to where it meets the transverse wave, can be determined, and hence the velocity of the strain wave can be calculated. The strain wave velocities determined using this method were compared with velocities calculated by two other methods, and were found to be consistent.

Smith *et al.* [1963] performed high velocity (up to 700 m/s) impact experiments on high-tenacity nylon and polyester yarns to investigate the resulting stress-strain response. In this investigation, it was assumed that the stress-strain behaviour of the yarns was independent of the strain rate. To perform the impact experiments, a yarn sample was clamped at one end and allowed to hang vertically. A 100 g weight was hung off the other end of the yarn to provide a constant tension on the yarn. Photographs of the event were taken to allow for the transverse strain wave velocity and the impact velocity to be determined. The breaking time of the yarns impacted was found to be dependent on the impact velocity.

The effect of yarn ply (the number of fibres in the yarn) and yarn twist on the ballistic response of textile materials was investigated by Figucia *et al.* [1971]. A number of different yarn types were

tested, including nylon, polyamide, and polypeptide, in an effort to characterize these materials for ballistic impact applications. Both low (100 %/min) and high (288,000 %/min) strain rate characterization tests were performed to determine tensile properties. The results of these tests were presented as ratios of the high strain rate tests to the low strain rate tests, which were referred to as "impact performance ratios". By increasing the degree of ply and twist of the yarns, the complexity of the yarn structure was increased. The impact performance ratios for each of the characterization tests were compared with the changes in complexity of the yarn structure, and it was observed that as complexity increases, the ballistic impact resistance of a textile material decreases. Figucia concluded that the reason for this was that the material was not able to translate its excellent low strain rate energy absorption characteristics to high strain rate situations.

In the investigation of transverse impact of textile yarns by Roylance [1977], the rate-independent theory developed by Smith *et al.* [1958] was considered to provide a "first-step guide to the design of impact resistant structures." In this investigation, Roylance observed that, although the energy absorption rate increases with increasing modulus, at the same time, the ductility decreases, which may result in reaching the optimum modulus for transverse critical velocity.

Knowledge of the ballistic impact response of yarns provides the foundation upon which the prediction of the ballistic impact behaviour of woven fabrics is based. Roylance [1980] made use of the ballistic impact behaviour of single yarns in determining the effect of yarn crossovers on the ballistic response. The investigation by Roylance yielded a numerical code which modelled two perpendicular yarns, crossing one another. This model considers the effect of the presence of a crossing, or secondary, yarn on the propagation of the longitudinal strain waves in a

primary yarn that has been transversely impacted. The yarns were treated as pin-jointed fibre elements, and the viscoelasticity of the fibres and inter-yarn friction were taken into account. The outputs of the model included the portion of the strain wave that was reflected at the crossover, the portion that was transmitted past the crossover, and the portion that was diverted at the crossover and began to move along the secondary yarn. By performing some computer-simulated impacts using this numerical model, it was observed that a greater portion of the strain wave was diverted rather than reflected. It was also observed that the effect of the crossover diminished as the friction between the yarns decreased.

2.3 Ballistic Impact of Fabrics

2.3.1 Experimental

The influence of ductility of fibres on the ballistic resistance of a fabric was investigated by Laible *et al.* [1973]. In this study, three variations of high moduli polyamide fibres were woven into fabrics and ballistically impacted. The three types of fibres all had high moduli, but varying levels of ductility. Testing was carried out per Military Standard MIL-STD-662, using a 5.58 mm (0.22″) diameter, 1.1 g (17 grain) fragment-simulating projectile (FSP). The ballistic limit, v_{50}, was determined from these tests, with the results indicating that the fabric made of the fibre with the greatest ductility had the highest value of v_{50}. The results were compared with results from nylon fabric, with the lower modulus, higher ductility fabric being comparable to standard nylon fabric. Thus, from the results of this study, Laible concluded that although a high modulus may be beneficial to ballistic protection ability, the ability of a material to plastically deform is also an important consideration in obtaining good ballistic resistance.

Wilde *et al.* [1973] performed ballistic impact experiments on single layers of high-tenacity nylon fabric. The targets were held tightly on all four edges within a steel frame. The projectiles used were 1.1 g (17 grain), bevel-faced cylindrical steel projectiles, 5.58 mm (0.22″) in diameter. Incident velocities ranged between 116 and 537 m/s. The impact velocity was measured by use of a chronograph, and high-speed photographs of the impact event were taken. Observation of the photographs revealed that in the early stages of penetration, fabric deformation is pyramidal in shape. In later stages, the fabric deformation becomes more conical in shape. The results of the impact experiments were presented as plots of projectile energy loss (ΔE) versus impact velocity (v_s), an example of which is shown in Figure 2.2.

The results of these experiments have helped to give a better understanding of the development and geometry of the transverse deformation of the fabric. Wilde found that the fabric responses, such as growth of the transverse deformation prior to and after penetration, and the energy absorbed during penetration, were strongly dependent on the impact velocity (in this investigation, constant mass projectiles were used). It was also observed that the transverse deformation of the fabric continued to grow both axially and radially, even after the projectile had penetrated the fabric.

The data generated from impact experiments performed by Wilde were further analyzed by Wilde [1974]. In this analysis, two different methods were used to determine the average stopping force developed by the fabric on the projectile. One method made use of results of projectile velocity loss, fabric-projectile interaction time and projectile mass to compute the average force. The other method made use of projectile energy loss data and the transverse deformation depth results. Both methods produced similar values for the average retarding force. Wilde [1974] also used the data and results produced by Wilde *et al.* [1973] to compare with

results of similar impact tests performed on single yarns. The comparison revealed that fabrics experience shorter projectile-fabric interaction times, smaller transverse deformation depths, and higher normalized retarding forces than yarn bundles. Wilde [1974] believed the reason for this was due to the restrictive effect of the woven yarns on each other in the fabric.

Laible *et al.* [1975] compared the ballistic impact resistance of Kevlar® 29 laminates to that of woven glass laminates. Ballistic impact tests were performed using a 9 mm (0.35″) diameter, 8 g (124 grain), full metal jacketed projectile, at velocities ranging from 335 to 396 m/s. Both single- and multiple-ply laminates were tested, so as to vary the areal density. Results of these tests indicated that, at equal areal densities, the Kevlar® fabric laminate had a greater ballistic resistance than the woven glass laminate, as fewer projectiles completely penetrated the Kevlar® targets. Laible also observed that the Kevlar targets showed less back face deformation and delamination than the glass targets. Cyclic bending, tensile, and interlaminar shear tests were also performed on both laminates to compare the mechanical properties of the Kevlar® and glass laminates. The results of these tests indicated that Kevlar® had survived a larger number of cycles of bending, had higher tensile strength and elongation-to-break than the glass, and had an interlaminar shear value greater than twice that of the glass. However, Laible suggested that actual wear tests should be performed to determine how the fabrics withstand mechanical abuse from service conditions.

A new experimental method of determining the ballistic limit of armour materials was presented by Figucia [1980]. This new methodology, developed by the U. S. Army Natick Research and Development Command (NARACOM), was developed to reduce the cost and time involved in conventional ballistic impact experiments used to determine v_{50}. This new procedure was based

on the observed relationship between energy absorption and areal density, and yields a term, called the Ballistic Performance Indicator (B.P.I.), which can be used to predict v_{50} values. The slope of an absorbed energy vs. areal density curve is taken to be the B.P.I. for the fabric, represented in units of J/kg/m^2. The experimental procedure involves testing a fabric over a range of areal densities, at impact velocities of 213, 274 and 366 m/s. The specimens are held between two aluminum plates in a specialized fixture which can be moved vertically and rotated to ensure that the boundary conditions are the same for every part of the target penetrated. Testing is performed at each velocity, while varying the areal density of the fabric. Striking and residual velocity data, measured using electronic Lumiline screens, are used in the calculations of energy absorption. When the energy absorption of the fabric is 50 to 60 % of the projectile energy, the testing procedure is stopped. Although this method involves very low values of areal densities (0.17 to 1.02 kg/m^2), it can be used to accurately predict the v_{50} values for more practical areal densities (~ 6 kg/m^2). Figucia used this method to test five Kevlar® fabrics. The values of v_{50} predicted using the B.P.I. values were in good agreement with v_{50} values measured from conventional impact tests. The B.P.I value was also used to indicate whether or not a fabric could be used successfully in ballistic applications. When plotting the B.P.I value against nominal fabric weight (the weight of a single layer of fabric presented in units of g/m^2), for example, it was observed that the ballistic performance decreased as the nominal fabric weight increased. From this, Figucia concluded that on an energy absorption to weight basis, lighter fabrics are more resistant to ballistic impact, i.e., it is better to use more layers of a lighter fabric than to use fewer layers of a heavy fabric to improve ballistic resistance. The relationships of the B.P.I. value with fabric cover and weave type were also investigated.

The effect of projectile geometry on the ballistic response of woven fabrics was investigated by Montgomery *et al.* [1982]. Two types of impact tests were performed on Kevlar® fabrics, with the data from both tests being presented as energy absorption as a function of projectile geometry. Four different projectile geometries were used, ranging in bluntness from flat to pointed. The first type of impact test was the conventional v_s - v_r test, in which the projectile completely penetrates the fabric and the impact and residual velocities are measured. The velocity range used for this test was 200 to 600 m/s. Both single- and multiple-ply targets of Kevlar® 49 were tested, as well as single-ply targets of Kevlar® 29. The second type of test used was the clay test, which is commonly used by law enforcement agencies to determine the ballistic response of body armour. Targets consisting of 10 layers of Kevlar® 49 were placed in front of a clay block and impacted by the four different projectile geometries. The velocity range for this test was 200 to 400 m/s. In this test, the impact velocity and the depth of the deformation in the clay block were measured.

Montgomery performed a statistical analysis on the v_s - v_r data. They concluded that at high impact velocities (greater than the v_{50} value), the more blunt the projectile is, the more quickly it is slowed down by the fabric. They suggested that the reason for this was that pointed projectiles are able to push through the yarns of the fabric with greater ease, and thus are not slowed down as much. At lower impact velocities, the opposite observation was made. This was believed to be due to the decreased stability of the more pointed geometries at lower velocities, causing the projectile to yaw and strike the fabric at an angle allowing more fabric to take part in energy absorption. It was also observed that as the number of layers of the target increased, the effect of projectile geometry on energy absorption was less "noticeable".

The results of the clay test performed by Montgomery indicated that the fabric deformation due to impact was pyramidal in shape, which agrees with observations made by Wilde *et al.* [1973]. The size of the deformation in the clay block increased with increasing velocity for all projectile geometries, but the degree of this increase was less for the blunt projectiles. Montgomery suggested that the reason for this was that blunt projectiles come into contact with more yarns during impact than the pointed projectiles do, and thus the amount of fabric involved in energy absorption increases. As a result, the degree of transverse deformation was less.

Prosser [1988a] performed ballistic impact tests on multiple layers of nylon fabric using FSP's of diameters ranging from 3.8 to 12.7 mm (0.15 to 0.50″). Impact and residual velocities were measured using a chronograph system. Impact velocities ranged between 61 and 732 m/s, and the projectiles impacted the targets with 0° obliquity. The data obtained from these experiments were presented as v_s - v_r plots. It was observed from these experiments that yarns crossing the point of impact had stretched with respect to the rest of the material, and also that some yarns were fused to cross yarns near the periphery of the impact point. Prosser suggested that this was due to frictional heat during passage of the projectile.

Prosser also compared the number of yarns broken in the top and bottom layers to that broken in the interior layers. It was observed that the greatest number of yarns broken occurred in the first two layers that the projectile penetrated, whereas the final two layers penetrated had the least amount of broken yarns. The number of yarns broken in the interior layers was relatively constant. Prosser believed that this variation in broken yarns was due to slippage of the yarns during penetration. The final two layers of fabric were not supported on their back by other layers of fabric, and thus the projectile could easily slip through the yarns due to the lateral movement of the yarns. This resulted in fewer broken yarns, but is not, however, beneficial to

ballistic resistance as it allows the projectile to penetrate the fabric with greater ease. In the initial two layers, the presence of the subsequent layers backing these first two trapped the yarns, keeping them from laterally moving. Therefore, less slippage of the yarns occurred causing more yarns to break. Prosser also experimented using panels composed of 1 to 80 layers of Kevlar® fabric. A 5.58 mm (0.22″) diameter FSP, impacted at 0° obliquity, was used in these experiments. The results and observations obtained from these experiments were very similar to those obtained for nylon.

In a continuation of the work performed by Prosser, the failure mechanism of ballistic nylon panels due to impact by chisel-nosed FSP's was investigated (Prosser, 1988b). Observation of data and photographs obtained from ballistic impact experiments performed by Prosser [1988a] revealed that the yarns in the fabric appeared to fail due to a shear mechanism and not by tensile failure when impacted by the chisel-nosed FSP's. In coming to this conclusion, Prosser [1988b] noted that there appeared to be uneven strain around the point of impact, indicating that yarns in one direction failed sooner than yarns in the other direction of the weave. It was also observed that the ends of the failed yarns were smooth, indicating shear failure and not a tensile break. To further investigate the effects of the edges of the FSP on the failure mechanism of nylon and Kevlar® yarns, Prosser [1988b] performed experiments to determine the yarns breaking strengths. The yarns were looped over bars of different cross-sectional shapes, ranging from round to a triangular shape with an edge of 150° angle at the apex. The ends of the yarns were clamped together and then pulled until the yarns failed. The breaking strengths of the yarns were recorded. The results indicated that the yarns looped over the round bar failed at various places along the yarn, which Prosser [1988b] suggested was a tensile mechanism of failure. The yarns looped over the triangular bars, however, failed where the yarn was in contact with the edge of

the bar. Prosser [1988b] proposed that this type of failure was due to a cutting, or shear, mechanism. It is assumed by Prosser [1988b] that these results can be applied to ballistic impact events, and thus he concludes that the ballistic performance of nylon and Kevlar® fabrics may be improved by improving the shear strength of these fabrics.

Taylor and Vinson [1990] produced an experimental program consisting of approximately 185 shots into targets composed of 1 to 5 layers of Kevlar® 29, in which the impact and residual velocities were measured. Projectiles consisted of 5.58 mm (0.22″) diameter, round nose projectiles and 9 mm (0.357″) diameter semi-wad cutter, flat nose projectiles, with impact velocities of 240, 310, and 380 m/s. Taylor and Vinson found that for complete penetration tests, the average failure strain for a given impact velocity is not dependent on the number of layers in the target. They concluded that for complete penetration experiments, results from one type of projectile can be used to predict penetration of another projectile as long as the impact velocities are the same. The data acquired was used to validate an analytical model developed by Vinson and Zukas [1975].

The ballistic impact response of Spectra®, Kevlar®, and graphite fabrics were investigated by Hsieh *et al.* [1990]. Included in this study was the investigation of the projectile energy loss due to frictional heat and the energy absorbed by the fabric due to breakage of the yarns. A projectile with a 50° conical-shaped, steel tip was used in these ballistic impact experiments, at velocities of 360 m/s. The velocity prior to and during the impact event was measured using a micro-velocity sensor device developed by Zee *et al.* [1989]. This device is based on the rationale that when a magnet is passed through a coil, an induced current is generated. Both multiple-ply, fabric-reinforced composites and fabrics without resin were tested. The results of these impact

tests suggested that the Spectra®-reinforced composites absorbed a larger amount of energy than both the Kevlar® and the graphite-reinforced composites. The results also indicated that for the three types of composites tested, the amount of energy absorbed increased almost linearly with increasing target thickness. Hsieh normalized this energy loss data with both thickness and areal density, and found that the Spectra® composites had the highest energy absorption density, followed by Kevlar®, while graphite composites had the worst. Hsieh also commented that the presence of the resin in the Spectra® and Kevlar® composites restricted these fibres from allowing the full potential of their ductility to be achieved. This restriction confined the deformation of the ductile Spectra® and Kevlar® fibres to areas close to the point of impact.

To observe the influence of delamination, Hsieh repeated the ballistic impact experiments using targets made of individual layers of the impregnated fabrics stacked together. The energy absorption of these stacked layers, when compared to that of the composite plates, showed little difference in neither the Spectra® nor Kevlar®. With graphite, however, the composite plate absorbed more energy than the stacked layers. The effect of pure fabric on ballistic impact behaviour was investigated by testing targets which contained no resin in their central region. Some resin was, however, placed around the region to be impacted to hinder any slippage of the yarns in the fabric during the impact event. The results of these tests indicated that the pure fabric targets absorbed only half the amount of energy that was absorbed by the fabric-reinforced composites. From these results, Hsieh proposed that the fibre properties are very important parameters involved in energy absorption during impact, and that in fabric-reinforced composites, more of the energy absorbed during impact is due to fibre breakage.

An overview of current hard and soft ballistic armour systems was presented by Segal [1991], and characteristics of an optimum fabric for use in soft armour applications were suggested. These characteristics included maximum strain wave velocity, maximum crossover density, maximum friction between the yarns of the fabric, minimum amount of crimp, and minimum moisture absorption. A United States patent has been obtained for a fabric with these characteristics. This fabric is currently being used in police personal body armour, and has been proposed for use in military applications. Segal presented a brief overview of military ballistic material specification and testing standards, which include MIL-C-44050 and MIL-STD-662E, respectively. MIL-C-44050 covers the ballistic requirements of p-aramid fabrics, whereas MIL-STD-662E covers the ballistic resistance of all types of military armour materials. Segal also briefly discussed two civilian protective armour testing standards, NIJ-0101.03 and PPAA-STD-1989-05.

Ballistic impact experiments using Spectra Shield™ laminated composites were performed by Lin and Bhatnagar [1992]. Spectra Shield™ is a material produced from Spectra®-1000 fibres and Kraton® 1107D thermoplastic resin. In this investigation, a cross-plied (0,90) prepreg formed by compression molding was used. Three different areal densities of the Spectra Shield™ material were tested using 5.58, 7.62, and 12.70 mm (0.22, 0.30, and 0.50″, respectively) diameter FSP's. Testing was performed in accordance with MIL-STD-662E. Plots of impact energy (E_s) versus residual energy (E_r) for each type of FSP were produced from the impact test results. From these plots, Lin and Bhatnagar observed that a linear relationship existed between E_s and E_r for the Spectra Shield™ composites tested. The critical energy, E_c, was defined as the value of the intercept of the E_s - E_r plot with the x-axis, i.e. the value of the lowest striking energy at which penetration occurred. Lin and Bhatnagar also compared results

of the Spectra Shield™ to Spectra® fabric composites. This comparison is given as a plot of FSP diameter versus areal density, and is shown Figure 2.3.

From this comparison, Lin and Bhatnagar concluded that for larger projectile diameters and lower areal densities (above the line in Figure 2.3), Spectra® fabric composites had a better ballistic resistance. At smaller projectile diameters and higher areal densities (below the line in Figure 2.3), Spectra Shield™ composites were more resistant. For projectile diameters and areal densities on the line in Figure 2.3, the energy absorption capabilities of both types of composites were believed to be the same.

The influence of friction between yarns on the ballistic impact behaviour of woven fabrics was investigated by Briscoe and Motamedi [1992]. Ballistic impact experiments were performed on single layers of plain and satin weaves of Kevlar® 29, and a "crowsfoot" weave of Kevlar® 49. Three different degrees of yarn lubrication were investigated for each of the weaves. These included cleaned yarns (no lubrication), as-received yarns (slightly lubricated), and intentionally lubricated yarns. The targets for the impact tests were circular in shape, and were pre-tensioned before being placed between two flat steel rings. The width and shape of the clamping device were varied. The impact and residual velocities were measured using IR emitters and sensors. The targets were impacted with 6.35 mm (0.25″) diameter steel ball bearings, at impact velocities ranging from 50 to 250 m/s. The event was also photographed, which revealed that increasing the lubrication of the yarns allowed the fabric to handle more strain and fibre pull-out before the projectile completely penetrated the fabric. The results of these experiments indicated that the fabric system which will dissipate the greatest amount of energy during the impact event is one which has high friction between the yarns, and thus, low lubrication.

Cunniff [1992] tested single plies of various soft armour materials, including Kevlar® 29, Spectra®-1000, and nylon. The projectiles used were chisel-nosed FSP's. The targets were clamped between thick aluminum plates with varying aperture sizes. From these experiments, the energy absorption characteristics were determined, and plots of fabric energy versus impact velocity were made. The maximum energy absorbed was found to occur at the ballistic limit. At velocities greater than the ballistic limit, it was observed that the size of the aperture did not have any effect on the ballistic response of the fabric. At velocities close to the ballistic limit, however, the ballistic response of the target appeared to be strongly influenced by the aperture size. Cunniff also observed that there appeared to be no clear relationship between the clamping pressure exerted on the fabric by the test fixture and the ballistic resistance of the fabric, however, no experimental data is given to support this statement.

Cunniff (1996) also performed impact experiments using 0.1, 0.3, 1.0, and 4.1 g (2, 4, 16, and 64 grains, respectively) right circular cylindrical projectiles. The targets used in these experiments consisted of 8, 16, 18, 22 and 54 layers of Kevlar® 29. The targets were impacted at impact angles of both 0° and 45° obliquity. The data generated from these experiments were represented as plots of v_{50} versus the number of plies of fabric in the target. The results were used to support an analytical model developed by Cunniff [1996].

Shim *et al.* [1995] performed ballistic impact experiments on single-ply Twaron® fabric for use in the verification of their numerical code. Impact velocities ranging from 140 to 420 m/s were obtained in these experiments using a spherical steel projectile of 9 mm (0.35″) in diameter. The vertical sides of the specimens were clamped to hold the fabric in place. Impact and residual velocities were measured using two pairs of laser-diodes. Observation of the specimens after

impact revealed that only yarns near the impact point were broken. It was also observed that the clamped yarns in contact with the projectile during penetration experienced fraying at their clamped edges, whereas unclamped yarns experienced unraveling at their edges.

Walsh *et al.* [1996] performed quasi-static penetration and low velocity impact experiments on woven Spectra® fabric composites. The purpose of their study was to investigate and establish a set of failure criteria to aid in the development of a model of the ballistic impact response of a fabric. The targets tested included single-ply woven Spectra® fabric without resin (dry fabric), and single- and multiple-ply woven Spectra® fabric-reinforced composites (with 25 % by weight of resin). The quasi-static penetration and low velocity impact tests were performed at 0.0002 m/s and 3.8 m/s, respectively. The penetrator used for these tests resembled a 1.1 g (17 grain) FSP. During testing, targets were held in a specialized fixture such that no slippage of the targets occurred. This fixture consisted of two steel plates with serrated inner surfaces, connected with a series of bolts which could be adjusted to provide sufficient clamping pressure. The effect of the addition of resin on the impact response of a fabric was also investigated. From the results of this investigation, Walsh concluded that the method of penetration of a dry fabric was quite different from that of a fabric-reinforced composite. In the dry fabric, Walsh observed that not as many yarns were broken because some of the yarns slipped over the tapered edges of the FSP. In a fabric-reinforced composite, however, it was observed that more yarns were broken. Walsh believed the reason for this to be due to the restrictive nature of the resin matrix, suppressing slippage of the yarns. For both target types, Walsh suggested that the major energy absorbing mechanism was that of fibre straining.

The distribution of kinetic energy in single-ply and multiple-ply Kevlar® Ht fabrics due to ballistic impact was investigated by Laine and Vähäkangas [1996]. Various steel projectile types, including the right circular cylinder, spherical ball, and the NATO STANAG 2920 shape were used. Laine and Vähäkangas suggested that the energy absorbed by a fabric impacted ballistically is distributed into four different mechanisms. These include strain energy, work of elongation to break, kinetic energy of the yarns along the fabric, and kinetic energy of the deformation cone in the direction of impact. The mechanical properties of the yarns in the fabric, including tensile breaking strength and elongation at break, were measured by testing yarns that were unraveled from the fabric. Laine and Vähäkangas observed that these values were lower than those measured from yarns that had never been woven. Residual velocity of the projectile, the transverse and elastic wave velocities, and the projectile-fabric interaction time were measured during the impact event. The multiple-ply fabric targets were examined after the impact event to determine the number of broken yarns in each layer of the target. Laine and Vähäkangas observed that the projectile-fabric interaction time per ply was lower for the multiple-ply targets than for the single-ply targets. The effect of moisture in the fabric on the ballistic response was also investigated. Laine and Vähäkangas observed that the presence of moisture in the fabric decreased the friction between the yarns of the fabric, therefore lowering the value of the ballistic limit (v_{50}).

A summary of the experimental work discussed is shown in Table 2-2.

2.3.2 Analytical Models

One of the earliest analytical models dealing with impact of fabrics was developed by Wilde *et al.* [1973]. This simplified analytical model predicts the projectile energy loss in a fabric that has

been ballistically impacted. The model requires inputs of the deformation size and velocity, both measured from experiments. A diagram of this model, known as the Broken Orthogonal Yarn (BOY) model, is shown in Figure 2.4.

The BOY model makes several assumptions, the first of which is that the sum of the strain and kinetic energies, confined to areas within the boundary of the deformation cone of the fabric, is the energy lost by the projectile during penetration. The deformation cone is the conical-shaped area of out-of-plane fabric deformation resulting from projectile impact. A second assumption is that this strain energy is confined to the broken orthogonal yarns passing through the point of impact within the boundary of the deformation cone. Thus, strain energy in yarns outside the boundary and in unbroken yarns within the boundary is neglected. A third assumption of this model is that the kinetic energy is due to the out-of-plane motion of the fabric within the deformation cone, therefore neglecting any in-plane motion along the yarns of the fabric outside of the boundary of the deformation cone. Although the BOY model is able to predict, to a fair degree, the projectile energy loss during impact, neglect of the previously mentioned terms may lead to errors in model predictions.

Vinson and Zukas [1975] developed a mathematical model which made use of strain wave propagation equations and conical shell theory to predict the mechanics of ballistic impact of fabrics. The model assumes that the fabric behaves as a homogeneous, flexible plate, and ignores strain energies and the effect of yarn crossovers on the ballistic performance. It does, in spite of these omissions, predict projectile velocity relatively accurately, as is shown in Figure 2.5.

The model requires inputs of projectile and target geometries, and certain material properties such as the ultimate material strain and modulus. The model assumes that the failure strain of the fibres in the fabric does not depend on the number of layers in the target. Due to this assumption, the model is able to predict the ballistic impact behaviour of a multiple-layer target using inputs from single-layer target impacts. Vinson and Zukas suggested that future work involving an extensive experimental program should be performed to determine the limitations of the model and to suggest any improvements that could be made to the model. This was accomplished by Taylor and Vinson [1990], and has been described previously in Section 2.3.1.

The analytical model developed by Leech *et al.* [1979] approximates the arrest of a projectile in both a linear and non-linear system, assuming the materials are linear-elastic. The model assumes that the transverse deformation of orthogonally woven fabric resulting from impact is rhomboidal in shape. The foundation of the model is based on a variational principle known as Hamilton's Principle. This principle takes into account both kinetic and strain energies, and thus allows the model to predict the total impact effect, in the impact region, by integrating the local impact effects of the single yarns which make up the material. One advantage of the model developed by Leech is that, since it is analytical, the solution of the model involves an ordinary differential equation. Also, the model presents the solution in terms of system properties (pre-strain and fabric densities) and impact variables (impact velocity and projectile mass). The results of this model agree quite well with experimental results.

Prosser [1988a] developed a mathematical model to predict the critical impact velocity, v_c (the minimum velocity at which penetration occurs), and the v_{50} of a fabric panel ballistically impacted by an FSP. The model is able to predict v_c, v_{50}, the average projectile deceleration, and the average force required to penetrate an interior layer for both non-bonded and bonded systems.

The model is based on the assumption that the energy lost by the projectile as it penetrates the interior layers of a fabric panel is constant, and depends on the number of layers in the target and not the impact velocity.

Parga-Landa and Hernandez-Olivares [1995] developed an analytical model, based on the conservation of momentum, which considers the penetration mechanics of soft armour materials. This model assumes that the fibres of the armour materials are linear-elastic until failure, and that every layer of the armour helps to slow down the projectile until that layer reaches its failure strain. To apply this model to actual woven soft armour materials, the effect of the yarn crossovers of these materials had to be considered. When a projectile strikes a fabric, longitudinal strain waves propagate outward along the yarn bundles, away from the point of impact. When these waves reach a yarn crossover, they are partially reflected. It was observed by Roylance and Wang [1980] that the velocity of a wave in a fabric, c', is a fraction of the wave velocity in a single fibre, c, that is,

$$c' = \frac{c}{\alpha} \tag{2.1}$$

where α is known as Roylance's coefficient. Parga-Landa and Hernandez-Olivares made use of Roylance's coefficient in their wave velocity calculations. Friction forces between the two overlapping yarn bundles at the crossovers were also considered in the development of their model. One of the model inputs is the dynamic modulus, **E**, of the yarns in the fabric. Due to experimental scatter involved in determining this value, Parga-Landa and Hernandez-Olivares used a range of values for **E** in their model predictions. Thus, the model is able to predict ballistic limit curves (v_{50} versus surface density) with a high degree of accuracy when compared

with published experimental results (determined by Du Pont de Nemours), as is shown in Figure 2.6.

The method of regressional analysis was used by Cunniff [1996] to predict the energy absorption characteristics of fabric armour materials. This model assumes that the energy involved in the impact response of the fabric is a combination of both strain energy (due to fibre elongation) and kinetic energy (due to the fabric's out-of-plane deformation). Another assumption made by the model is that at the instant the projectile is stopped by the fabric, the impact velocity of the projectile equals the critical velocity of the system, and both the fabric and the projectile are at rest. Thus, the kinetic energy of the system is zero. At much higher impact velocities, the impact event is assumed to be entirely inelastic, and thus the strain energy of the system is zero. The model also accounts for the decrease in projectile velocity due to air drag, and assumes that the projectile impacts the fabric at 0° obliquity.

A summary of the analytical models discussed is given in Table 2-2.

2.3.3 Numerical Models

Roylance *et al.* [1973] made use of a direct analysis approach to develop a finite element code to model the ballistic impact response of fabrics. This code was originally developed for single-yarn impact, and contains a viscoelastic material model within the code. This numerical code simplifies the yarn crossovers in the fabric as pin-joints, as shown in Figure 2.7.

The model neglects any slippage at the yarn crossovers, and does not take into account the effect of projectile geometry. The code predicts v_s versus v_r curves of ballistic impact which agree well with experimental results, as shown in Figure 2.8.

Use of this model has predicted that most of the ballistic energy lost by the projectile during a penetration event is absorbed by the orthogonal fibres passing through the point of impact. Fibres other than those passing through the impact point are basically ineffective. Roylance concluded that knowledge of the response of a single fibre to ballistic impact is very useful in determining the fundamental response of a fabric to impact. However, due to the fabric construction and material properties of a fabric armour system, single fibre properties alone cannot predict a fabric's impact response.

The increase in strain of a woven fabric due to reflections of strain waves at yarn crossovers was modelled by Freeston and Claus [1973]. The model is based on the theory that when a fabric is impacted, longitudinal strain waves travel in the yarns away from the point of impact. These strain waves are partially reflected at yarn crossovers. These reflected strain waves cause the strain in the fabric to be magnified, with the maximum strain occurring at the point of impact. The model neglects the effects of creep and stress relaxation of the yarns in its predictions, and assumes that the point of impact is "perfectly reflecting". The model plots the predicted results as amplitude of strain versus position for various times after impact. With this model, Freeston and Claus concluded that yarn crossovers do not greatly impede the movement of longitudinal strain waves in a fabric.

The fabric code developed by Roylance *et al.* [1973] was reviewed by Roylance and Wang [1980]. In this review, Roylance and Wang discussed in greater detail the various component models making up the fabric code, and investigated the stability and convergence of the predicted solutions of the code. Roylance and Wang then used this code to predict impact results for four orthogonally woven materials, namely nylon, Kevlar® 29, Kevlar® 49, and graphite. Due to the lack of dynamic fibre properties, Roylance and Wang made use of static fibre properties as inputs

for the model. They make a note, however, that the use of static properties, especially the yarn breaking strain, may lead to slight discrepancies in the predicted results. Despite this, the results indicated that the yarn modulus, **E**, was a very important factor in the development of strain in the fabric at the impact point. To compensate for the effect of **E** on the strain in the fabric, Roylance and Wang normalized the strain values by the value of strain developed in a yarn impacted at the same impact velocity. For all four fabrics, the time after impact at which the first peak in strain values occurred was observed to be linearly related to $\mathbf{E}^{1/4}$. These results were plotted to produce a master curve, shown in Figure 2.9, which can be applied to all four materials.

Roylance and Wang suggested that this curve could be used to produce strain versus time curves for any fabric, given the dynamic yarn modulus and impact velocity. They do note, however, that the master curve shown in Figure 2.9 was produced from impact data at high velocities and may not be valid at lower impact velocities.

Leech and Adeyefa [1982] developed a numerical model to predict the dynamics of ballistic impact of woven fabrics. The model is able to accurately predict the characteristics of the transverse wave fronts. The model is based on the stress wave theory method of characteristics, and makes use of Hamilton's principle to determine the equations of motion. Results of velocity-time and displacement-time predicted by this model are in good agreement with experimental data. The model, however, is not suitable for impact predictions involving viscoelastic woven materials.

Cunniff [1992] also made use of the fabric code developed by Roylance *et al.* [1973], but modified the model into what Cunniff called the "Natick direct analysis method model". Cunniff

suggested that this modified version provides a more extensive description of the projectile geometry than the model developed by Roylance *et al.* [1973].

The effect of interface friction on the ballistic impact response of woven aramid fabric has been investigated by Briscoe and Motamedi [1992]. A numerical code, based on a first-order model of the quasi-static penetration event, was developed to predict the ballistic impact energy dissipation characteristics of the aramid fabric. The main considerations of the model are the influences of friction between the fibres which make up the yarns of the fabric, and the friction between the yarns themselves. This model, unlike the model developed by Roylance *et al.* [1973], is much simpler and assumes that the shape of the transverse deformation of the fabric is dependent upon the test fixture supporting the fabric, and not the velocity of the induced strain waves. The quasi-static deformation model was found to predict the ballistic penetration process quite well. It was found that both the quasi-static and the ballistic deformation processes are related to the stiffness of the fabric. Since the stiffness of a fabric is greatly influenced by the interface friction, the influence of lubrication of fibres and yarns is an important consideration.

Ting *et al.* [1993] further modified the fabric code developed by Roylance *et al.* [1973] to include the effect of slippage of the yarns at clamps and at yarn crossovers. This modified version is able to deal with multiple-layer fabrics impacted by a range of projectile geometries. A graphical interface was also added to this code, which allows the user to view the strain in the target as the impact event occurs. The predictions of the code, with respect to yarn slippage in single layer fabrics, agree well with experimental observations made by Cunniff [1992] and Prosser [1988b], who found that the ballistic performance of woven fabrics decreases as slippage at the yarn crossovers increases.

The effect of an increase in temperature in woven Spectra® armour during ballistic impact was simulated numerically by Prevorsek *et al.* [1994]. Heat generated by both friction between the projectile and fabric, and by straining of the fibres, were considered. This latter term, however, was found to be negligible. The model makes a few assumptions, the first being that the density and thermal conductivity of the fabric do not change with temperature. The model also assumes that, due to the very short duration of the impact event (about 16 μs) and the very poor heat conducting ability of Spectra® fabric, the increase in temperature resulting from projectile impact is confined to a very small layer of fabric adjacent to the projectile.

Shim *et al.* (1995) developed a numerical code to predict the ballistic impact response of single-ply, plain woven polymeric fabrics, such as PPTA poly(p-phenylene-terephtalamide) and Twaron®, which is similar to Kevlar®. The code accounts for the viscoelastic nature of polymeric materials by incorporating a three-element viscoelastic constitutive model into the code and, like the model developed by Roylance *et al.* [1973], by treating the fabric as a network of pin-jointed fibre elements. The three-element viscoelastic constitutive model is shown in Figure 2.10, where K_1 represents the stiffness of the primary bonds in the fibres, K_2 represents the stiffness of the secondary bonds in the fibres, and μ_2 represents the viscosity of the yarns in the fabric.

The transverse deformation of the fabric due to impact is predicted by the code to be pyramidal in shape. The input requirements for the code include projectile geometry, impact velocity, and the fabric's boundary conditions and mechanical properties. The code must also be given the criteria as to when an element should fail. In addition to viscoelasticity considerations, the model incorporates the effect of yarn crimp into its code. This is accomplished by making the

assumption that crimping is responsible for a fraction of the total strain in the fabric, and that this fraction does not create any stresses. The energy absorption results predicted by this model agree well with experimental results, however, some errors may occur because this model does not take into account the ability of the fibres to slip past one another during penetration.

A parametric study was also performed on the model developed by Shim to determine the degree of influence, on ballistic impact response, of certain parameters in the numerical code. The parameters investigated were the stiffness of the primary bonds, the fraction of strain due to crimp, viscoelastic effects, and the failure strain of the fibres. The study revealed that the ballistic response is greatly influenced by the primary bond stiffness and the fibre failure strain. The influence of crimping strain and viscoelastic effects have a less, but still significant effect on the ballistic response.

Lomov [1995] developed a numerical model to simulate the ballistic impact response of a multiple-ply woven fabric structure. Lomov [1996] extended this model to account for oblique impacts, i.e., when the projectile impacts the target at an angle other than 0° (normal impact). The model requires inputs of projectile geometry, impact angle, target geometry, elastic moduli of the yarn, and the maximum tensile strains of single yarns. A complete list of model inputs is given in Table 3. The model assumes that no slippage of yarns occurs within a layer of fabric and that the layers fail sequentially, one after another. The model takes into account that the strength of the yarns decreases when woven into a fabric, due to crimping. To show the accuracy of the model, predictions were made simulating experiments found in literature. The predicted results were compared with the experimental results. Figure 2.11 shows the projectile exit velocity, v_r, and the height of the deformation, d, as functions of the projectile velocity, v_s, for both experimental (dots) and predicted (lines) results. For the results shown, the angle of impact

was 0°. Figure 2.12 shows the predicted and the experimentally observed deformation for the normal impact. A typical diagram of the projectile position and fabric deformation generated by the model for an oblique impact is shown in Figure 2.13.

A summary of the numerical models discussed is given in Table 2-3.

2.4 Conclusions

This review of the literature on the ballistic impact of textile armour materials provides a comprehensive summary of past and present work in this area, and reveals the presence of some significant gaps in both experimental work and analytical/numerical modelling.

2.4.1 Experimental

A lack of generality appears to exist in the test methods used by many researchers, as many of the experiments documented in the literature did not follow a standard test procedure, and were performed to determine the ballistic limit for a specific target/projectile system. Knowledge of the ballistic limit of a system alone does not give the entire story of how well an armour system will protect against a ballistic threat, as serious injury can still occur due to significant back-face deformation of the armour material.

2.4.2 Analytical/Numerical Modelling

Very few of the analytical and numerical models currently available are able to accurately predict the ballistic response of complex armour systems. The lack of an accurate predictive tool which brings together extensive experimental results and comprehensive modelling techniques emphasizes the need for an accurate, robust, experimentally-verified model able to predict the response of a textile armour system when impacted by any type of projectile.

Table 2-1: Summary of Experimental Work (? Indicates that information was not given)

Name	Materials Tested	Projectile Information	Test Fixture	Velocity Range	Main Considerations
Smith et al. (1963)	high-tenacity nylon and polyester yarns	5.58 mm diameter rifle bullets with prong-shaped tips	clamped at one end, a 100 g weight at other	up to 700 m/s	stress-strain response
Figucia et al. (1971)	nylon, polyamide and polypeptide yarns	?	?	strain rates of 100 %/min and 288,000 %/ min	ply and twist
Laible et al. (1973)	high modulus polyamide	5.58 mm diameter, 1.1 g FSP	as per MIL-Std-662	as per MIL-Std-662	ductility
Wilde et al. (1973)	single-ply, high-tenacity nylon	bevel-faced steel, 5.5 mm diameter, 1.1 g	all edges clamped in steel frame	116 - 537 m/s	development of transverse deformation
Laible et al. (1975)	single- and multiple-ply Kevlar®29 and woven glass fibre	9 mm, 8 g full metal jacketed	?	335 - 396 m/s	comparison of ballistic resistance
Figucia (1980)	single- and multiple-ply Kevlar®	1.1 g FSP	held between two Al plates	213, 274, 366 m/s	fabric weight fabric cover weave type
Montgomery et al. (1982)	single- and multiple-ply Kevlar®	5.58 mm, 1.5 g projectiles, four different geometries, ranging in bluntness	clay block placed behind target	200 - 600 m/s	projectile geometry
Prosser (1988)[a]	single- and multiple-ply nylon and Kevlar®	3.8 to 12.7 mm diameter steel FSP's	?	61 - 732 m/s	number of broken yarns in each layer
Taylor, Jr. and Vinson (1990)	single- and multiple-ply Kevlar®29	5.58 mm diameter, round nose and 9 mm diameter semi-wad cutter, flat-nose	?	240, 310, 380 m/s	?
Hsieh et al. (1990)	multiple-ply Spectra®, Kevlar®, graphite fabrics and fabric-reinforced composites	50° conical, steel tip	?	360 m/s	influence of delamination on projectile energy loss

Table 2-1: Summary of Experimental Work (continued)

Name	Materials Tested	Projectile Information	Test Fixture	Velocity Range	Main Considerations
Lin and Bhatnagar (1992)	multiple-ply Spectra Shield™ laminated composites and Spectra® fabric composites	5.58, 7.62 and 12.7 mm diameter FSP's	in accordance with MIL-STD-662E	in accordance with MIL-STD-662E	comparison of ballistic resistance
Briscoe and Motamedi (1992)	single-ply Kevlar®29 (plain and satin weaves) and Kevlar®49 (crowsfoot weave)	6.35 mm diameter steel ball bearing	pre-tensioned targets, clamped between steel rings of varying width and shape	50 - 250 m/s	inter-yarn friction
Cunniff (1992)	single-ply Kevlar®29, Spectra®, and nylon	chisel-nosed FSP	held between thick Al plates, varying aperture sizes	?	clamping pressure
Shim et al. (1995)	single-ply Twaron®	9 mm, spherical steel	vertical sides clamped	140 - 420 m/s	clamping vs. not clamping
Cunniff (1996)	multiple-ply Kevlar®29	0.1, 0.3, 1.0 and 4.1 g right circular cylinder	?	?	effect of changing areal density on V_{50}
Walsh et al. (1996)	single-ply dry Spectra® fabric, single- and multiple-ply Spectra®-reinforced composite	1.1 g FSP	two steel plates with serrated inner surfaces, connected with bolts	0.0002 m/s and 3.8 m/s	resin vs. no resin
Laine and Vähäkangas (1996)	single- and multiple-ply Kevlar® Ht	steel right circular cylinder, spherical ball, and NATO STANAG 2920 shape	two steel frames	?	distribution of kinetic energy

Table 2-2: Summary of Analytical Models (? Indicates that information was not given)

Name	Model Inputs	Model Outputs	Assumptions
Wilde et al. (1973)	• deformation cone size • projectile velocity • specific breaking energy of yarn • yarn mass	• projectile energy loss during penetration • velocity in fabric	• sum of strain and kinetic energies is the energy lost by projectile during penetration • strain energy in yarns outside deformation boundary and unbroken yarns within boundary are neglected • kinetic energy due to in-plane motion of yarns outside boundary is neglected
Vinson and Zukas (1975)	• projectile geometry, mass and velocity • fabric thickness • ultimate fabric strain and fabric modulus (as a function of strain rate) • fabric density	• velocity-time history • ballistic impact behavior of multiple-ply targets from single-ply target data • maximum deflection	• fabric behaves as a homogeneous, flexible plate • ignores strain energies • ignores effect of crossovers • failure strain of fibres does not depend on the number of layers in target
Leech et al. (1979)	• fabric areal density and modulus • fraction of yarns in warp and weft • projectile mass • striking velocity • fabric thickness	• velocity and displacement histories	• materials are linear-elastic • transverse deformation is rhomboidal in shape • no movement of the fabric in the plane of the target • Hamilton's principle holds
Prosser (1988)[a]	• areal density • number of layers in target • striking velocity • projectile mass and geometry • residual or critical velocity (determined experimentally)	• critical impact velocity • ballistic limit (v_{50}) • average projectile deceleration • average force to penetrate an interior layer for both bonded and non-bonded systems	• projectile energy loss as the projectile penetrates the interior layers is constant, and depends on the number of layers in the target and not the impact velocity
Parga-Landa and Hernandez-Olivares (1995)	• target properties: dynamic modulus of fibres, fibre volumetric density, yarn diameter, yarn spacing, yarn fracture strain, target dimensions, layer spacing, number of layers • projectile mass, diameter, incident surface • impact velocity	• ballistic limit curves (v_{50} versus surface density) • impact force • displacement and velocity of layers and projectile	• fibres are linear-elastic until failure • every layer helps to slow down the projectile until that layer reaches its failure strain • projectile is rigid • spacing between layers is constant • projectile decelerates uniformly from one layer to the next • properties of material remain constant during impact • neglects friction between the projectile and target

Table 2-2: Summary of Analytical Models (continued)

Name	Model Inputs	Model Outputs	Assumptions
Cunniff (1996)	• critical velocity (highest striking velocity where no penetration occurs) • striking velocity • projectile mass and shape • areal density	• v_s - v_r curves	• absorption energy is combination of both strain and kinetic energy • impact velocity equals critical velocity, and both target and projectile are at rest, at the instant the projectile is stopped by the fabric

Table 2-3: Summary of Numerical Models (? Indicates that information was not given)

Name	Model Inputs	Model Outputs	Assumptions	Features
Roylance et al. (1973)	• static fibre properties • striking velocity • projectile mass • fabric geometry	• v_s - v_r curves • strain-time history • strain and energy distributions	• neglects slippage at the crossovers • neglects effect of projectile geometry	• originally developed for single yarn impact • simplifies yarn crossovers as pin-joints • approximates impact as a point
Freeston, Jr. and Claus, Jr. (1973)	• longitudinal strain wave velocity • fraction of wave reflected at crossover	• strain amplitude-time history	• neglects effects of creep and stress relaxation • the impact point is perfectly reflecting • neglects wave velocity dispersion effects	• assumes impact point is perfectly reflecting
Roylance and Wang (1980)	• static fibre properties (tensile modulus, fracture strain, mass, yarn denier) • fibre failure criteria	• v_s - v_r curves • shape and size of deformation cone • strain wave propagation	• neglects slippage at the crossovers • neglects effect of projectile geometry	• used model by Roylance et al. (1973)
Leech and Adeyefa (1982)	• fibre properties (density and elastic modulus) • transverse wave velocity	• transverse wave front characteristics • velocity-time curves	?	• based on theory method of characteristics • makes use of Hamilton's principle • defines solution by deflections at each crossover
Cunniff (1992)	• striking and residual velocity data • yarn denier • failure criteria • number of layers • areal density • projectile mass and geometry	• strain-distance from impact curves • transverse deflection-distance from impact curves	• strain wave velocity is constant	• modified model by Roylance et al. (1973) to produce the "Natick direct analysis method model" • does not need to approximate impact as a point • a parametric study of this code can be performed quite easily
Briscoe and Motamedi (1992)	• wave propagation velocities • yarn modulus and density	• energy dissipation characteristics • indentation vs. displacement curves	• the geometry of the transverse deformation depends on geometry of test fixture and not the strain wave velocity • wave velocity is constant	• based on first-order model of quasi-static penetration event • considers the friction between the fibres and between the yarns

Table 2-3: Summary of Numerical Models (continued)

Name	Model Inputs	Model Outputs	Assumptions	Features
Ting et al. (1993)	• striking velocity • areal density • crossover density • failure criteria	• strain vs. position from impact point curves • a display of the uni-directional strain • v_s - v_r curves • deformation contour plot	?	• modified the model by Roylance et al. (1973) to simulate multiple-layer fabrics • includes effect of slippage at yarn crossovers and at clamps • has graphical interface to view strain in target during penetration • simplifies yarn crossovers as pin-joints
Prevorsek et al. (1994)	• projectile density, heat capacity, and thermal conductivity • fibre density, heat capacity, thermal conductivity and friction coefficient • striking velocity	• temperature profile at the interface of the projectile and fabric	• the density and thermal conductivity of the fabric do not change with temperature • the increase in temperature resulting from projectile impact is confined to a very small layer of fabric adjacent to the projectile	• considers heat generated due to friction
Shim et al. (1995)	• projectile geometry • impact velocity • target boundary conditions • mechanical properties of fabric • failure criteria	• transverse deformation shape • energy absorption vs. impact energy curves • v_s - v_r curves	• yarn crimping is responsible for a fraction of the total strain in the fabric • neglects the ability of the fibres to slip past one another during penetration	• treats fabric as a network of pin-jointed fibre elements • incorporates a three-element viscoelastic constitutive model • incorporates effect of yarn crimp
Lomov (1995), (1996)	• projectile geometry • each layer is characterized by yarn count, yarn spacing, weave tightness coefficient, yarn linear density, elastic modulus, yarn diameter • maximum tensile strains of single yarns • impact angle (Lomov, 1996)	• v_s - v_r curves • deformation height - v_s curves • deformation profiles • projectile penetration profiles for normal and oblique impacts • velocity-time, deformation-time and strain-time curves	• no slippage of yarns occurs within a layer of fabric • layers fail sequentially, one after another • deformation of yarn is linear • projectile is rigid	• accounts for decrease in strength of yarns when woven due to crimping • accounts for projectile nose shape • accounts for oblique impacts (Lomov, 1996)

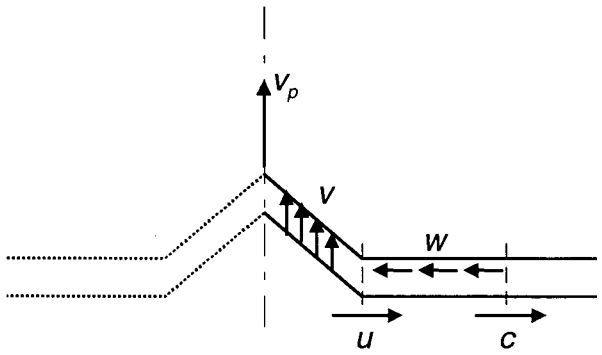

Figure 2.1: **Schematic of impacted yarn, symmetric about the center line (where v is the velocity of the material in the transverse direction, v_p is the velocity of the projectile, w is the velocity of the material moving towards the impact point between the longitudinal strain wavefronts, u and c are the velocities of the transverse and longitudinal waves, respectively).**

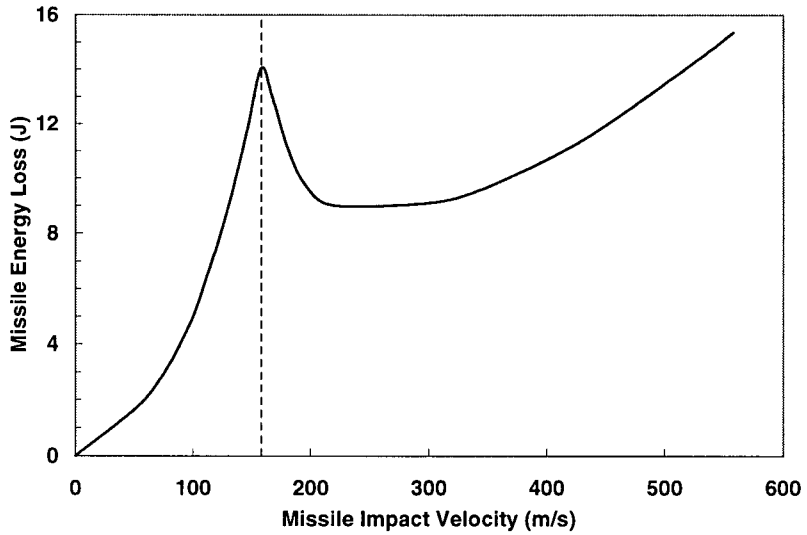

Figure 2.2: **Projectile energy loss versus impact velocity, where the dashed line indicates the average impact velocity at which penetration does or does not just barely occur. (Reproduced from Wilde *et al.* [1973])**

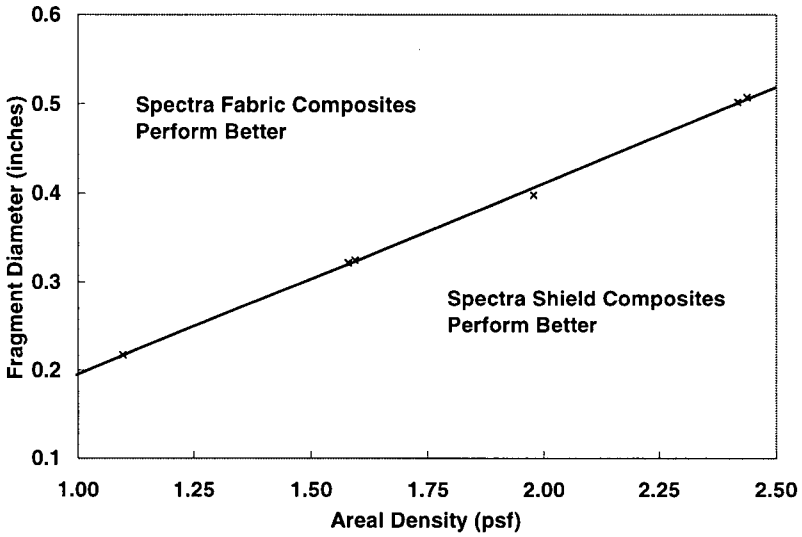

Figure 2.3: Comparison of the ballistic performance of Spectra Shield™ composites and Spectra® fabric composites. (Reproduced from Lin and Bhatnagar [1992])

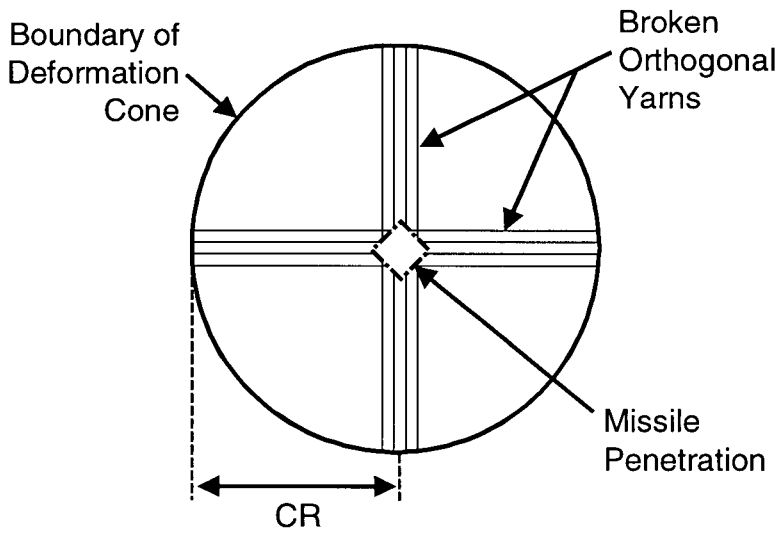

Figure 2.4: BOY model. (Reproduced from Wilde *et al.* [1973])

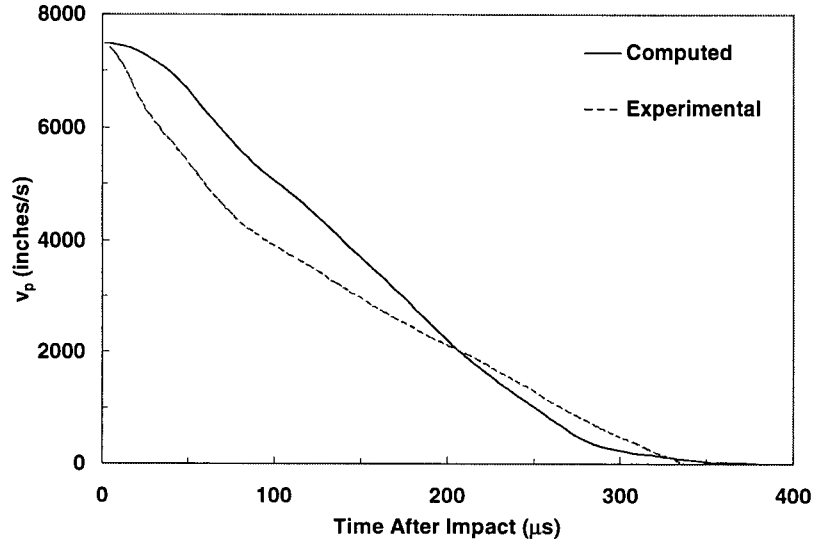

Figure 2.5: Penetration velocity: model predictions and experimental data. (Reproduced from Vinson and Zukas [1975])

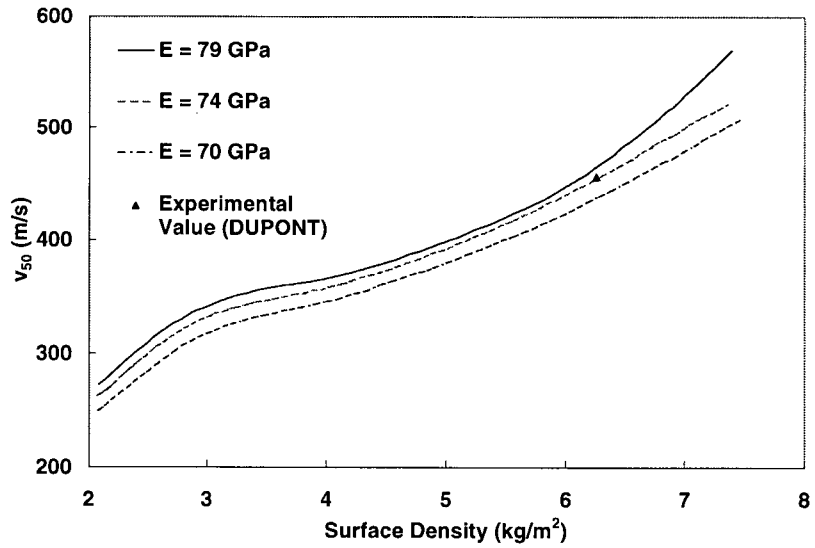

Figure 2.6: Ballistic limit curve: model predictions and experimental data. (Reproduced from Parga-Landa and Hernandez-Olivares [1995])

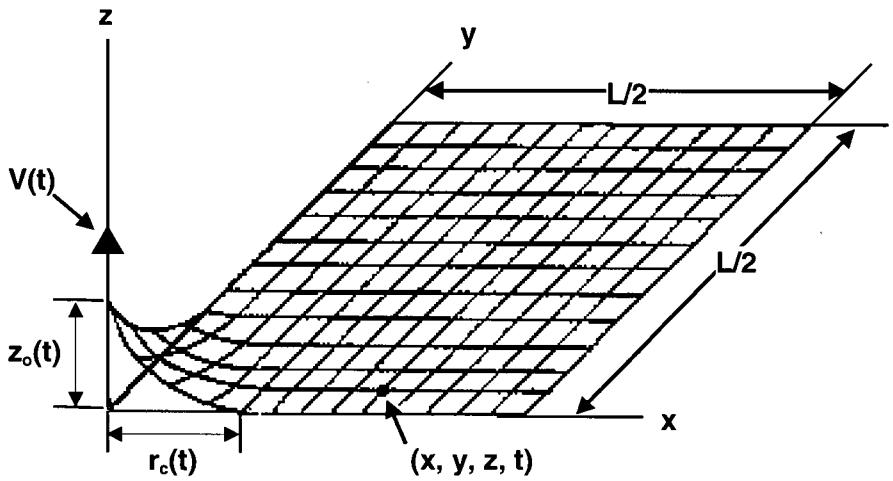

Figure 2.7: **Model simplification of yarn crossovers as pin-joints. (Roylance and Wang [1980])**

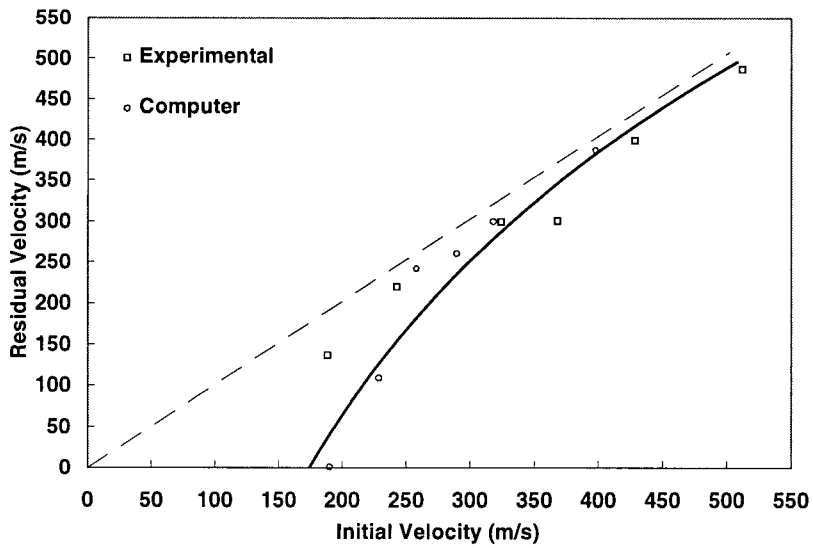

Figure 2.8: **Impact velocity versus residual velocity curve of ballistic impact: model predictions and experimental data. (Reproduced from Roylance *et al.* [1973])**

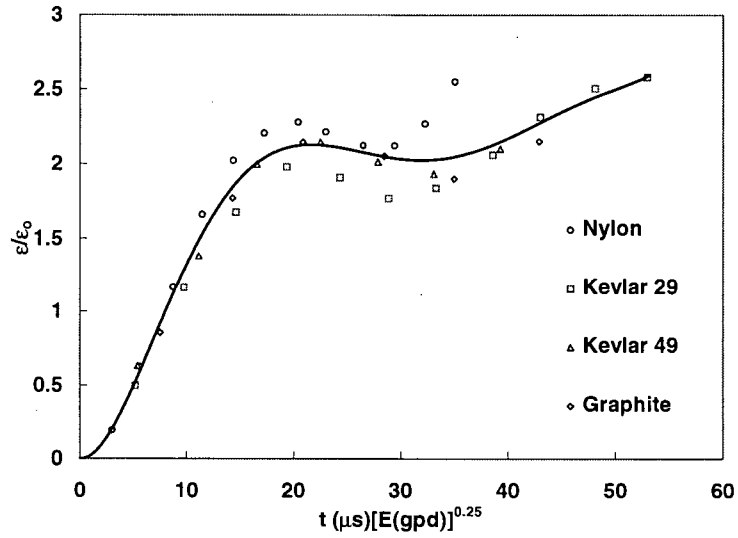

Figure 2.9: Master curve. (Reproduced from Roylance and Wang [1980])

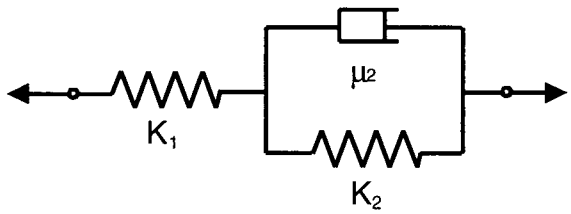

Figure 2.10: Three-element viscoelastic constitutive model. (Reproduced from Shim *et al.* [1995])

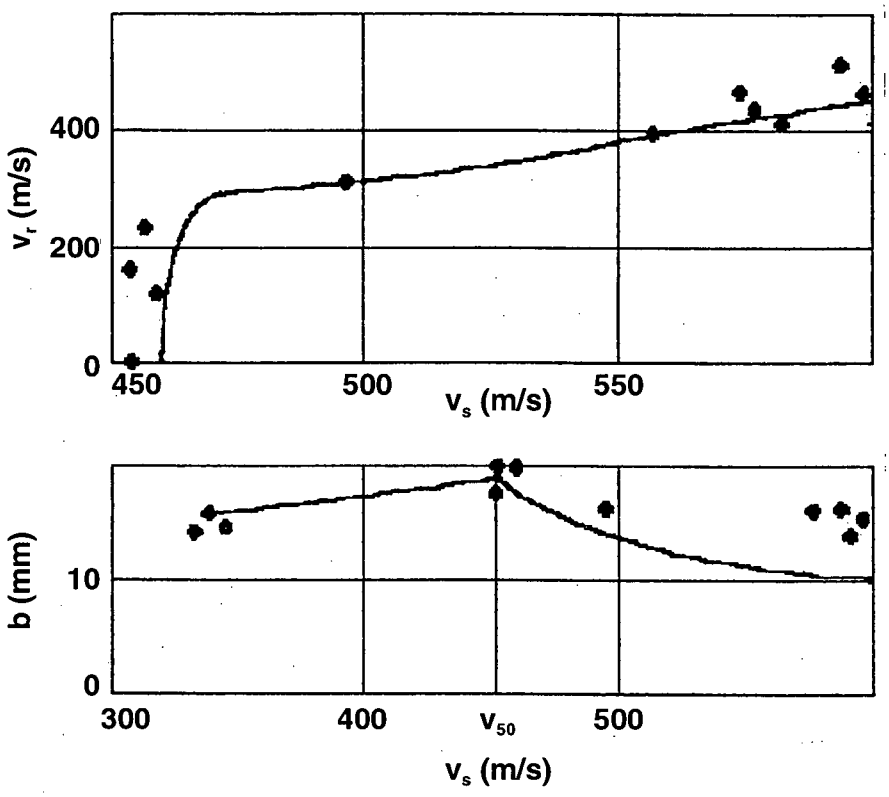

Figure 2.11: Predicted and experimental results from normal impact. (Lomov [1996])

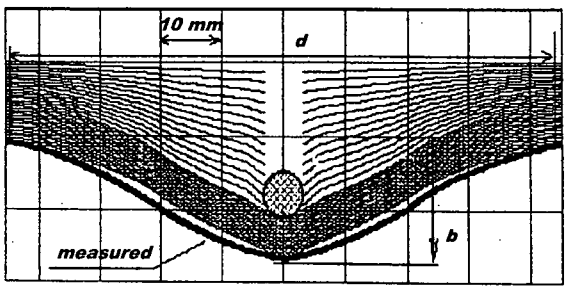

Figure 2.12: Predicted and measured (observed) deformation from normal impact. (Lomov [1996])

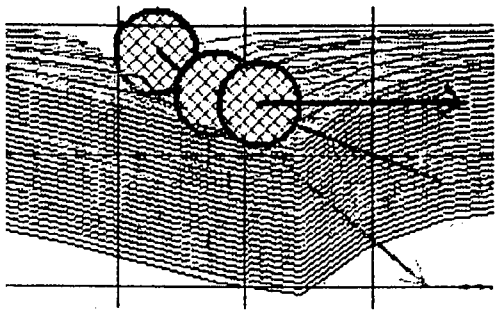

Figure 2.13: Simulated diagram of oblique impact. (Lomov [1996])

Chapter Three: Ballistic Impact Tests Using a High Speed Video Camera

3.1 Introduction

This chapter discusses the ballistic impact experiments performed at the Defence Research Establishment Valcartier (DREV), Quebec. The ballistic test equipment, targets, test fixture, and projectiles used in the experiments are described. The two measurement techniques used, a high speed video camera and optical sensors, are discussed. A summary of the test procedure performed on each target is described.

3.2 Test Components

3.2.1 Gas Gun

The gun used to perform the ballistic impact tests at DREV was a smooth bore gas gun with a 5.58 mm (0.22″) diameter barrel. The gas gun made use of pressurized helium/nitrogen to provide the necessary driving force to propel the projectile down the barrel. A complete description of the gas gun used at DREV can be found in Kraak [1994].

3.2.2 Projectiles

Ballistic impact experiments were performed using 2.8 g (43 grain) blunt aluminum cylindrical projectiles approximately 46 mm (1.81") in length, and 1.1 g (17 grain) aluminum fragment simulating projectiles (FSP), approximately 18 to 19 mm (0.71 - 0.75") in length. The 1.1 g projectiles had conical (with a 120° cone angle), hemispherical, and blunt nose shapes. All projectiles, schematics of which are shown in Figure 3.1, were 5.38 mm (0.21") in diameter. The length of the projectiles was adjusted to give the appropriate weight. Due to the size difference

between the projectile diameter and the gun barrel, a small cylinder of styrofoam, 5.58 mm (0.22″) in diameter and 12 mm (0.47") in length, was placed directly behind the projectile in the gun barrel prior to every test. The purpose of this foam piece was to provide a tighter seal in the gun barrel.

3.2.3 Targets

The targets used in these ballistic impact experiments were composed of 8 and 16 plies of Kevlar® 129. All targets were 400 mm x 400 mm (15.7" x 15.7"), and were stitched at the four corners to hold the plies together. The physical and mechanical properties of Kevlar® 129 yarn, as well as the physical properties of the Kevlar® 129 woven fabric used, are given in Table 3-1 and Table 3-2, respectively.

3.2.4 Test Fixture

The targets were clamped to a back plate which had a square opening, 305 mm x 305 mm (12" x 12"). The top and bottom edges of the targets were clamped using square rods, with three c-clamps applying the clamping pressure to each rod, as shown in Figure 3.2. The vertical sides of the target were not clamped, providing free boundary conditions.

3.3 Measurement Techniques

3.3.1 Optical Sensors

A set of two optical sensors were used to determine the initial velocity of the projectile in the experiments. The sensors, shown in Figure 3.3, were located at the end of the gas gun barrel, and were spaced a distance of 76 mm (3") apart. As the projectile passed the first sensor, a counter was triggered. The time taken for the projectile to reach the second sensor was recorded by the

counter. By knowing the distance between the sensors, and using the time recorded by the counter, the initial velocity of the projectile could be calculated.

3.3.2 High Speed Video Camera (HSVC)

An ultra high speed video camera, shown in Figure 3.4, was used to take photographs of the target deformation during the ballistic impact experiments. The camera is an OPTIKON™ HSFC Model HS4/100, consisting of four small cameras which all look through the same lens. The lens used with the camera was an APO-RODAGON-N 150 mm lens, with an aperture of 1:4. The camera is capable of taking four images per impact event, with an exposure time of 1 μs for each image. The camera is triggered when the projectile passes the first optical sensor. The time at which each image is taken, known as the time delay, is set manually.

3.4 Experimental Procedure

3.4.1 Testing

Due to the size of the target and the easy maneuverability of the test fixture, each specimen could be impacted more than once. A pattern of dots (evident in Figure 3.2) was marked on the front (impact) face of the target to aid in the alignment of each shot and to ensure that no two shots impacted the same yarns in the target. The distance between each shot, and the distance between any target edge and a shot was at least 51 mm (2"). After each shot, the target was removed from the test fixture, flattened and then re-clamped to the test fixture. This was done to ensure that the boundary conditions were approximately the same for each shot. The initial projectile velocity for the ballistic impact tests ranged from 303 to 458 m/s. The distance between the end of the gun and the targets, which influences the time delay of the camera, was arbitrarily set between 76 mm (3") and 178 mm (7"). A schematic showing the relative positions of the gas gun, target,

and high speed video camera is given in Figure 3.5. A summary of the tests performed is given in Table 3-2.

3.4.2 Post-Test Target Analysis

In the experiments performed using the 2.8 g projectiles, a post-test analysis was performed on each impact site to determine the number of broken yarns in each ply. This was accomplished by observing the impact site under a low powered microscope, and counting the number of broken yarns to the nearest ¼ yarn.

3.4.3 Calculation of Time Values for Video Images

A calculation was performed for the 2.8 g (43 grain) blunt projectile tests to determine if the projectiles were experiencing any deceleration due to air drag. The calculation and the results, given in Appendix A, show that deceleration is negligible, and therefore, the velocity determined by the optical sensors was taken to be the impact velocity in all tests.

The time at which impact occurred was found using the impact velocity and the distance the projectile had travelled from when it triggered the video camera (at the first optical sensor, located 76 mm (3") from the end of the gun barrel) until the projectile impacted the target. For images in which the projectile could be seen prior to impact, the time delay for the image was found from the impact velocity and the known distance the projectile had travelled. This value was found to be slightly less than the time delay values set manually and recorded by the video camera acquisition program. The difference between these two values was determined and used to correct the time values for the remaining images. For tests in which this was not possible, the first image was used as a reference point, and the times of the remaining images were taken with respect to the first image.

Table 3-1: Physical and mechanical properties of Kevlar® 129 yarn (Pageau [1997]).

Property	Value
Tensile Strength	3378 MPa (2.35 N/tex)
Tensile Modulus	96 GPa (66.8 N/tex)
Elongation at Break	3.3 %
Specific Gravity	1.44 g/cm^3

Table 3-2: Physical properties of Kevlar® 129 fabric (Pageau [1997]).

Property	Value
Weave	Plain 1x1
Linear Density	840 denier (93.3 tex)
Mass	204 g/m^2
Yarn Crimp	≤ 3 % difference between warp and weft
Woven Fabric Count	11 yarns/cm (warp and weft)
Fibre Tenacity	20 g/denier (warp and weft)

Table 3-3: Summary of tests performed at DREV.

Test	Number of Plies	Projectile	Impact Velocity (m/s)	Perforation/ No Perforation
#L1	8	2.8 g, blunt	278	N
#L2			341	N
#L3			341	N
#L4			343	N
#L5			303	N
#L12	16		401	N
#L13			404	N
#L14			397	N
#L15			431	N
#L16			459	N
#C19	8	1.1 g, 120° conical	325	N
#C20			325	N
#C21			383	P
#H22	8	1.1 g, hemispherical	383	P
#H23			360	P
#H25			328	N
#H26			324	N
#S28	8	1.1 g, blunt	329	N
#S29			357	N
#S31			378	N
#S32			398	N

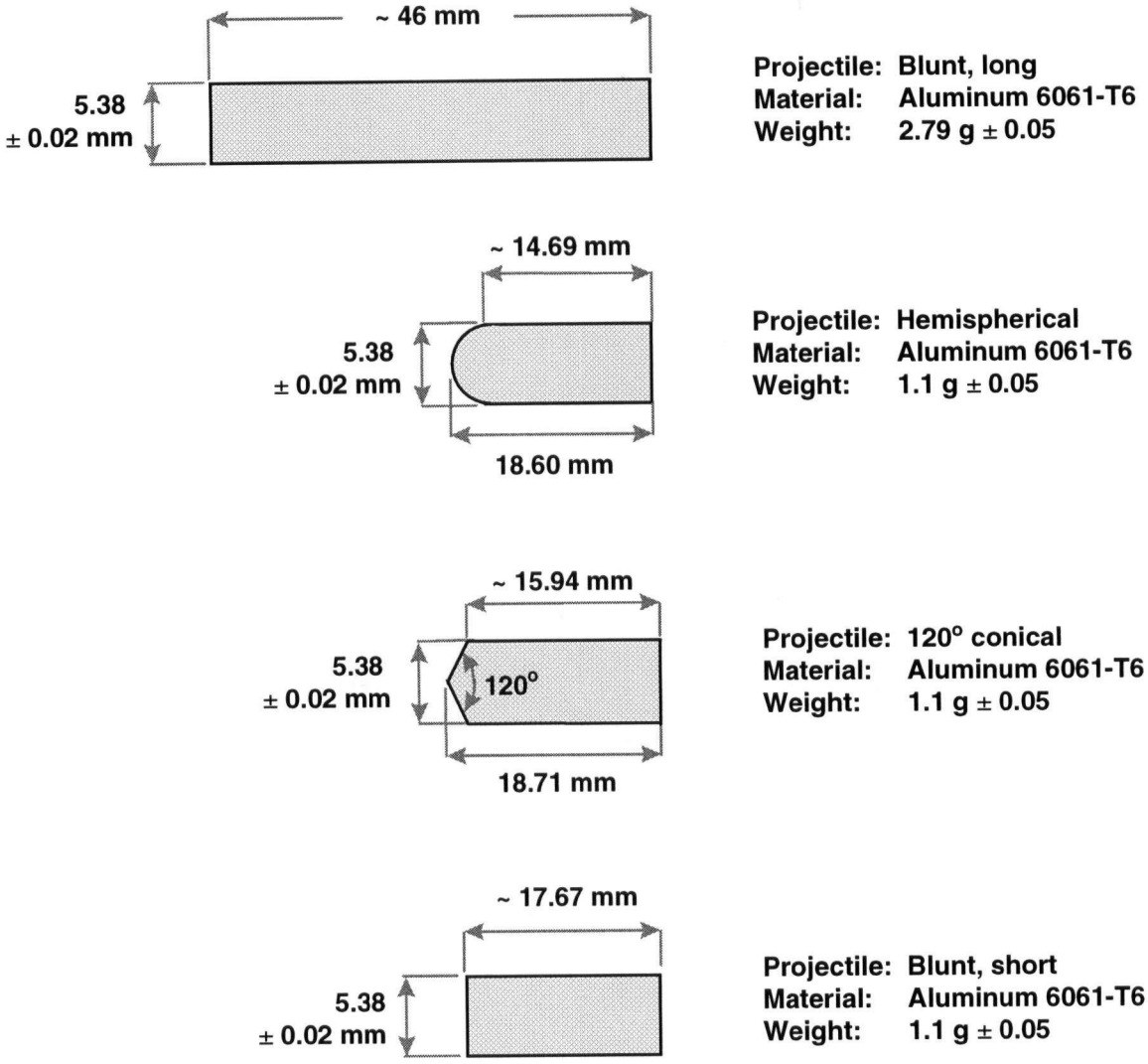

Figure 3.1: Projectiles used in ballistic impact experiments at DREV.

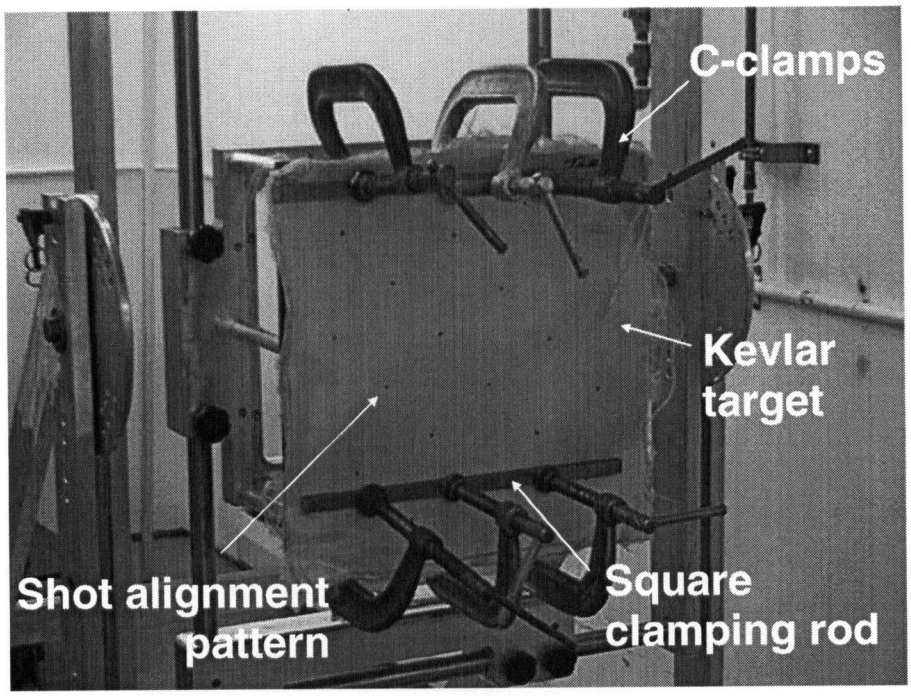

Figure 3.2: Kevlar® 129 target clamped in DREV test fixture.

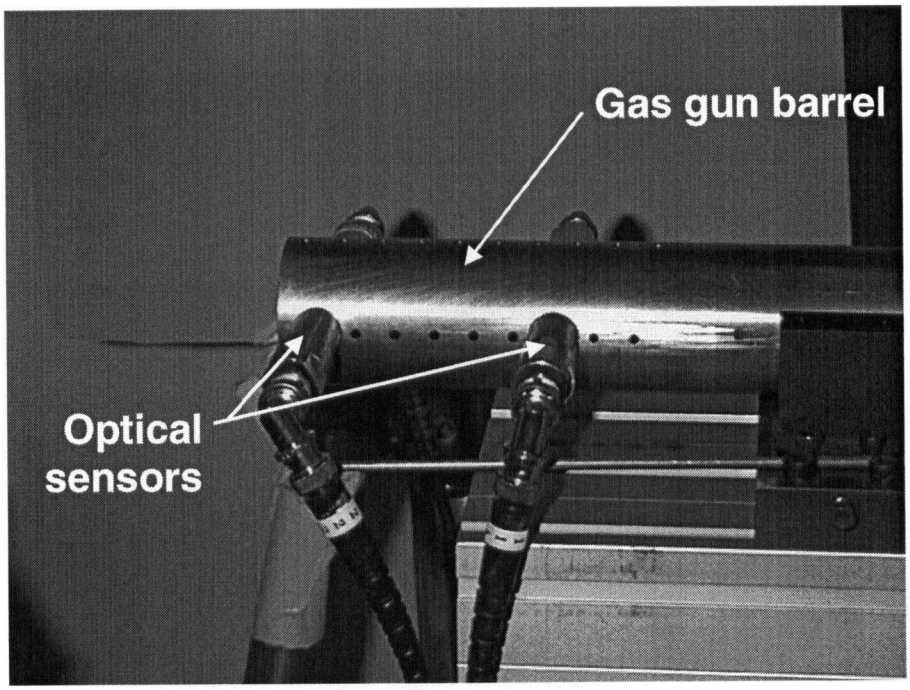

Figure 3.3: Optical sensors attached to end of gas gun at DREV.

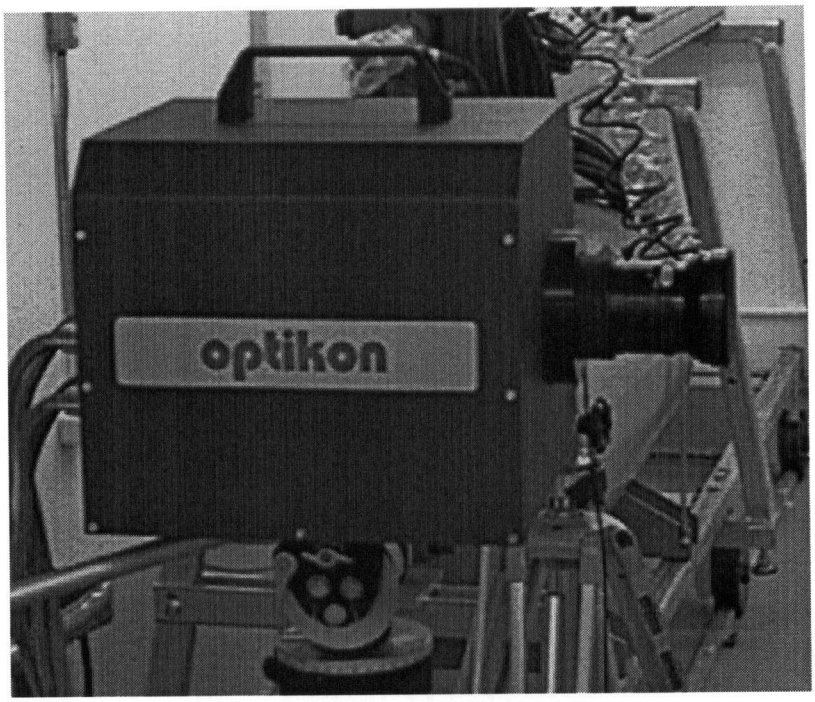

Figure 3.4: Optikon™ high speed video camera.

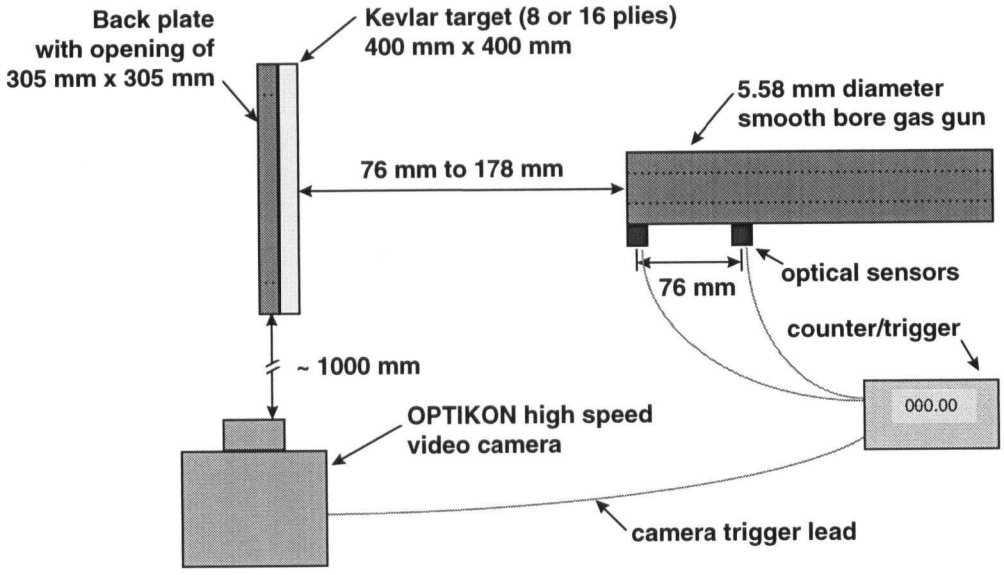

Figure 3.5: Schematic of test set-up at DREV.

Chapter Four: Ballistic Impact Tests Using the ELVS

4.1 Introduction

This chapter describes the ballistic impact experiments performed using The University of British Columbia Enhanced Laser Velocity System (ELVS) measurement technique. The ballistic test equipment, measurement technique, targets, test fixture, and projectiles used in the experiments are described. A summary of the test procedure performed on each target is presented.

4.2 Test Components

4.2.1 Powder Gun

A powder gun with a 5.58 mm (0.22") diameter Remington riffled barrel was used to fire the projectiles in the ballistic impact experiments performed at UBC. The powder gun set-up, shown in Figure 4.1, consists of a universal receiver, a barrel, a blast deflector, and a catchment chamber. The blast deflector was used to reduce the amount of smoke and unburned powder resulting from firing a projectile, and the catchment chamber was used to stop any projectiles that perforated the targets.

The powder gun was first calibrated using 2.8 g (43 grain) blunt aluminum cylindrical projectiles, shown in Figure 4.2. These projectiles were the same as those used in the actual ballistic impact tests discussed in this chapter. The gun powder used for this series of calibration tests and for all ballistic impact tests performed at UBC was Hodgdon H450. This lower energy powder was used in these experiments to obtain a more stable burn, and hence, more repeatable velocities.

With more energetic powders, e.g. Bullseye®[2], problems arose when testing at lower velocities (200 to 300 m/s) due to the small amounts of the more energetic powder required.

The calibration procedure was required to determine the relationship between the amount of gun powder used (in units of grains) and projectile energy. To perform the calibration procedure, the projectiles were loaded into Remington 22-250 brass casings, which contained a pre-determined amount of gun powder. The projectile and casing were then loaded into the barrel of the powder gun, and fired. This was repeated for a range of powder amounts from 9 to 15 grains. The velocity of the projectiles in these "no target" tests was determined using the ELVS, described in detail in Section 4.3. A plot of the powder amount versus projectile energy is given in Figure 4.2, showing both calibration data and a linear curve fit to the data.

4.2.2 Projectiles

The projectiles used for these experiments were 2.8 g (43 grain) blunt aluminum cylinders, 5.38 mm (0.21") in diameter and approximately 45 mm in length. The length of the projectiles was adjusted to give the correct weight. These projectiles, shown in Figure 4.2, were similar to those used in the ballistic impact experiments discussed in Chapter 3, with the only difference being that the projectiles used at UBC had a 'skirt' machined on the back end of the projectile to allow the projectile to properly fit into the brass bullet casings. The projectiles discussed in Section 3.2.2 did not have this skirt on their back end because a smooth bore gas gun was used.

[2] manufactured by Hercules Incorporated.

4.2.3 Targets

The targets used in these experiments were composed of 8 and 16 plies of Kevlar® 129, the same material used for the targets discussed in Chapter 3. The targets were 330 mm x 330 mm (13" x 13"). The physical and mechanical properties of Kevlar® 129 yarn, and the physical properties of the Kevlar® 129 woven fabric used can be found in Tables 3-1 and 3-2, respectively.

4.2.4 Test Fixture

A fixture to hold the fabric target during impact testing was designed and constructed at UBC. Figure 4.4 shows a detailed schematic of both the front and back plates of the test fixture. The test fixture, adapted from the NATO-STANAG-2920 standard test frame, clamps the target between ridges on two circular plates, 444 mm (17.5") in diameter. A cross-section showing how the fabric target is clamped between the ridges is shown in Figure 4.5. The two plates are held together using eight 12.7 mm (0.5") coarse thread, counter bored allen screws. A torque can be applied to the screws to ensure the two plates are tightly clamped. The ridges consist of 7.9 mm ($^5/_{16}$") square rods glued into grooves in the circular plates. The edges of the inner most rod were sanded down to eliminate any cutting of the fabric by the sharp edges of the rod when the target was clamped in the fixture.

The test fixture is capable of clamping the targets on all four sides. In the experiments performed for this thesis, however, the targets were clamped only at the top and bottom. This was accomplished by gluing only the top and bottom rods onto the circular plates, and not attaching the side rods. The reason for using this partial clamping was to match the boundary conditions of the tests performed using the 2.8 g (43 grain) projectiles at DREV (Section 3.2.4).

The test fixture is attached directly onto the catchment chamber of the existing powder gun set-up at UBC using two 25.4 mm (1") bolts, such that the center of a target in the test fixture aligns with the center of the gun barrel, as shown in Figure 4.6. The opening through which the target is impacted is a square with dimensions of 203 mm x 203 mm (8" x 8"). This is smaller than the opening in the NATO-STANAG-2920 standard test frame (300 mm x 300 mm), and was necessary so that the UBC test fixture could be easily attached to the existing powder gun set-up. A slot was machined into the front (impact) face of the test fixture to allow the laser sheet of the ELVS to be placed close to the target. A photograph of the test frame and the experimental set-up is shown in Figure 4.1.

4.3 UBC Enhanced Laser Velocity System (ELVS)

The ELVS measurement technique was used in all impact experiments performed at UBC. The system, shown in Figure 4.7(a), allows for continuous measurement of projectile displacement before and during a ballistic impact event. The basis of this method is quite simple. A sheet of laser light is emitted from a diode laser (#1 in Figure 4.7(a)) and diverges in both the horizontal and vertical planes. The diode laser contains specialized line generating optics which produce a sheet of light with relatively uniform intensity along the width, except at the edges. The diverging sheet then passes through two plano-cylindrical lenses. The first of these (#2) collimates the sheet in the horizontal plane, while the second (#5) collimates the sheet in the vertical plane. An aperture (#3) and neutral density filter (#4) are placed between the two cylindrical lenses to block out the edges of the sheet which are of significantly non-uniform intensity, and to reduce the overall intensity of the laser sheet, respectively. The result is a sheet of laser light with uniform width, thickness and intensity. In the ELVS, the width of the laser

sheet is 25.4 mm (1.0") and the thickness is 1 mm (0.04"). The laser sheet is then focused by a symmetric-convex collector lens (#6) onto the active area of a silicon PIN photo-detector (#7) which reads the intensity of the laser sheet. The sheet intensity is then recorded as a voltage by an oscilloscope. All components of the system are mounted on special mounting equipment to allow for optimum alignment. Lexan sheets are placed in front of the second cylindrical lens (#5) and the collector lens (#6) to protect these two lenses from any debris or unburned gun powder which may be ejected during a ballistic impact test. A more detailed description of the components in the ELVS, including part numbers, is given in Appendix B.

4.3.1 Principle of Operation of the ELVS

The basic principle of the method is shown in Figure 4.7(b), with the corresponding voltage-time curve from an actual impact test, given in Figure 4.8. In this ballistic test, the projectile was 12.6 mm (0.5") longer than the width of the laser sheet. While the projectile is out of the sheet (up to position A in Figure 4.7), the oscilloscope shows full voltage, or 100 % intensity (up to position A in Figure 4.8). As the projectile moves from position A to B, it blocks out the sheet and the intensity drops in proportion to the amount of light blocked. The minimum voltage, corresponding to an intensity of 0 %, does not drop to 0 V because the photo-detector registers background light. Since the projectile is longer than the sheet, it continues to block out the sheet until the back end of the projectile reaches the front of the sheet, i.e. from B to C. This results in a "null" period where the intensity of the sheet stays constant at 0 %. From position C to E the projectile leaves the sheet causing the intensity to rise with a corresponding rise in voltage. Position D is the point at which impact occurs. From this point, until the end of the voltage-time curve, the data recorded provides a continuous measurement of the impact event. The distance between the target and the laser sheet is not fixed and can be adjusted to whatever is required.

In order to convert the voltage measurements from the impact event into useable displacement data, the relationship between voltage and displacement must be obtained by performing a calibration test. Once this is obtained, the velocity, acceleration, force and energy values can be determined by performing simple mathematical calculations on the data.

A complete description of the ELVS, including the calibration procedure and the data analysis, is given in detail in Appendix B.

4.4 Experimental Procedure

4.4.1 Testing

Due to the smaller size of the targets tested at UBC and limitations of the test fixture, each target was impacted only once. The targets were placed a distance of 21 to 22 mm (0.83 - 0.87") from the laser sheet of the ELVS. The initial projectile velocity for the ballistic impact tests ranged from 267 to 428 m/s. A summary of the tests performed at UBC, and a comparison of the experimental set-up and test conditions at UBC and at DREV (Chapter 3) using the 2.8 g (43 grain) aluminum blunt projectiles, are given in Table 4.1 and Table 4.2, respectively.

4.4.2 Post-Test Target Analysis

A post-test analysis was performed on each target to determine the number of broken yarns in each ply. This was accomplished by observing the impact site under a low powered microscope, and counting the number of broken yarns to the nearest ¼ yarn.

Table 4-1: Summary of ballistic impact tests performed at UBC.

Test Number	Number of Plies	Impact Velocity (m/s)	Perforation/ No Perforation
o291	8	314	N
o301	8	344	N
o311	8	341	N
o312	8	298	N
o313	8	428	P
n272	8	366	N
n282	8	267	N
d121	16	375	N
d122	16	359	N
j201	16	364	N

Table 4-2: Comparison of the ballistic impact tests performed at UBC and DREV, using the 2.8 g (43 grain) blunt aluminum projectiles.

TEST CONDITION	UBC	DREV
Target material	Kevlar® 129	
Target size (mm)	330 x 330	400 x 400
Back plate opening (mm)	203 x 203	305 x 305
Clamping conditions	clamped at top and bottom	
Gun	rifled barrel powder gun	smooth bore gas gun
Measurement technique(s)	ELVS	high speed video camera optical sensors
Distance between initial velocity measurement and target (mm)	21 - 22	127 - 178
Impact velocity range (m/s)	267 - 428 (8 ply tests) 359 - 375 (16 ply tests)	278 - 343 (8 ply tests) 397 - 459 (16 ply tests)

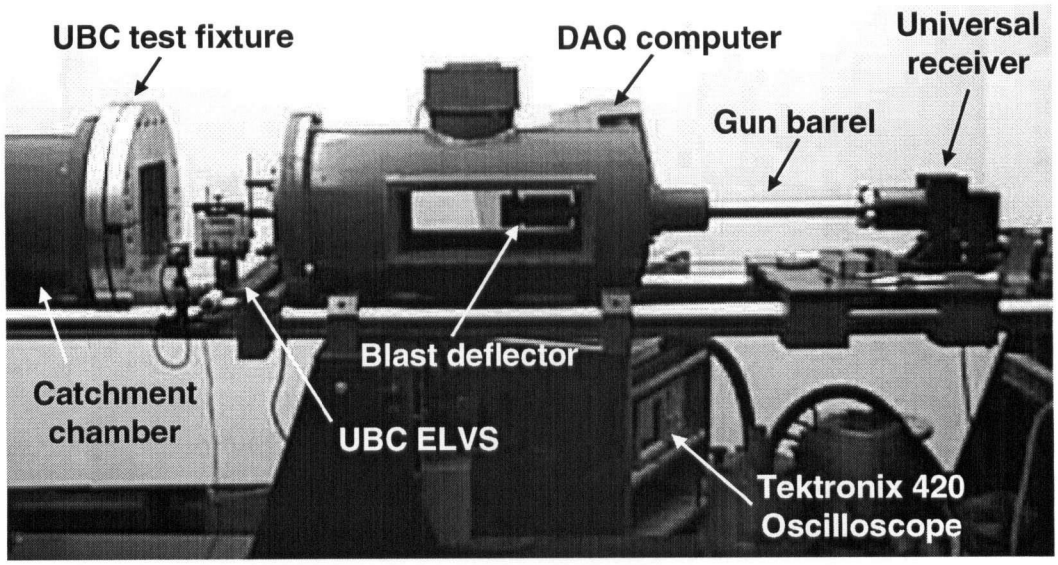

Figure 4.1: **Photograph of experimental set-up at UBC, including powder gun, measurement system, test fixture and catchment chamber.**

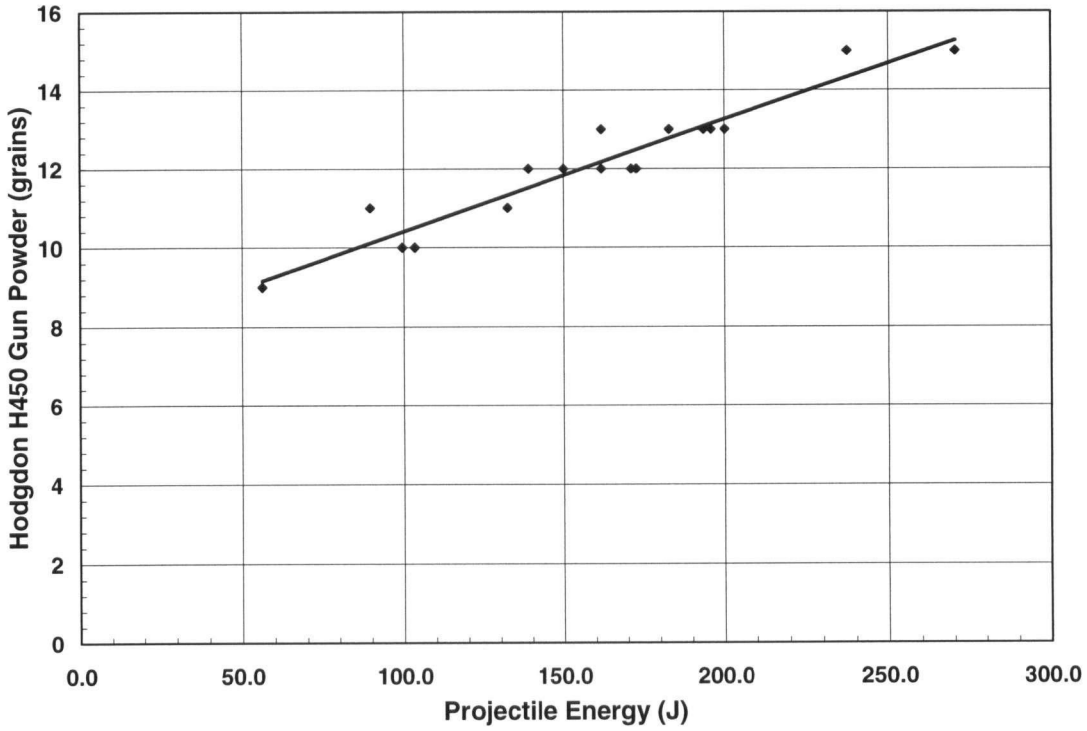

Figure 4.2: **Relationship between amount of gun powder and projectile energy using Hodgdon H450 gun powder, showing calibration data and a fitted curve.**

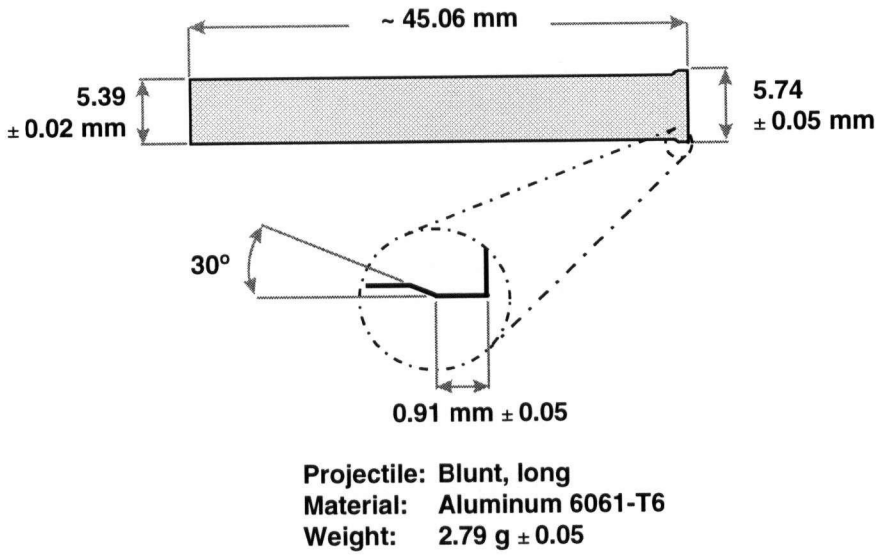

Figure 4.3: The 2.8 g aluminum cylindrical projectile used at UBC.

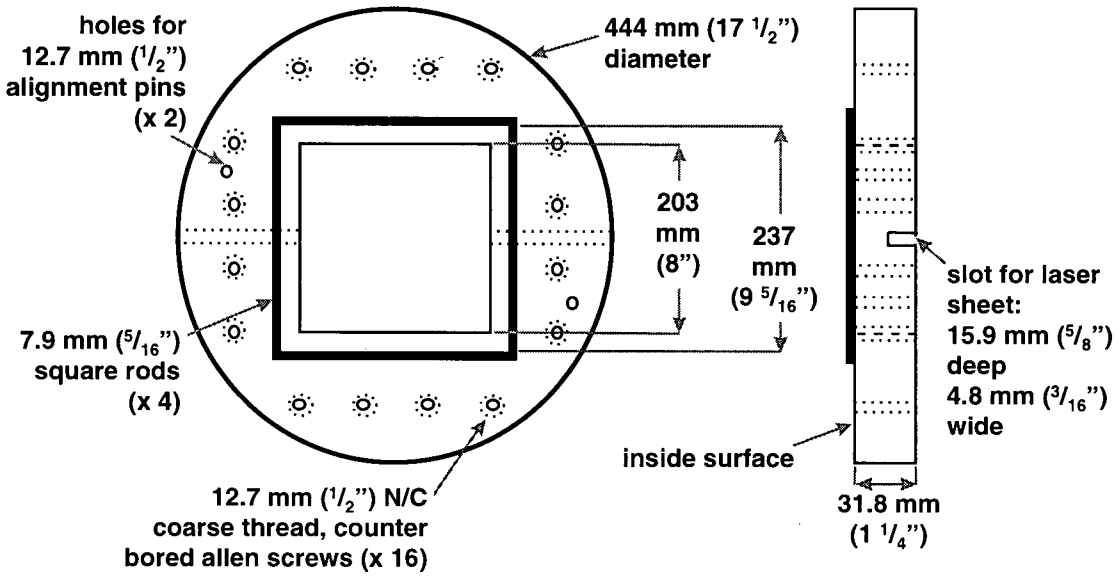

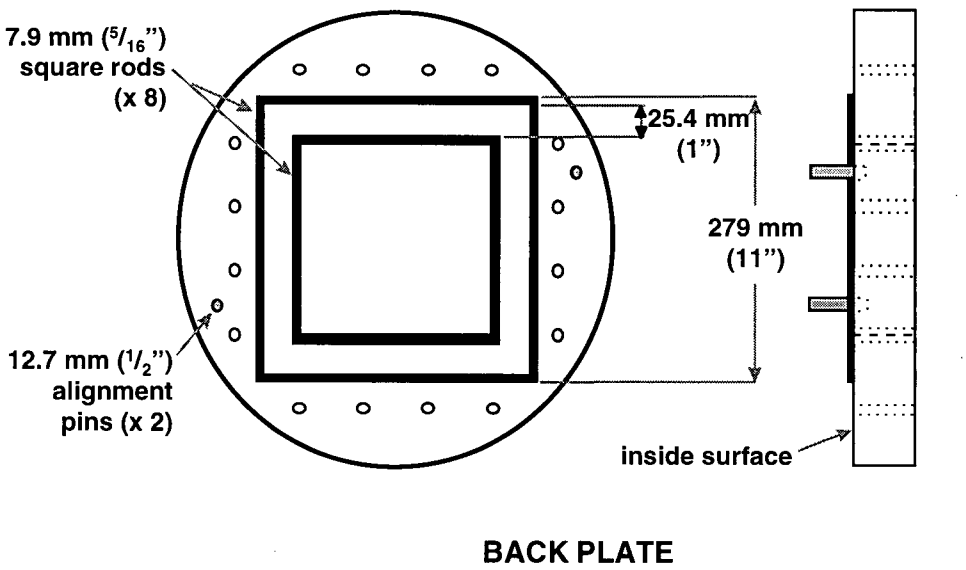

Figure 4.4: Detailed schematics of UBC test fixture, showing front and back plates.

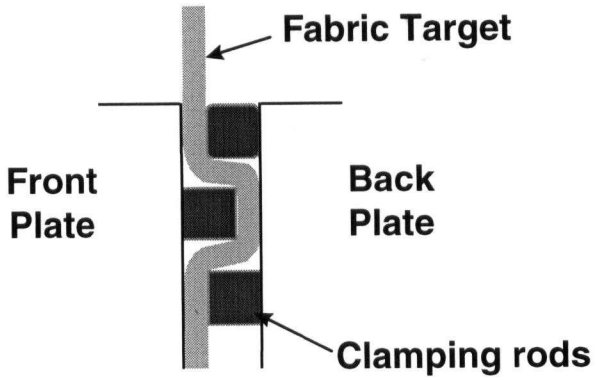

Figure 4.5: Fabric clamped between ridges in UBC test fixture.

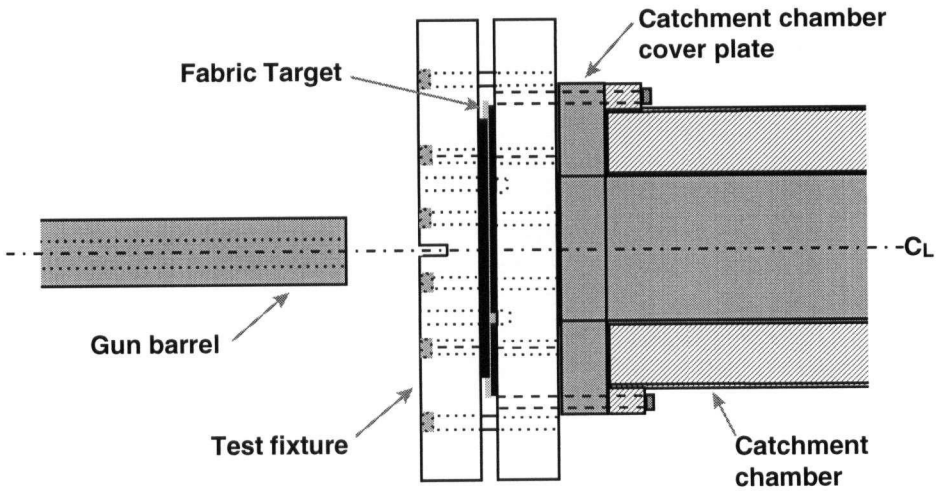

Figure 4.6: Schematic of UBC test fixture, showing alignment with existing power gun set-up.

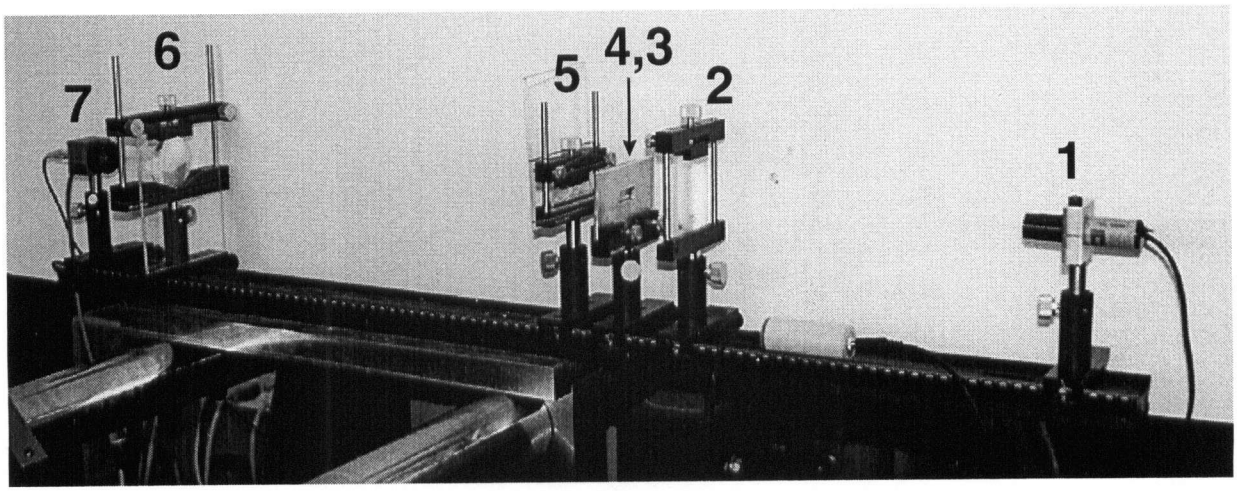

(a)

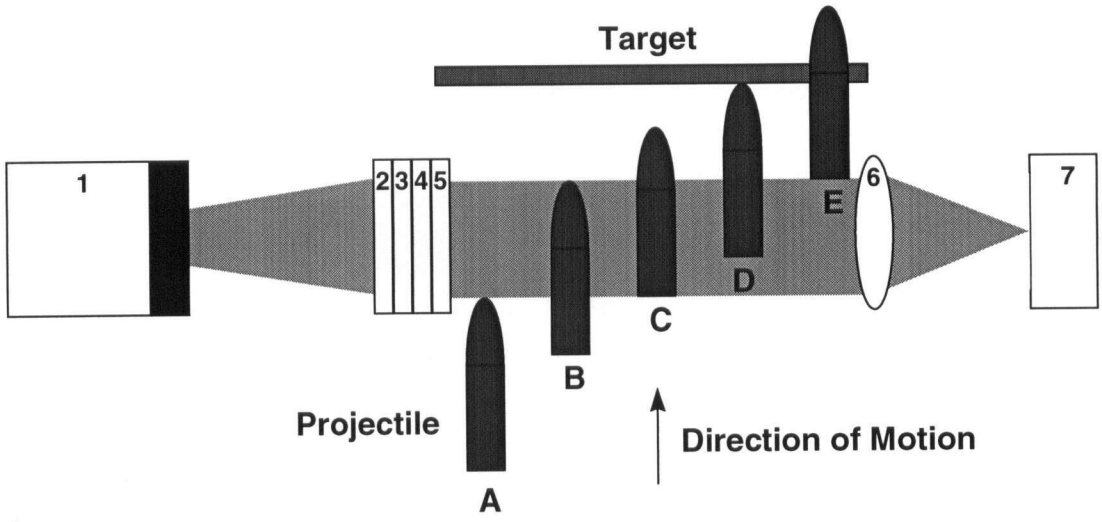

(b)

Figure 4.7: **The ELVS (where 1 is the line laser, 2 is the first cylindrical lens, 3 is the aperture, 4 is the neutral density filter, 5 is the second cylindrical lens, 6 is the collector lens, and 7 is the photodetector). (a) photograph of the system, and (b) schematic showing the principle of operation of the system.**

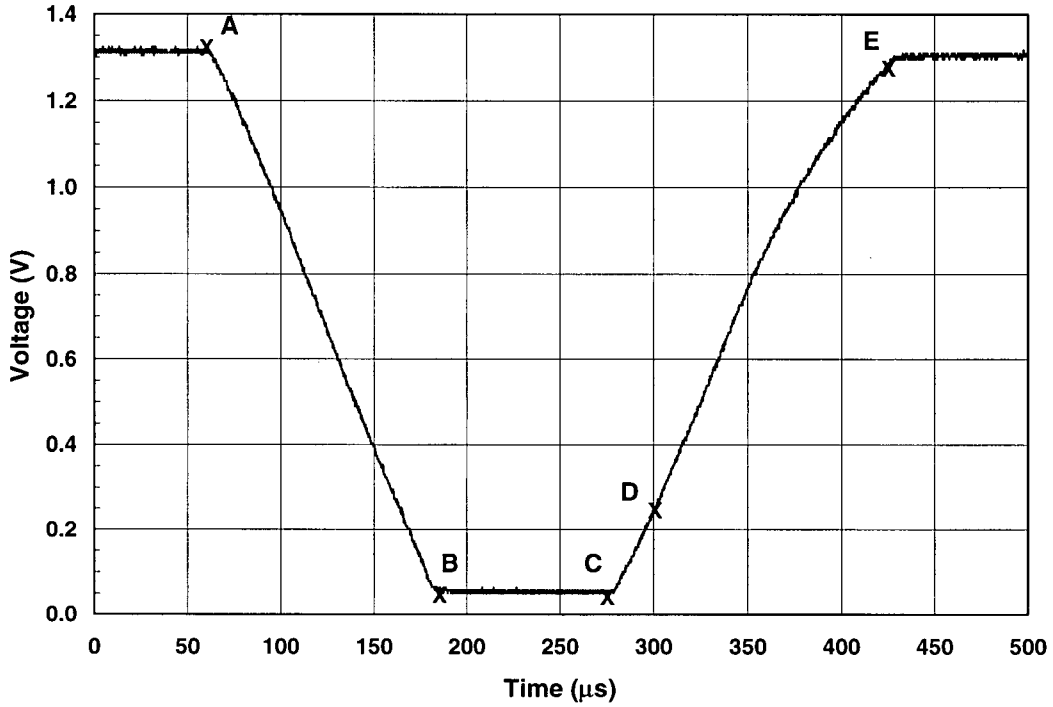

Figure 4.8: **A sample voltage-time curve from a ballistic impact test with points A to E corresponding to points in Figure 4.7(b).**

Chapter Five: Results and Discussion

5.1 Introduction

This chapter presents and discusses the results from all ballistic impact tests performed for this thesis. The ballistic impact response of textile materials is shown to involve both a local and a global deformation mechanism. The size of the fabric deformation resulting from both a perforating and a non-perforating test are compared, and some interesting conclusions regarding energy absorption are presented. A combination of the video camera and the ELVS results is shown to provide a more complete displacement history of the impact event.

5.2 High Speed Video Camera Results

5.2.1 1.1 g (17 grain) Projectiles

A total of 11 tests were performed using the 1.1 g (17 grain) projectiles for which video images were obtained. Only 5 tests, however, will be presented here to provide a representation of the deformation history of a fabric when ballistically impacted by these projectiles. The remaining images are shown in Appendix C. Figures 5.1 and 5.2 show the video images from the ballistic impact of 8-ply Kevlar® targets using the 120° conical and the hemispherical tipped projectiles, respectively. For each projectile, two tests are presented, one in which the projectile perforated the target (a) and one in which the projectile was stopped (b). In Figure 5.1(a), test #C21, the impact velocity, v_s, was 383 m/s. The projectile perforated the target and had a residual velocity, v_r, of 253 m/s. The target absorbed 45 J of energy, or 56 % of the projectile incident energy. In Figure 5.1(b), test #C20, v_s was 325 m/s. The projectile was stopped by the target, and by definition, all of the projectile incident energy (58 J) was absorbed. In Figure 5.2(a), test #H22,

v_s was 383 m/s and v_r was 287 m/s. The target absorbed 35 J, or 44 % of the projectile incident energy. In Figure 5.2(b), test #H25, v_s was 328 m/s and the target absorbed 59 J. An interesting observation can be made by looking at the size of the fabric deformation in Figures 5.1 and 5.2. In image C in Figure 5.1(b), where there is no perforation, the deformation size is greater than in image C of Figure 5.1(a), where the projectile has already perforated the target. The difference in deformation size between a perforating and non-perforating event is even more evident in image C of Figure 5.2, and would imply that the size of the fabric deformation is not an indication of when failure will occur. Furthermore, it is interesting to note in Figures 5.1(b) and 5.2(b), that the material at the point of contact with the projectile appears to actually conform to the shape of the projectile nose.

Figure 5.3 shows the video images obtained from a test using the 1.1 g (17 grain) blunt-tipped projectiles. For this test, #S31, v_s was 378 m/s and the total energy absorbed was 79 J. In all tests performed using the 1.1 g (17 grain) blunt projectiles, the projectiles were stopped by the target.

The images previously presented indicate that there is both a local and a global deformation mechanism which occur during the ballistic impact of fabrics. The local mechanism can be seen in Figures 5.1(b) and 5.2(b), where local deformation at the point of contact of the target material with the projectile is evident. The global mechanism can be seen in the formation of the overall fabric deformation. Energy absorption is greater when there is significant global deformation. The extent of this global deformation, however, appears to be dependent upon the local deformation mechanism. It is this local deformation mechanism, or local straining of the fabric, which "decides" if failure of the material will occur. The local-global deformation response is discussed further in Section 5.2.3.

Figure 5.4 shows a plot of the absorbed energy ($E_{absorbed}$) versus the impact energy (E_s) for all of the ballistic impact tests performed using the 1.1 g (17 grain) projectiles. The general trend of the curves for the hemispherical and 120° conical projectiles are typical of those observed in the literature (see Figure 2.2 in Chapter 2), in which, by definition, $E_{absorbed}$ is equal to E_s up to the point where the projectile perforates the target. This point is known as the ballistic limit of the material, which in this case appears to occur around 59 J, or 327 m/s. After this point, $E_{absorbed}$ decreases with increasing E_s. It has been observed in the literature for different projectile-target systems (Cunniff [1992], Wilde et al [1973]) that after failure of the target occurs, $E_{absorbed}$ first decreases, and then later starts to increase again at higher values of E_s. The reason for this latter behaviour remains unclear, however, a possible explanation could lie within the exchange between the local and global deformation response of the material.

The fabric deformation due to ballistic impact is assumed to be in the shape of a pyramid (Cunniff [1992], Leech *et al.* [1979]), the base of which is shown schematically in Figure 5.5. For each image in which the target deformation was visible, the depth, d, and base, b, shown in Figure 5.5, were measured. These values for the 1.1 g (17 grain) projectile tests are given in Table 5-1.

5.2.2 2.8 g (43 grain) Projectiles

Figure 5.6 shows video images obtained from the ballistic impact tests performed using the 2.8 g (43 grain) blunt projectiles. Test #L2, in which an 8-ply target was impacted, is shown in Figure 5.6(a), and test #L13, in which a 16-ply target was impacted, is shown in Figure 5.6(b). In test #L2, v_s was 341 m/s and the total energy absorbed by the target was 163 J. In test #L13, v_s was 404 m/s and the total energy absorbed was 229 J. In all tests performed using the 2.8 g

projectiles, the projectile was stopped by the target, and therefore, by definition, the target absorbed 100 % of the projectile incident energy. The depth and base measurements of the fabric deformation are given in Table 5-2.

It must be noted that all of the 2.8 g (43 grain) blunt projectiles used in the impact tests experienced some degree of plastic deformation, i.e. mushrooming of the projectile tip. In the two ballistic tests, #L13 and #L16, the projectile experienced both mushrooming and bending. To observe the effect of the projectile deformation on the displacement results, displacement measurements were taken from the video images for both the projectile back-end displacement and the target back-face deformation, where possible. The maximum difference between these two measurements was 2 mm for the 8-ply targets and 5 mm for the 16-ply targets. Both of these values were on the order of the projectile deformation due to mushrooming. It should be noted that the 1.1 g (17 grain) blunt projectiles experienced minimal deformation, whereas the 1.1 g (17 grain) hemispherical and 120° conical projectiles did not experience any deformation.

For the 2.8 g (43 grain) blunt projectile tests, the results of the post-test analysis in which the number of broken yarns in each ply was determined, are given in Tables 5-3 and 5-4 for the 8-ply and 16-ply targets, respectively.

5.2.3 Discussion of Video Camera Results

A common way of presenting data from ballistic impact tests is to show the relationship between the absorbed energy, $E_{absorbed}$, and the impact energy, E_s. As E_s increases, $E_{absorbed}$ increases linearly (by definition) until it reaches the ballistic limit of the material, where it then decreases. As mentioned previously in Section 5.2.1, there appears to be a combined local and global deformation response of textile materials to ballistic impact. An analogy to this local-global

response of the material is a series of two springs, shown in Figure 5.7. The smaller spring is analogous to the local deformation, and involves a small volume of material in contact with the projectile. The larger spring is analogous to the global deformation of the target, and involves a greater volume of material in the deformation process. As shown in this figure, the energy absorbed due to the local mechanism, E_{local}, is significantly smaller than the energy absorbed due to the global mechanism, E_{global}, and therefore, E_{local} is assumed to be negligible. A force is now applied to the springs, representing the target being impacted by the projectile. The total energy absorbed by the target, E_{total}, is absorbed via the global deformation mechanism, i.e., E_{total} is approximately equal to E_{global}. In the spring analogy, the larger spring is stretched (deformed) as a result of the force being applied, while the small spring is unaffected. As the impact energy (the force applied to the spring) increases, it will eventually reach the ballistic limit of the material where perforation occurs (the small spring will eventually break), and therefore, the energy absorbing capability of the global deformation mechanism cannot be utilized. Thus, it would appear as if the maximum value of E_{global} is a function of the local deformation mechanism.

The energy absorbed versus impact energy plot for the tests performed using the 1.1 g (17 grain) projectiles, shown in Figure 5.4, together with the video images in Figures 5.1 and 5.2, clearly support this analogy. Up until a substantial amount of damage (perforation) occurs, the target absorbs all of the projectile incident energy in the formation of the deformation pyramid. At the projectile incident energy where the target fails locally, in perforation, the energy absorption decreases. From these results, it would also appear that the nose shape of the projectile plays a major role in local deformation response, and hence perforation of the fabric.

5.3 ELVS Results

Figure 5.8 shows the results from ballistic impact tests performed on 16-ply Kevlar® targets, where the impact velocity ranged from 359 to 375 m/s. The projectile displacement-time, velocity-time, force-time, force-projectile displacement, and absorbed energy-projectile displacement curves are presented for these tests. In all of the ballistic impact tests performed on 16-ply Kevlar® targets, the projectile was stopped. From the force-projectile displacement curve, the maximum force obtained using the ELVS is found to be approximately 13 to 15 kN. Theoretically, the point at which the force becomes positive should correspond to the impact point. Due to the flexible nature of the target and the presence of unburned gun powder preceding the projectile, however, the point at which the force is positive could only be determined to within ±2 mm. This explains the reason for the slight variation in the curves at the origin of the plot.

Figure 5.9 shows some of the results from ballistic impact tests performed on 8-ply Kevlar® targets. A total of 7 tests were performed on the 8-ply targets, with impact velocities ranging from 267 to 428 m/s. In this chapter, however, only two are shown, one in which the projectile perforated the target and one in which the projectile was stopped. The results of the remaining 5 tests are given in Appendix D. In test UBC #o313, in Figure 5.9, the projectile perforated the target with a v_s of 428 m/s. In test UBC #n282, v_s was 267 m/s and the projectile was stopped. The projectile displacement-time, velocity-time, force-time, force-projectile displacement, and absorbed energy-projectile displacement curves are shown for both tests.

The force-projectile displacement results for all of the 8-ply targets are plotted onto one curve, shown in Figure 5.10. As in the case with the 16-ply targets, the point at which the force is

positive could only be determined to within ±2 mm due to the flexible nature of the target and the presence of unburned gun powder preceding the projectile. From Figure 5.10, the maximum force is approximately 10 to 12 kN. The absorbed energy-projectile displacement curves are also plotted onto one graph, shown in Figure 5.11.

The results of the post-test analysis, in which the number of broken yarns in each ply was determined, are given in Tables 5-3 and 5-4 for the 8-ply and 16-ply targets, respectively.

5.3.1 Discussion of ELVS Results

Observation of the force-projectile displacement curves in Figure 5.10 reveals some interesting information about the ballistic response of the 8-ply targets. In the early stages of the impact event, the target responds in a linear behaviour, shown by the linearity of the initial part of the force-displacement curves. Once the curve reaches a peak value (10 to 12 kN), however, the force begins to decrease. In all the tests, with the exception of UBC #n272 and UBC #o313, the targets sustained very little damage in the form of broken yarns. Thus, the decrease in the force after the peak value could be attributed to slippage (pull-in) of the yarns at the boundaries, and/or a loss of elasticity of the target due to the formation of the deformation pyramid. In test UBC #o313, in which the projectile perforated the target, the peak force remains approximately constant over a displacement range of 2 mm. This plateau region might be associated with the force required to perforate each ply. It is interesting to note that the 2 mm of projectile displacement over which the force is observed to be constant correlates well with the overall thickness of the target. This observation is consistent with an observation made by Prosser [1988], in which he noted that the work required to perforate each of the interior plies of a 12-ply nylon target was approximately constant.

In the impact tests in which the target sustained minimal damage and the projectile was stopped, the values for the maximum energy absorbed in the measurable range, or "measurement window", of the ELVS are within 4 to 14 J of the projectile incident energy. The measurement window of the ELVS is equal to the width of the laser sheet, or approximately 25 mm. The maximum absorbed energy values for these tests do not reach the values of projectile incident energy, as expected, because the projectile leaves the measurement window before the event is over. In test #n272, shown with all of the 8-ply tests in Figure 5.11, the target sustained a substantial amount of damage before the projectile was stopped (5 plies were perforated). The energy absorbed increases to a value of 120 J, and remains somewhat constant at this value before increasing again to a value of approximately 159 J. After this point, the fabric has deformed to an extent such that the projectile has left the measurement window of the ELVS, and thus the measurements do not reach the projectile incident energy of 188 J. In test UBC #o313, only 126 J of energy was absorbed before the projectile perforated the target.

5.4 Comparison of the ELVS and Video Camera Displacement Results

In the ELVS ballistic impact tests using the 2.8 g (43 grain) blunt cylindrical projectiles, the targets deformed significantly compared to the measurement window of the ELVS, as mentioned in the previous section. For this reason, in most tests the system was not able to measure the projectile motion during the latter stages of the impact event, i.e., beyond 25 mm of displacement. The pictures obtained using the high speed video camera, however, were in most cases taken in the latter stages of impact, i.e. beyond 25 mm of displacement. By combining the results from both the ELVS and video camera, a more complete displacement history of the impact event was obtained.

The ELVS results for the 16-ply target tests are plotted with the video image results obtained for similar test conditions (same number of plies and impact velocities), and are shown in Figure 5.12. For these tests, the ELVS projectile displacement results (specifically UBC #d121 and UBC #d122) are lower than the video image results. In addition to the fact that the impact velocities in these tests were slightly lower than those obtained in the video camera tests, a possible reason for the difference in the displacement results is due to the overall stiffness of the target as a result of the clamping pressure. In the tests performed using the ELVS, the 16-ply targets could be clamped quite tightly due to the nature of the test fixture used, and thus the target was reasonably stiff. In the test fixture used with the video camera, it was physically more difficult to obtain a significant amount of clamping with the thick 16-ply targets, resulting in a target that was more loosely held. This problem did not occur with the 8-ply targets, as they could be clamped tightly in both test fixtures. To confirm this effect with the 16-ply targets, a test (UBC #j201) was performed with the ELVS in which the clamping pressure on the target was slightly less than that in the initial two impact tests. From the results of this test, also shown in Figure 5.12, it appears as if the stiffness of the target as a result of the clamping pressure could be a possible reason for the difference in results. However, more tests should be performed at even lower levels of clamping pressure to further investigate this effect.

The results for the 8-ply target tests are shown in Figures 5.13 to 5.16. It is apparent from these plots that there is good agreement between the ELVS and video image results.

5.5 Energy Absorbing Mechanisms

For the 2.8 g projectile tests in which video images were obtained, energy calculations were performed to determine how energy is being absorbed during a ballistic impact event. As

mentioned previously, the fabric deformation is assumed to form in the shape of a pyramid. The mechanisms which are assumed to contribute to the absorption of energy are the kinetic energy of the deformation pyramid, the strain energy in the deformation pyramid, and the energy to deform the projectile. In some tests, however, the projectile deformation was minimal.

5.5.1 Energy Absorbed by Target

When the projectile does not deform, the total energy absorbed by the target, $E_{absorbed}$, is found from:

$$E_{absorbed} = E_K + U \tag{5.1}$$

where E_K and U are the kinetic energy of the deformation pyramid and strain energy in the pyramid, respectively. Assuming that the material in the pyramid is moving at the same velocity as the projectile (Smith *et al.*, [1963]; Laine and Vähäkangas [1996]), E_K is found using:

$$E_K = \tfrac{1}{2} \cdot m_{pyramid} \cdot v_p^2 \tag{5.2}$$

where $m_{pyramid}$ is the mass of the material in the pyramid and v_p is the velocity of the projectile at any time. The mass of the deformation pyramid is found from:

$$m_{pyramid} = A_{surface} \cdot \rho_{areal} \cdot \eta \tag{5.3}$$

where $A_{surface}$ is the surface area of the deformation pyramid (in units of m^2), ρ_{areal} is the areal density of the material (having a value of 204 kg/m^2 for the Kevlar® 129 used), and η is the number of plies in the target (8 or 16). Referring to Figure 5.5, the surface area, $A_{surface}$, for the whole deformation pyramid is:

$$A_{surface} = \frac{1}{2} \cdot \frac{b}{\sqrt{2}} \cdot h \cdot 4 \tag{5.4}$$

where b is measured directly from the video images, and h is calculated from simple geometry and is found to be:

$$h = \sqrt{\frac{b^2}{8} + d^2} \tag{5.5}$$

where d is the depth of the deformation pyramid. The deformation pyramid base and depth measurements for the 2.8 g (43 grain) projectile tests, given in Table 5.2, are plotted onto a curve of base versus depth, shown in Figure 5.17. A linear relationship exists between the two measurement values, and thus b (and therefore, h) can be defined in terms of d.

The strain energy in the pyramid, U, is defined as:

$$U = \frac{1}{2} \cdot E \cdot \varepsilon^2 \cdot A_{surface} \cdot T \tag{5.6}$$

where E is the dynamic elastic modulus of the yarns in the fabric (96 GPa for the Kevlar® 129 used here (Pageau [1997])), ε is the strain in the pyramid, and T is the thickness of the target (2 mm for a 8-plies and 4 mm for 16-plies). It should be noted that the yarn modulus used in these calculations is the modulus determined at high strain rates (~1000 s^{-1}). The strain rates encountered in the impact tests for this thesis are on the order of 500 to 1000 s^{-1}, and thus the use of the dynamic elastic modulus is valid.

When the target does not sustain any damage and the projectile does not experience any deformation, it is reasonable to assume that the energy balance for the impact event is:

$$E_s = \frac{1}{2} \cdot \left(m_p + m_{pyramid}\right) \cdot v_p^2 + U \tag{5.7}$$

where E_s is the projectile incident energy and m_p is the projectile mass.

The strain in the pyramid is found by first finding the strain in a single yarn running through the deformation pyramid, and then integrating this to find the strain in the whole pyramid. Using Figure 5.18, the length of a strained yarn, l, in the pyramid is found to be:

$$l = L - 2 \cdot x + 2 \cdot x \cdot \sqrt{1 + \frac{4 \cdot d^2}{b^2}} \tag{5.8}$$

where L is the initial length of the yarn (in this case, L was 0.33 m) and x denotes the position of the yarn in the pyramid, as shown in Figure 5.18. The strain in this yarn, ε_{yarn}, is found to be (Smith [1956]):

$$\varepsilon_{yarn} = \frac{l - L}{L} = \frac{\left(L - 2 \cdot x + 2 \cdot x \cdot \sqrt{1 + \frac{4 \cdot d^2}{b^2}}\right) - L}{L} \tag{5.9}$$

The actual value for the strain in the pyramid is not known, and thus, as a first approximation, the strain in the pyramid is assumed to be constant and equal to the maximum strain of a yarn (the maximum strain occurs in a yarn passing through the apex of the pyramid, hence $x = \frac{b}{2}$). Substituting the known values into Equation 5.9, and putting all variables in terms of d, the strain in the pyramid is found to be:

$$\varepsilon = 1.8 \cdot d \tag{5.10}$$

Substituting Equation 5.10 into 5.6, and then using Equations 5.6 and 5.7, values for v_p are found for a range of pyramid depths, which are then used in Equation 5.2 to determine the kinetic energy. The strain and kinetic energy values are used to determine the total energy absorbed (Equation 5.1) for a range of pyramid depths. The values of absorbed, kinetic and strain energies predicted using the previous equations, as well as experimental results, are shown in Figures 5.19 and 5.20 for the 8-ply and 16-ply targets, respectively. From these figures, the simple mathematical model described above appears to reasonably predict the energy absorbed by the target in most of the tests.

5.5.2 Energy to Deform Projectile

In all tests performed using the 2.8 g (43 grain) blunt cylindrical projectiles, the projectiles experienced some degree of "mushrooming" at the projectile tip. The equation used to determine the energy required to deform the projectiles in this manner, assuming that the projectile material is rigid, perfectly-plastic, is:

$$E_{mushroom} = V_p \cdot \sigma_y \cdot \varepsilon_p \tag{5.11}$$

where V_p is the volume of the deformed part of the projectile, σ_y is the yield strength of the projectile material (Aluminum 6061-T6, taken to be 250 MPa), and ε_p is the strain of the projectile as a result of deformation. In the 8-ply tests, the average value of $E_{mushroom}$ was 4 % of the projectile incident energy. For the 16-ply tests, the average value of $E_{mushroom}$ was 12 % of the projectile incident energy.

In two of the 16-ply impact experiments performed using the video camera, #L13 and #L16, the projectile also experienced bending. By assuming that a segment of the projectile rotates about a plastic hinge, the energy required to bend the projectile, E_{bend}, is found using:

$$E_{bend} = \mathrm{M}_{bend} \cdot \theta_{bend} \tag{5.12}$$

where M_{bend} is the fully plastic bending moment and θ_{bend} is the bend angle. The bending moment is found using:

$$M_{bend} = \sigma_y \cdot \frac{4r^3}{3} \tag{5.13}$$

where r is the radius of the projectile. The energy absorbed in bending the projectiles was found to be minimal (an average value of 2 % of the projectile incident energy).

5.6 Discussion of Results

The predictions of energy absorption made by the simple mathematical model, presented with experimental results in Figures 5.19 and 5.20, appear to be in very reasonable agreement. It is interesting to note from these figures that initially in the impact event, most of the energy is absorbed in the form of kinetic energy of the pyramid. As the pyramid depth increases, however, the kinetic energy reaches a peak value and then decreases to a value of zero as the projectile comes to a stop. The strain energy increases slowly in the initial stages of the impact event, but as the pyramid depth increases, the strain energy increases very quickly. Thus, it would appear that the "first approximation" of the strain in the pyramid and the simple assumptions made in the energy calculations were very reasonable. It is interesting to note in Figure 5.20, for test UBC #j201, that the predicted results appear to be offset from the experimental results. As

mentioned previously, the clamping pressure for this test was reduced, and the difference between the two curves is most likely due to the slackness of the target.

Figure 5.21 shows the $E_{absorbed}$ versus E_s relationship for the tests performed on the 8-ply targets using the ELVS. The upper curve shows (by definition) the energy absorbed by the target when the projectile is stopped. The lower curve shows the maximum energy absorbed within the measurement window of the ELVS, and represents the energy absorbed at approximately 25 mm of displacement (i.e., the curve for a deformation pyramid with a depth of 25 mm). Once again, the same trend as seen in Figure 5.4 is observed. The $E_{absorbed}$ versus E_s relationship for a range of pyramid depth values for the same tests as in Figure 5.21 are plotted in Figure 5.22. It is interesting to note from both Figure 5.21 and 5.22 that in a test where the projectile is stopped, the majority of the energy has been absorbed in the first 25 mm of displacement. When referring to the images obtained from the video camera experiments (Figure 5.6), the deformation continues to grow significantly beyond 25 mm and it would appear as if a substantial amount of energy is still being absorbed. When these observations are combined with the information obtained from the ELVS, however, it becomes more apparent that the deformation growth in the latter stages of the impact event is not a result of the projectile energy being absorbed, but is a result of the energy that has already been absorbed by the target being re-distributed.

5.7 Summary

The following results were presented in this chapter:

1. Energy absorption in ballistically impacted fabrics involves both a local and global deformation response. The local response encompasses the local deformation of the fabric in direct contact with the projectile, and dictates if failure of the fabric will occur. The

global response involves the global deformation of the fabric and is manifested in the formation of the deformation pyramid. The bulk of the energy absorbed by the target appears to occur via the global deformation mechanism, however the *maximum* value of energy absorbed by the global mechanism is a function of the local response.

2. It would appear that the nose shape of the projectile plays a major role in local deformation response, and hence perforation of the fabric.

3. The maximum force attained within the measurement window of the ELVS is 10 to 12 kN for the 8-ply targets, and 13 to 14 kN for the 16-ply targets.

4. Fabrics appear to behave linearly up to the point at which the maximum force is attained.

5. Combination of the results obtained from the video camera images and the ELVS provides a more complete history of the impact event.

6. The combined video camera and ELVS results for the 16-ply targets indicate that the clamping pressure does influence the impact response of the target, as more tightly clamped targets are stiffer, resulting in a lower degree of deformation within a certain time.

7. The energy absorbed in deforming the aluminum projectiles was minimal for the 8-ply tests (an average of 4 % of the incident energy) but increased to an average of approximately 12 % for the 16-ply targets. The energy absorbed in bending the projectiles was negligible (2 % of the projectile incident energy).

8. For non-perforating impacts, a large part of the projectile incident energy is absorbed by the target during the first 25 mm of displacement. Substantial growth of the deformation

pyramid beyond this occurs due to a re-distribution of the energy that has already been absorbed by the material.

9. The simple mathematical model used to predict the total energy absorbed, the strain and the kinetic energy, in both 8 and 16-ply targets when impacted by 2.8 g (43 grain) blunt projectiles, is shown to be a very reasonable approximation.

10. Energy absorption in fabrics appears to be initially in the form of kinetic energy, which reaches some peak value before it starts to decrease. The energy absorption in the form of strain energy increases very slowly at the beginning, but as the kinetic energy decreases, the strain energy increases quickly.

Table 5-1: Measurements taken from video images of 1.1 g projectile tests (where Test #C, H and S correspond to tests using the 120° conical, hemispherical, and blunt projectiles, respectively).

Test	Image	v_s (m/s)	v_r (m/s)	Time after impact (μs)	Depth, d (mm)	Base, b (mm)	E_s (J)	$E_{absorbed}$ (J)
#C19	B	325	---	149	20	65	58	58
	C			299	23	96		
	D			449	25	115		
#C20	B	325	---	149	18	68	58	58
	C			299	21	80		
	D			449	21	94		
#C21	B	383	253	131	20	66	81	45
	C			281	21	77		
	D			431	22	85		
#H22	B	383	287	131	13	48	81	35
	C			281	14	66		
	D			431	15	73		
#H23	B	360	293	121	9	32	71	24
	C			271	11	50		
	D			421	13	70		
#H25	A*	328	---	0	6	15	59	59
	B			150	19	58		
	C			300	25	74		
	D			450	28	88		
#H26	B	324	---	179	21	66	58	58
	C			349	25	82		
	D			549	27	105		
#S28	B	329	---	108	17	44	59	59
	C			158	19	56		
	D			208	21	58		
#S29	A*	357	---	0	12	30	70	70
	B			179	25	59		
	C			349	29	85		
	D			549	32	100		
#S31	A*	378	---	0	18	53	79	79
	B			179	28	85		
	C			349	31	104		
	D			649	31	127		
#S32	A*	398	---	0	21	62	87	87
	B			179	30	80		
	C			349	32	102		
	D			749	31	134		

* indicates the tests in which image A was used as the reference for determining time after impact.

Table 5-2: Measurements taken from video images of 2.8 g projectile tests (where test #L1 to #L5 are for 8-ply targets, and test #L12 to #L16 are for 16-ply targets).

Test	Image	v_s (m/s)	Time after impact (μs)	Depth, d (mm)	Base, b (mm)	E_s (J)
#L1	C	278	79	14	51	108
	D		479	34	108	
#L2	B	341	67	14	44	163
	C		237	29	74	
	D		637	43	130	
#L3	B	341	167	23	67	163
	C		337	30	90	
	D		737	35	133	
#L4	B	343	167	24	76	165
	C		337	34	98	
	D		737	39	122	
#L5	B	303	180	24	69	129
	C		350	32	95	
	D		750	38	136	
#L12	D	401	90	20	56	225
#L13	B	404	58	16	48	229
	C		138	25	92	
	D		218	30	99	
#L14	B	397	80	18	66	221
	C		180	25	80	
	D		280	30	96	
#L15	D	431	263	34	90	260
#L16	C	459	174	24	85	
	D		324	31	90	295

Table 5-3: Results from post-test analysis performed on the 8-ply targets from both video camera and ELVS, for the 2.8 g (43 grain) blunt projectile tests.

Test	UBC #o291	UBC #o311	#L4	UBC #n272	UBC #o313
v_s (m/s)	314	340	343	366	428
Target	8-ply	8-ply	8-ply	8-ply	8-ply
# Broken Yarns in Ply:					
#1	8.75	10.00	7.75	11.25	10.50
#2	1.75	--	--	10.50	10.25
#3	--	--	--	9.50	10.25
#4	--	--	--	8.75	10.50
#5	--	--	--	6.25	9.00
#6	--	--	--	--	8.00
#7	--	--	--	--	7.75
#8	--	--	--	--	6.25
Total Broken Yarns	10.50	10.00	7.75	46.25	72.50

Table 5-4: Results from post-test analysis performed on the 16-ply targets from both video camera and ELVS, for the 2.8 g (43 grain) blunt projectile tests.

Test	UBC #j201	#L14	#L13	#L16
v_s (m/s)	364	397	404	459
Target	16-ply	16-ply	16-ply	16-ply
# Broken Yarns in Ply:				
#1	7.75	8.50	11.00	11.50
#2	--	--	8.50	9.00
#3	--	--	7.75	8.00
#4	--	--	5.00	8.00
#5	--	--	--	8.00
#6	--	--	--	7.75
#7	--	--	--	--
#8	--	--	--	--
...	--	--	--	--
#16	--	--	--	--
Total Broken Yarns	7.75	8.50	32.25	52.25

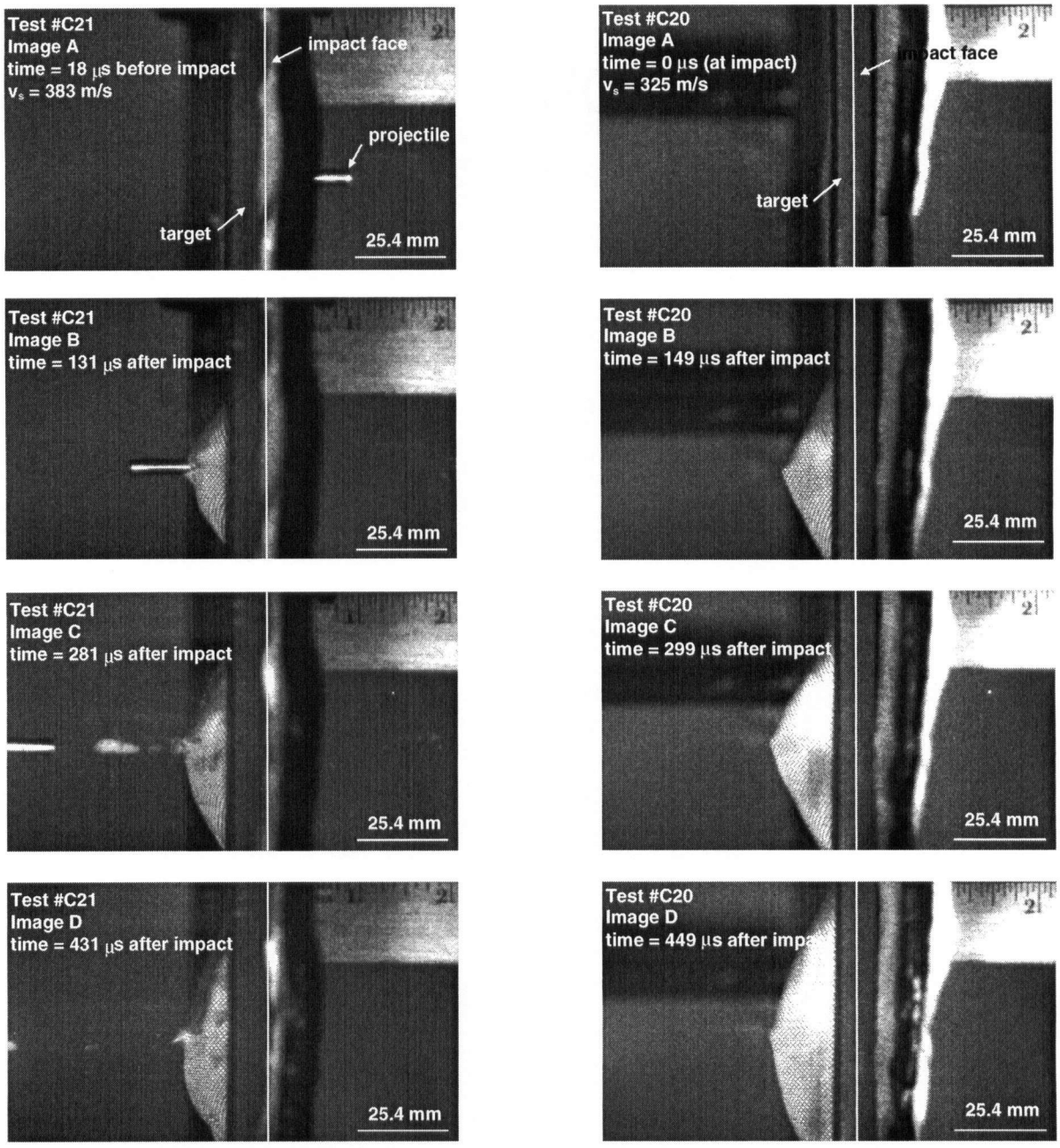

(a) (b)

Figure 5.1: **Video images showing ballistic impact of an 8-ply Kevlar® target by a 1.1 g aluminum projectile with 120° conical tip, where (a) is a test where the projectile perforated the target, v_s = 383 m/s and v_r = 253 m/s; and (b) is a test where the projectile was stopped, v_s = 325 m/s and v_r = 0 m/s.**

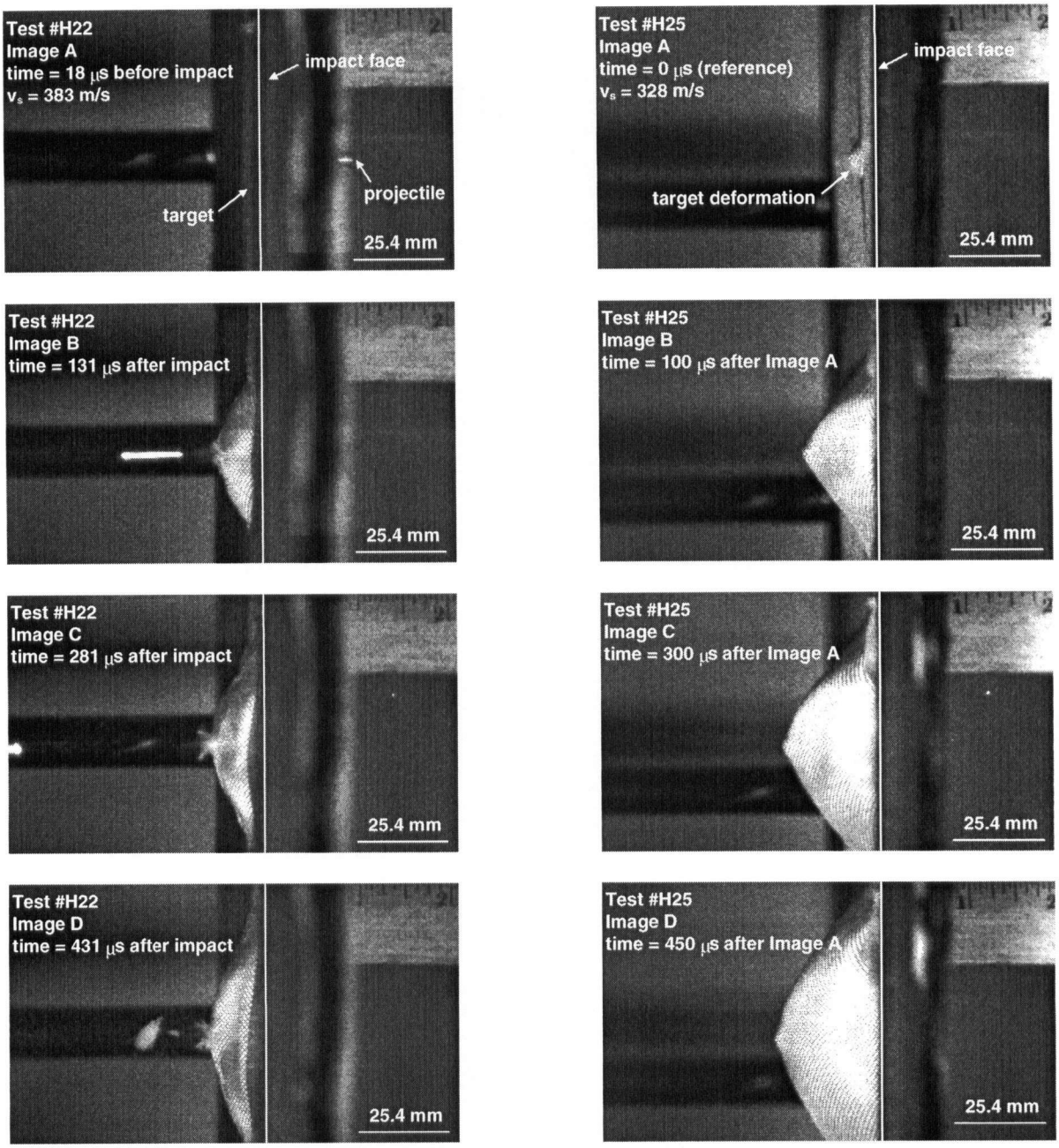

(a) (b)

Figure 5.2: **Video images showing ballistic impact of an 8-ply Kevlar® target by a 1.1 g aluminum projectile with hemispherical tip, where (a) is a test where the projectile perforated the target, v_s = 383 m/s and v_r = 287 m/s; and (b) is a test where the projectile was stopped, v_s = 328 m/s and v_r = 0 m/s.**

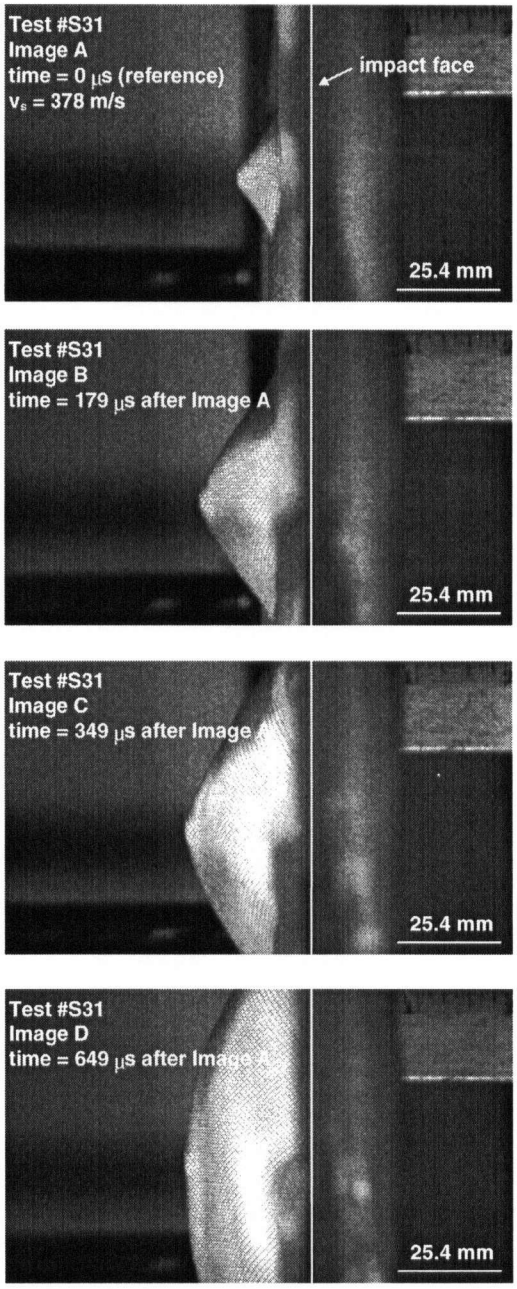

Figure 5.3: **Video images showing ballistic impact of an 8-ply Kevlar® target by a 1.1 g aluminum projectile with blunt tip, v_s = 378 m/s. In this test, the projectile was stopped.**

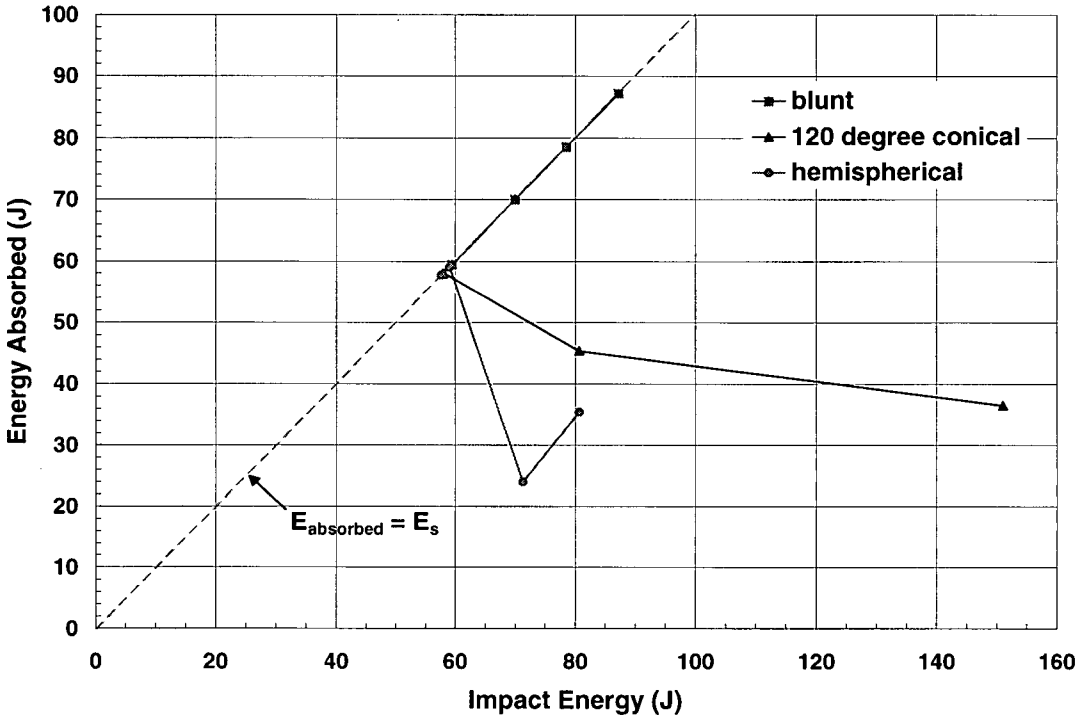

Figure 5.4: **Plot of the relationship between the absorbed energy ($E_{absorbed}$) and the impact energy (E_s) for the 1.1 g aluminum projectiles.**

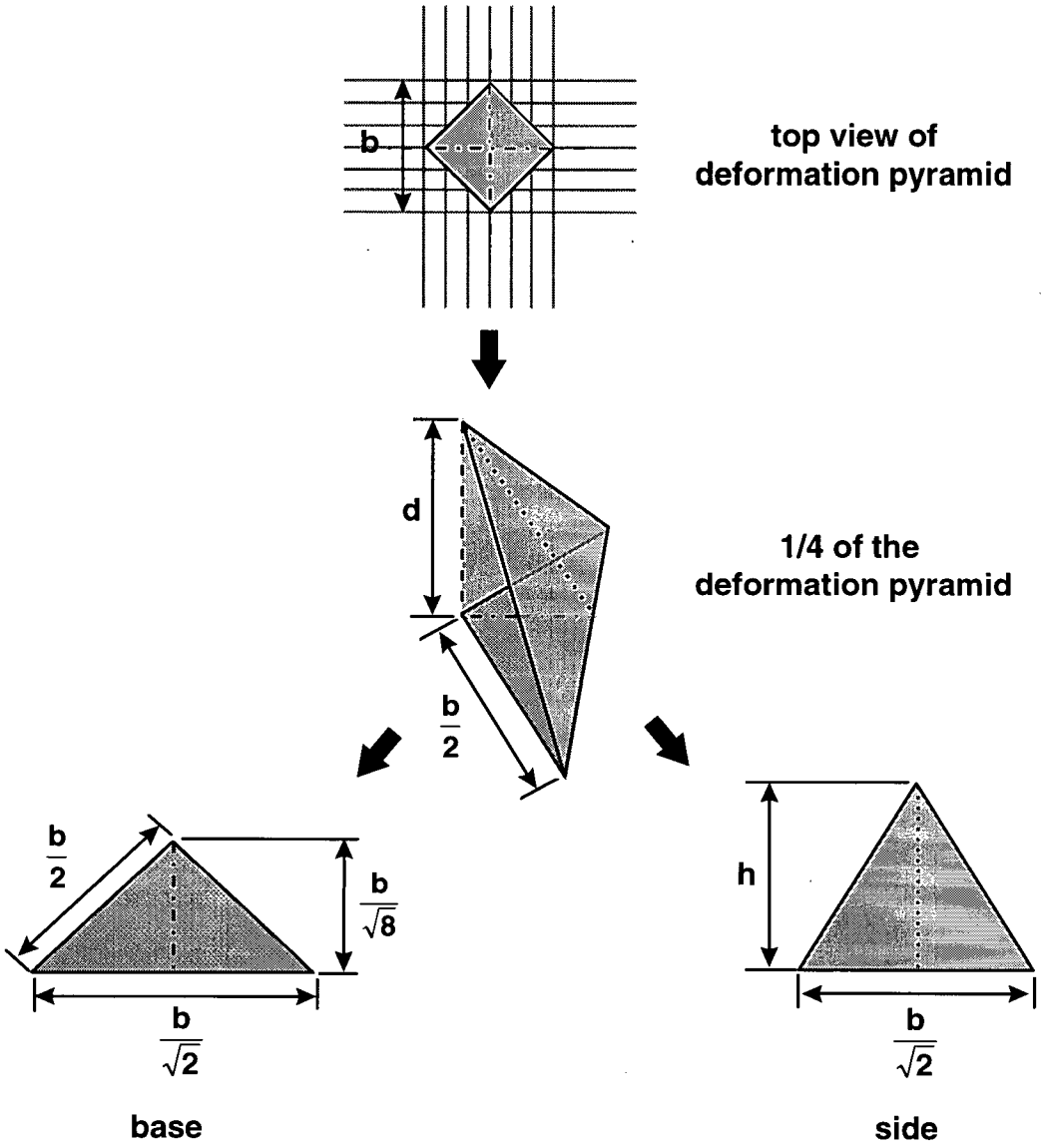

Figure 5.5: Schematic showing the fabric deformation (assumed to be a pyramid) and the measurements of the deformation pyramid used in the energy calculations.

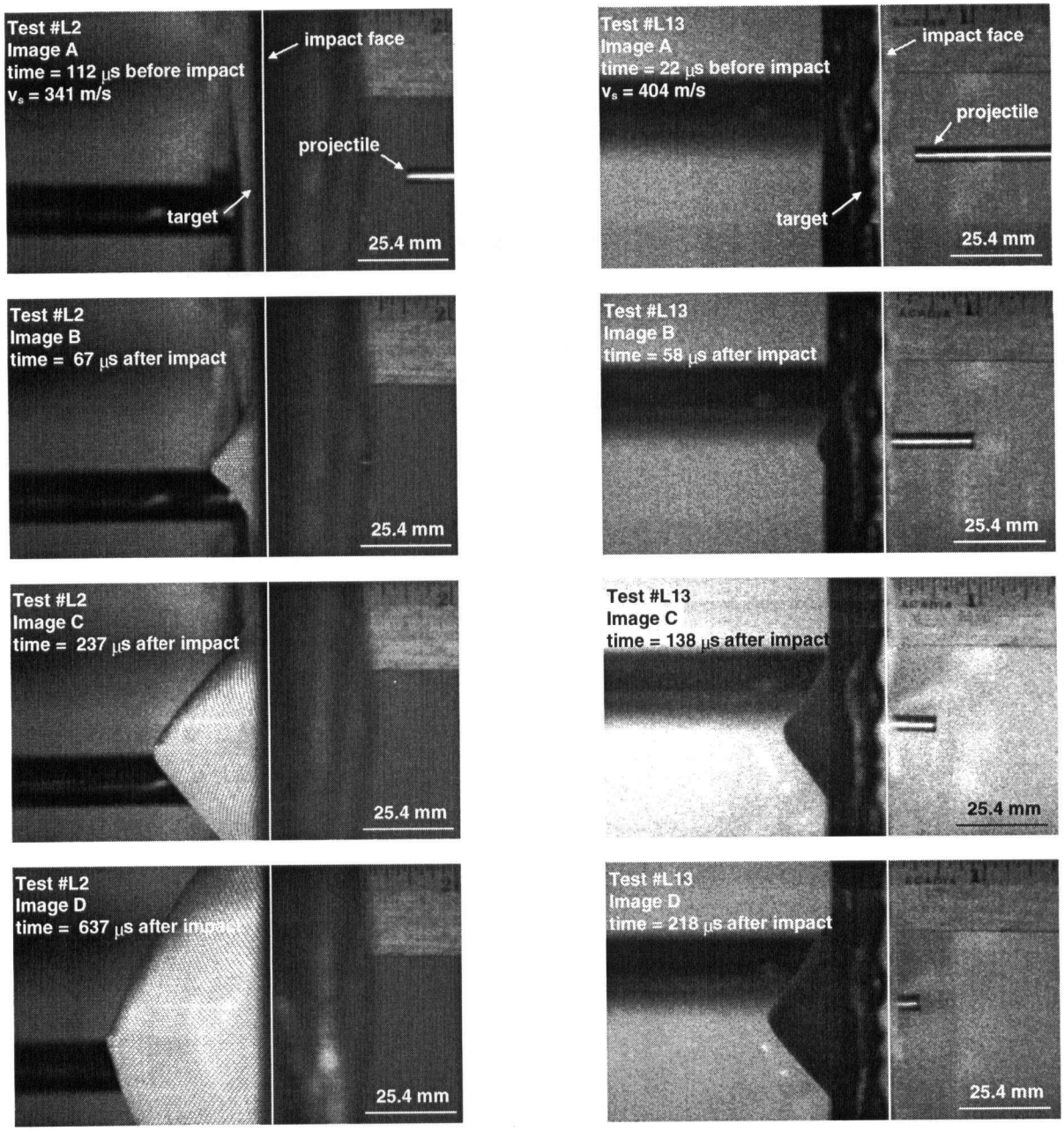

Figure 5.6: **Video images showing ballistic impact of (a) an 8-ply Kevlar® target, vs = 341 m/s; and (b) a 16 ply-Kevlar® target, vs = 404 m/s, by a 2.8 g blunt aluminum projectile. In both tests, the projectile was stopped.**

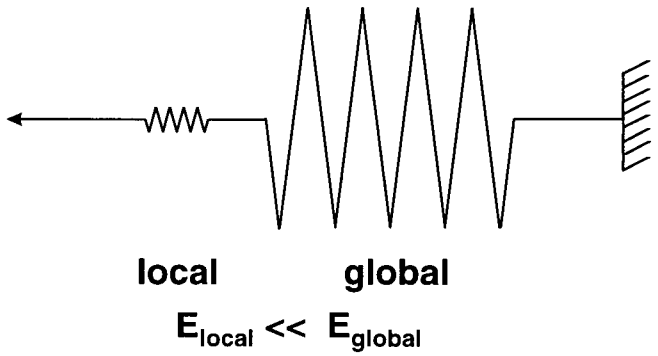

Figure 5.7: Analogy of springs in series to represent the local and global response of a ballistically impacted fabric.

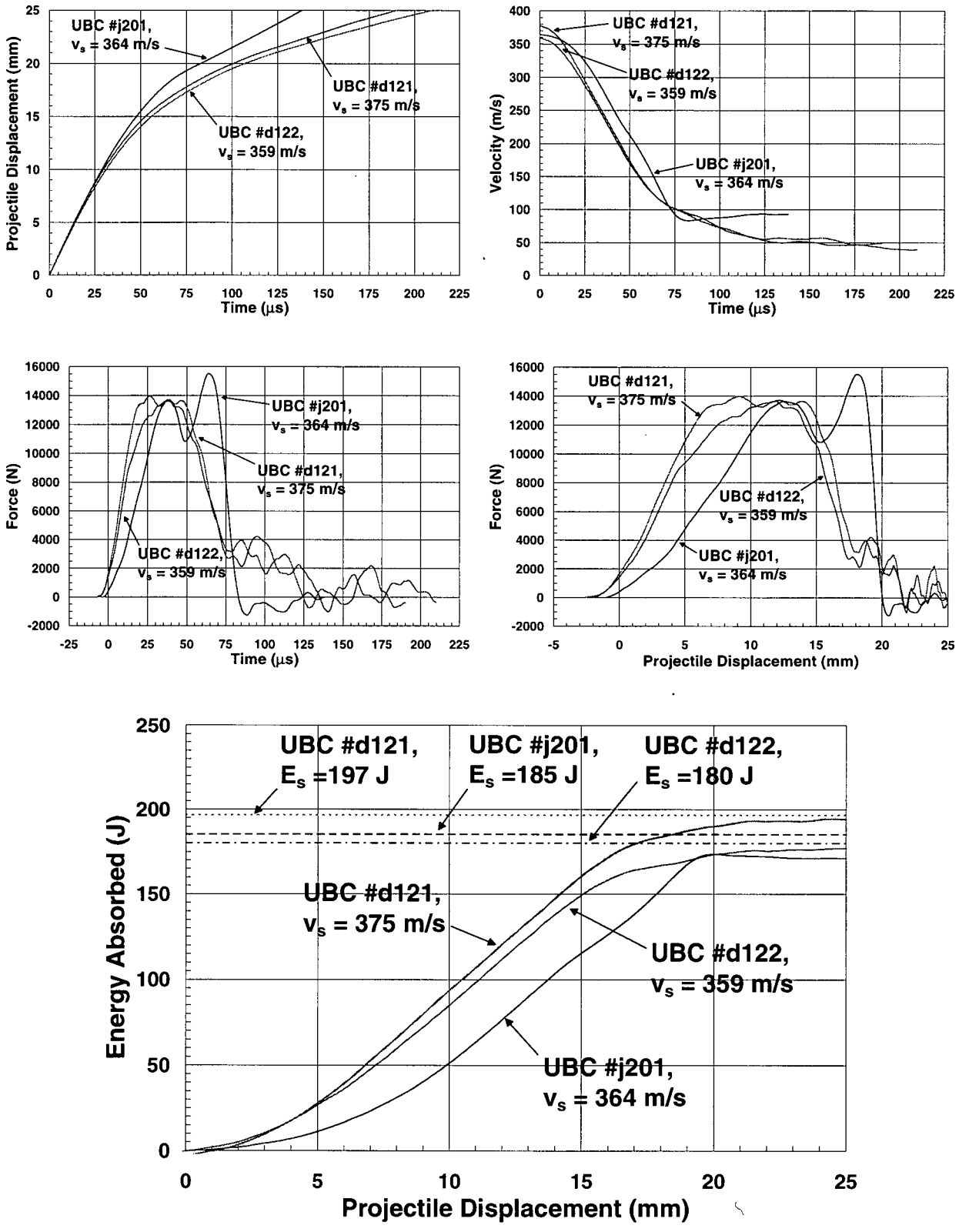

Figure 5.8: **ELVS results for the 16-ply targets impacted by 2.8 g (43 grain) blunt cylindrical projectiles.**

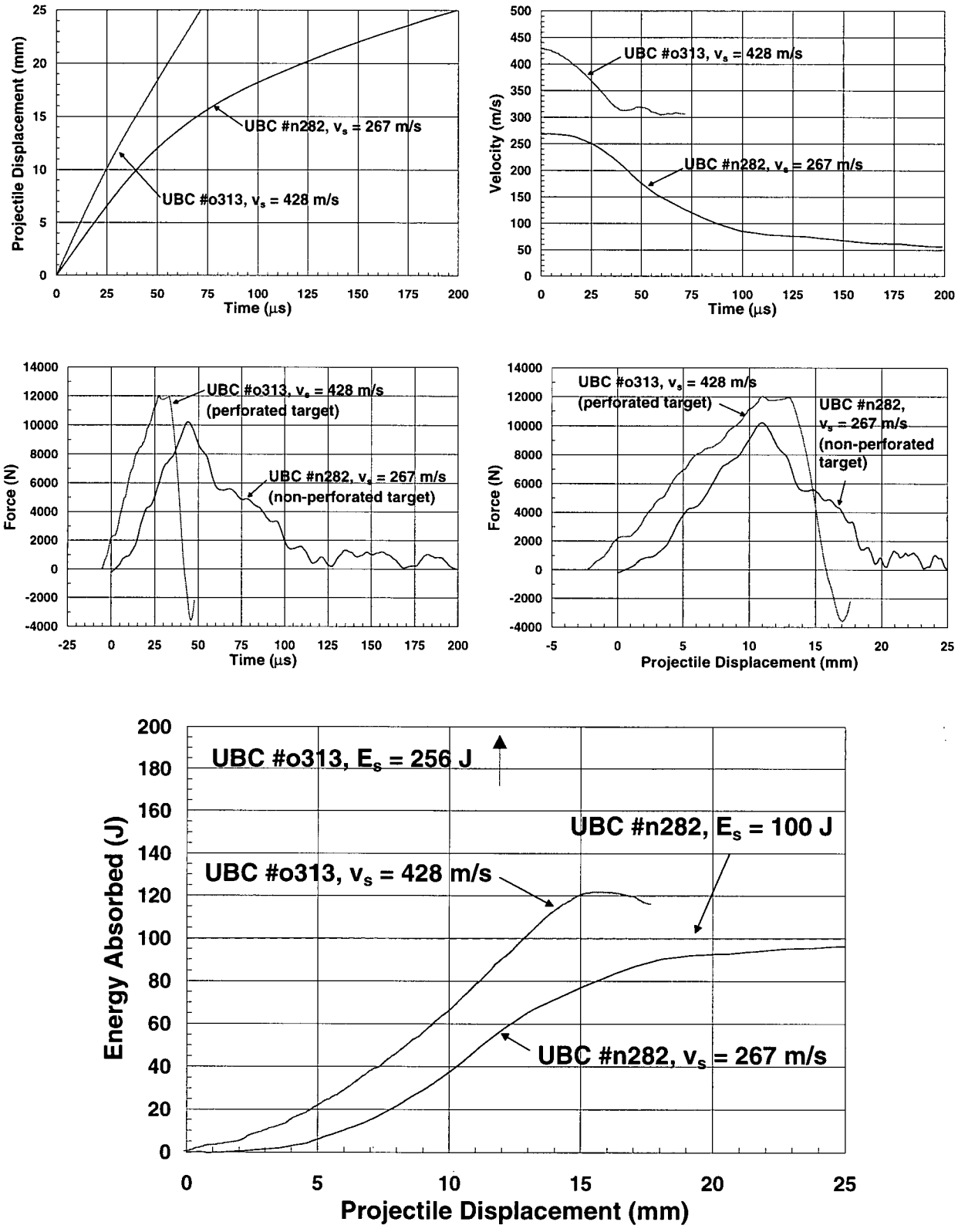

Figure 5.9: **ELVS results for two of the 8-ply targets impacted by 2.8 g (43 grain) blunt cylindrical projectiles. In UBC #o313, the projectile perforated the target and in UBC #n282, the projectile was stopped.**

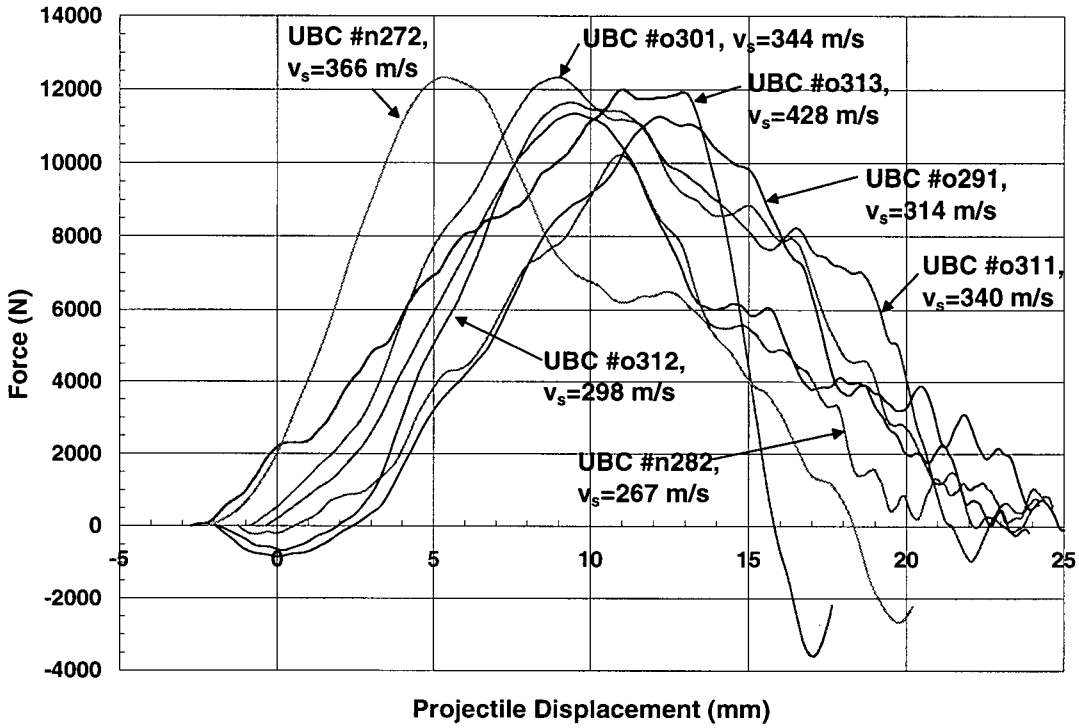

Figure 5.10: Force versus projectile displacement for all of the 8-ply targets impacted by 2.8 g (43 grain) blunt cylindrical projectiles.

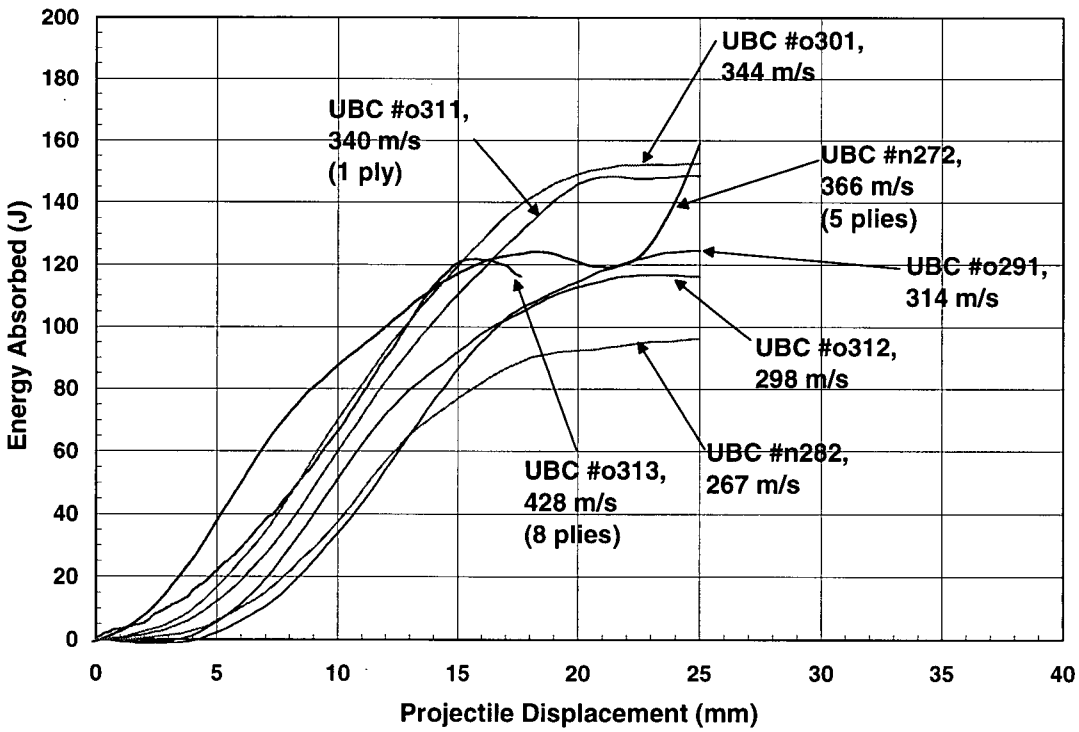

Figure 5.11: Energy absorbed versus projectile displacement for all of the 8-ply targets impacted by 2.8 g (43 grain) blunt cylindrical projectiles.

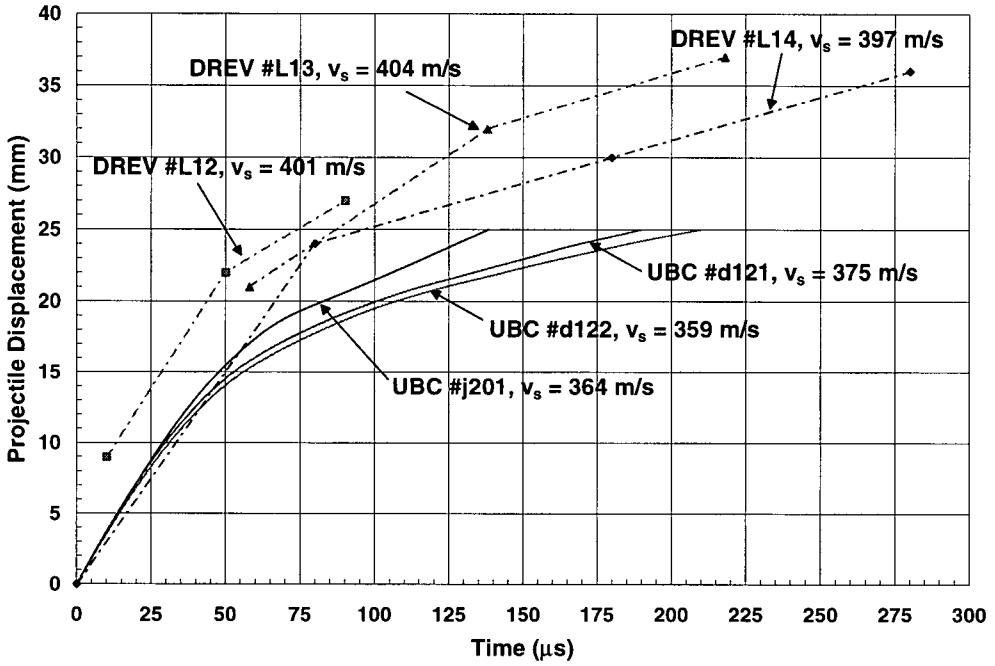

Figure 5.12: Comparison of video camera and ELVS displacement-time results for 16-ply Kevlar® 129 targets.

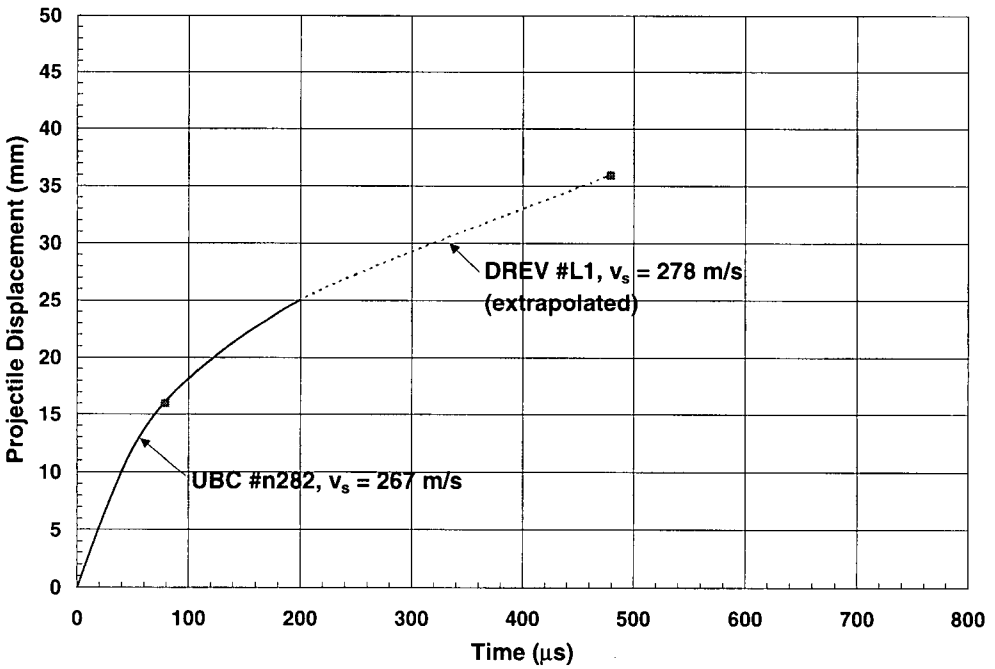

Figure 5.13: Comparison of video camera (DREV #L1) and ELVS (UBC #n282) displacement-time results for 8-ply Kevlar® 129 targets.

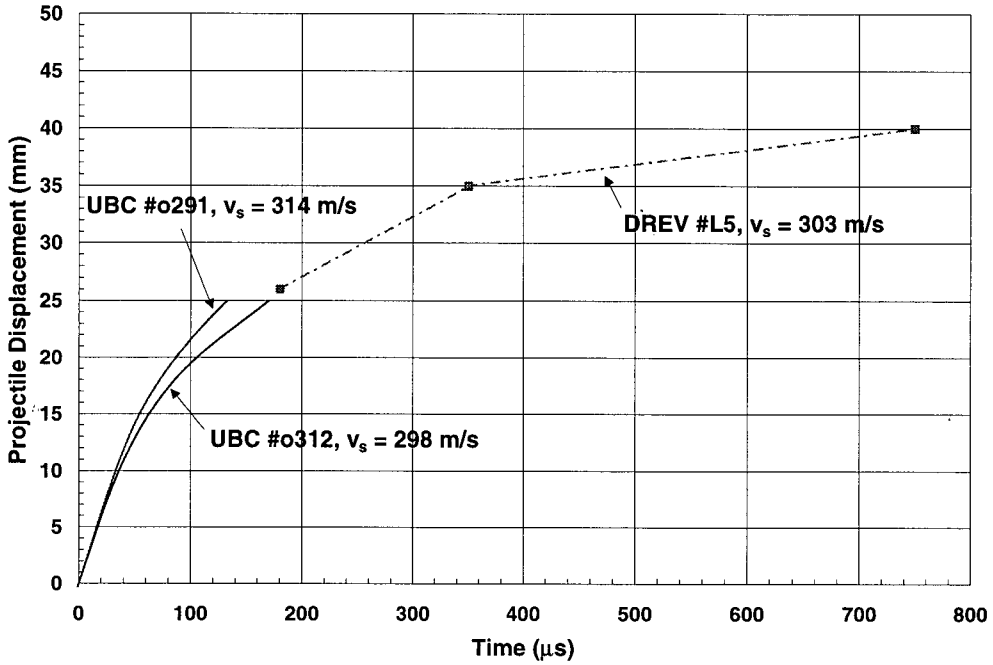

Figure 5.14: Comparison of video camera (DREV #L5) and ELVS (UBC #o291 and #o312) displacement-time results for 8-ply Kevlar® 129 targets.

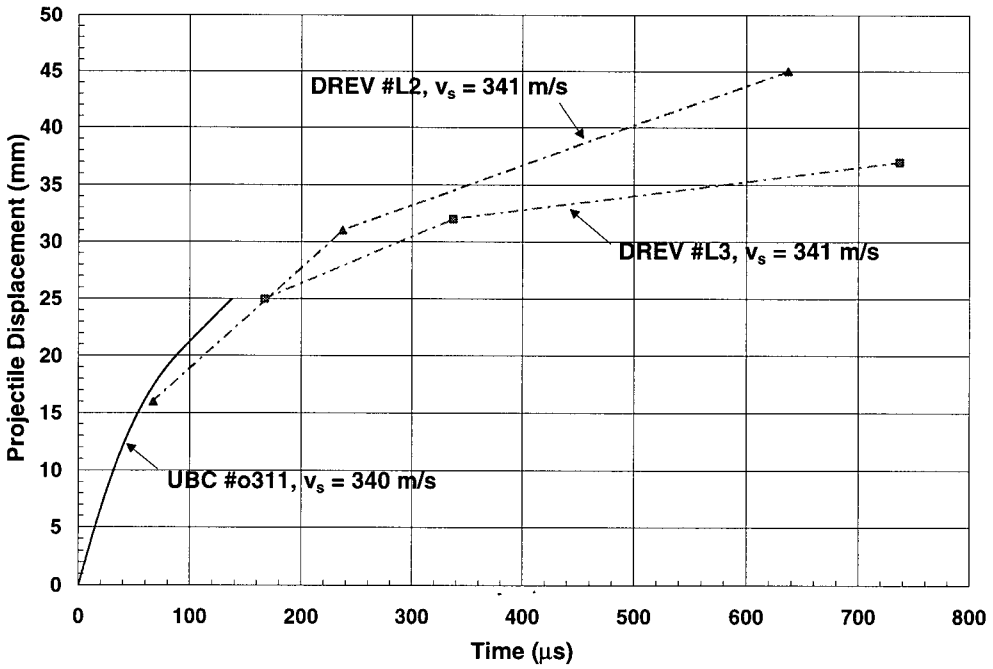

Figure 5.15: Comparison of video camera (DREV #L2 and #L3) and ELVS (UBC #o311) displacement-time results for 8-ply Kevlar® 129 targets.

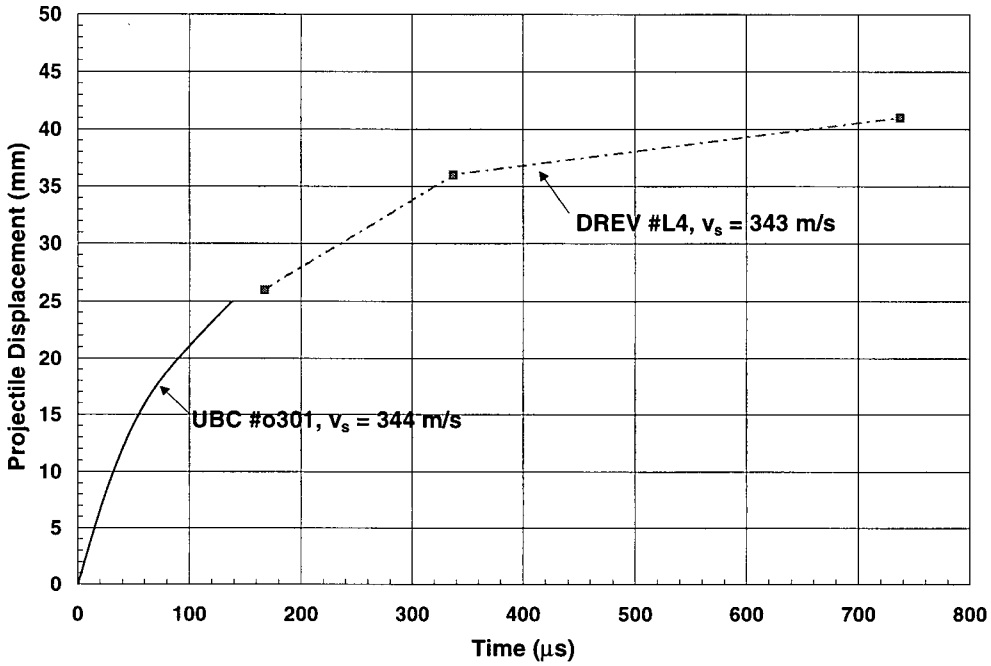

Figure 5.16: Comparison of video camera (DREV #L4) and ELVS (UBC #o301) displacement-time results for 8-ply Kevlar® 129 targets.

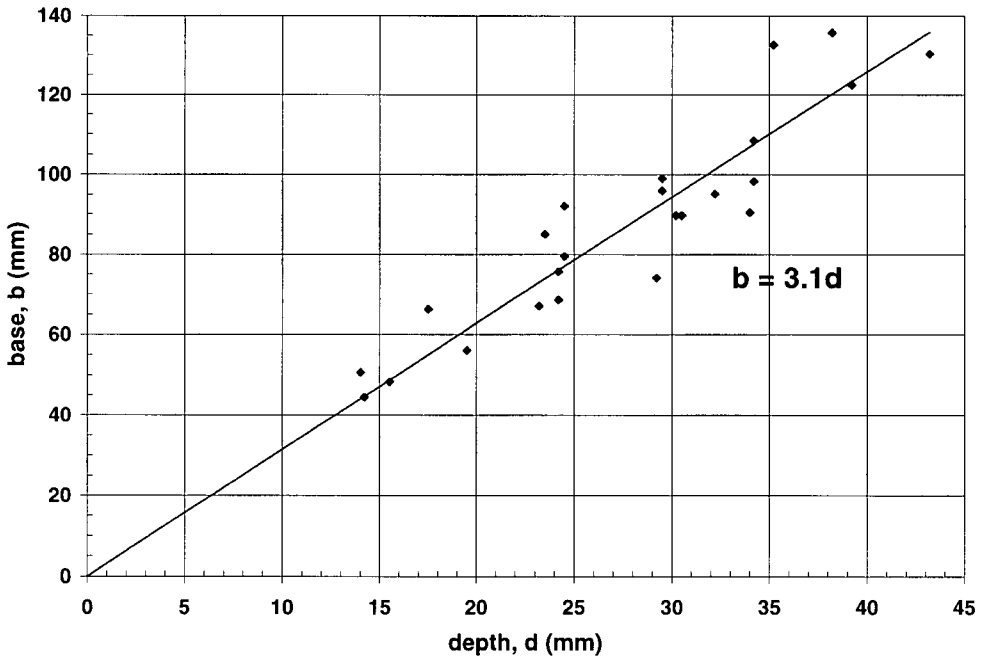

Figure 5.17: Relationship between the base, *b*, and depth, *d*, of the deformation pyramid for the 2.8 g (43 grain) projectile tests.

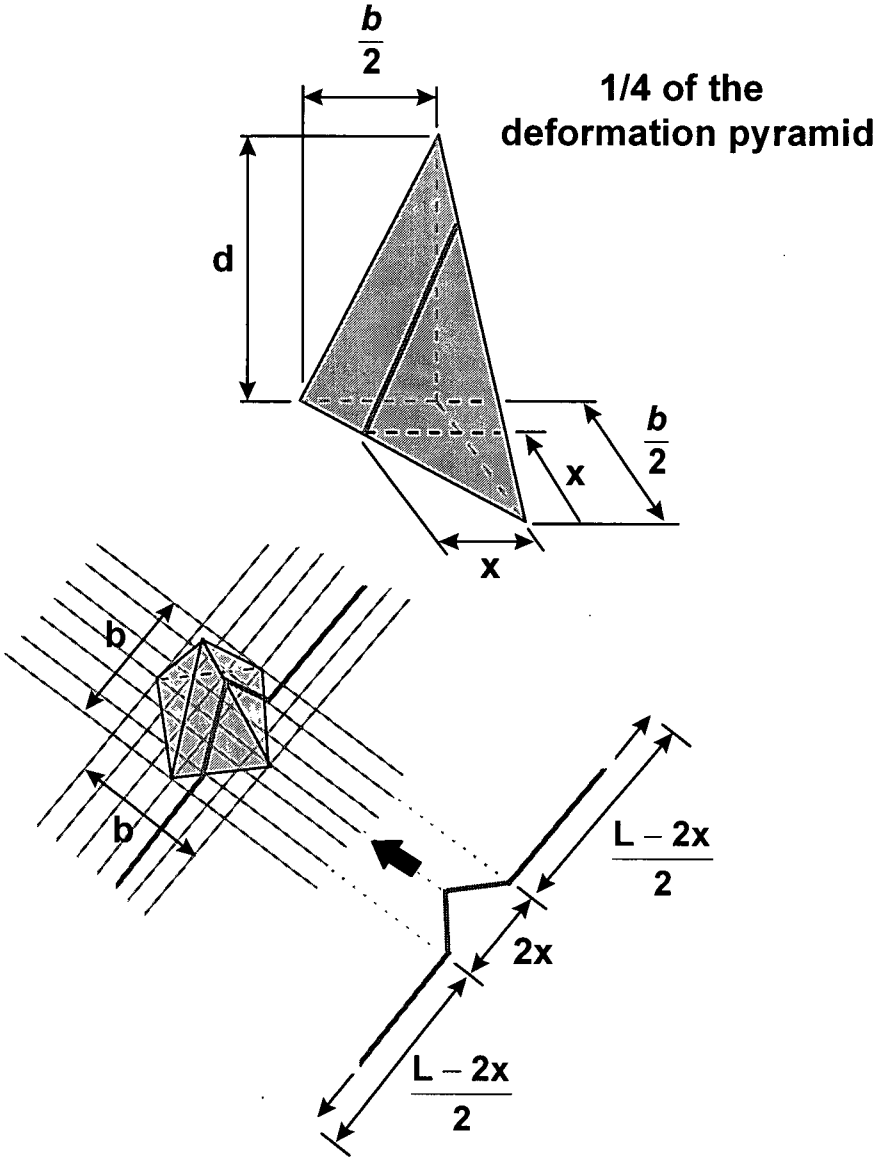

Figure 5.18: Schematic showing the measurements of the deformation pyramid used in the calculation of strain.

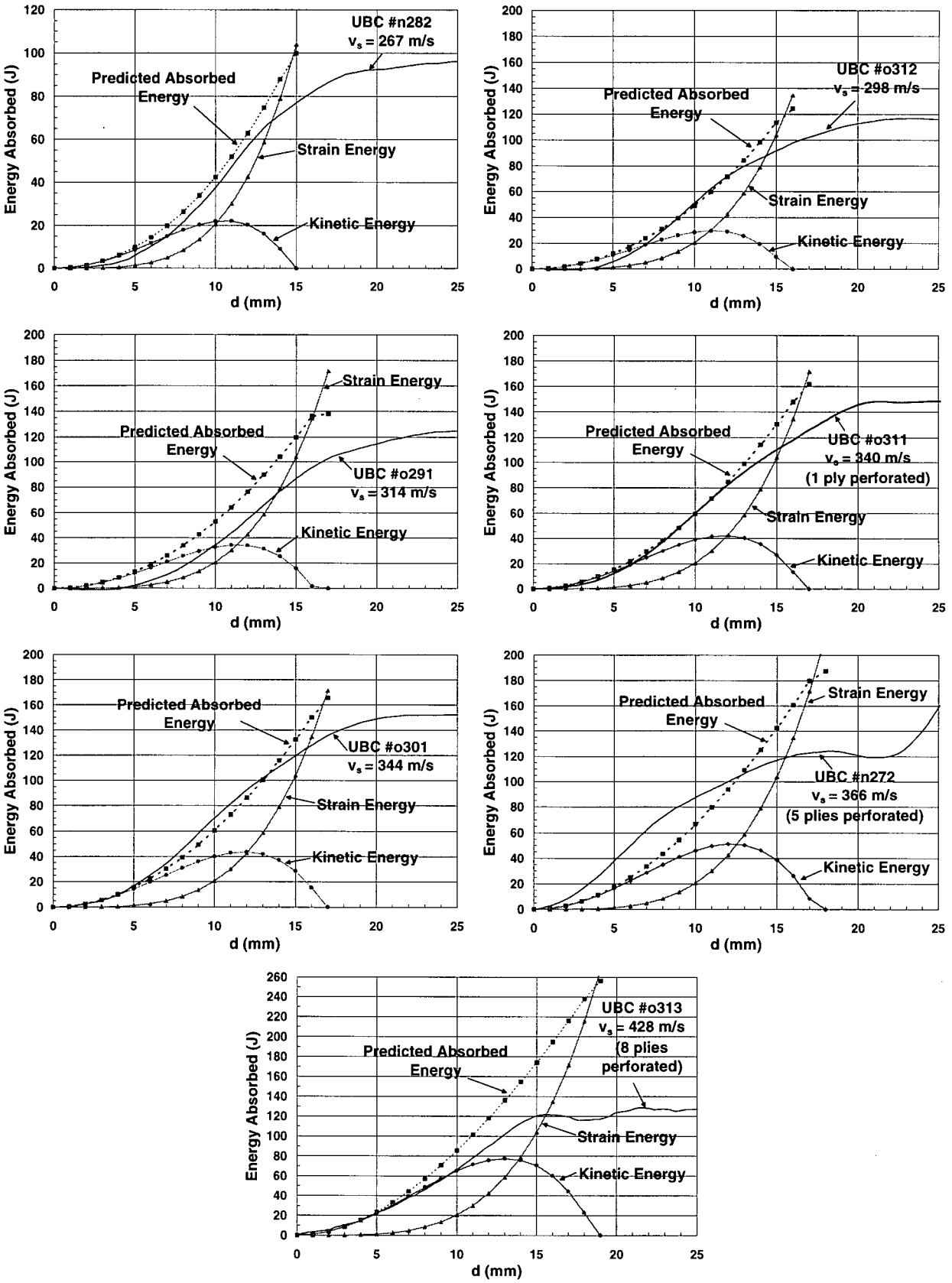

Figure 5.19: Energy absorbed versus pyramid depth for 8-ply targets, showing predicted (absorbed, strain and kinetic energy) and experimental results.

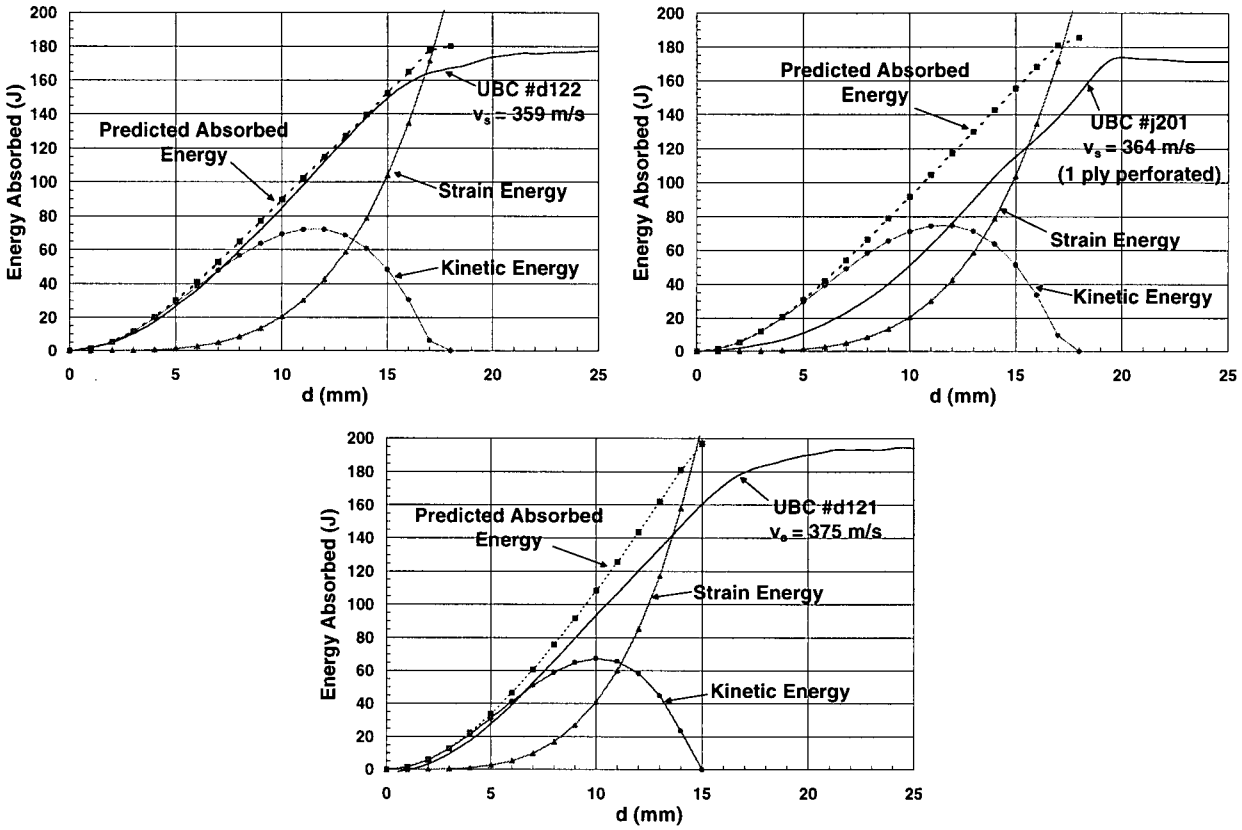

Figure 5.20: Energy absorbed versus pyramid depth for 16-ply targets, showing predicted (absorbed, strain and kinetic energy) and experimental results.

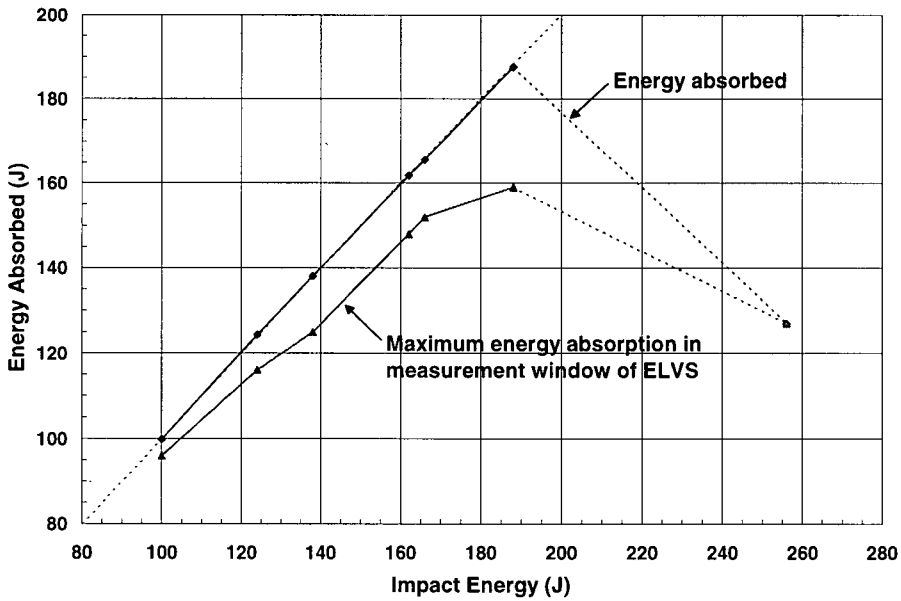

Figure 5.21: Absorbed energy versus impact energy for the 8-ply Kevlar® 129 targets impacted by 2.8 g (43 grain) projectiles, showing both the energy absorbed in the measurement window of the ELVS and the maximum energy absorbed.

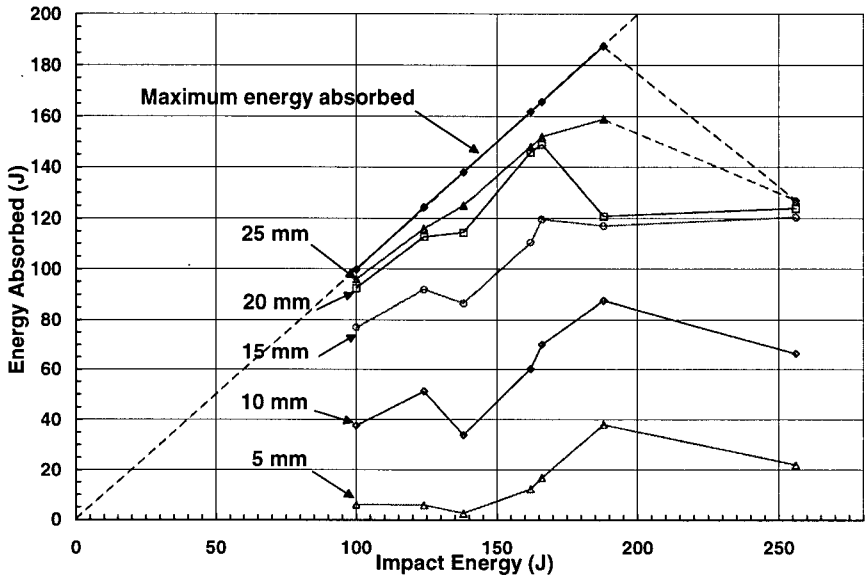

Figure 5.22: **Absorbed energy versus impact energy for the 8-ply Kevlar® 129 targets impacted by 2.8 g (43 grain) projectiles, showing the maximum energy absorbed and the energy absorbed at different values of pyramid depths.**

Chapter Six: Conclusions and Future Work

6.1 Introduction

Conclusions are drawn from the results and discussion presented in Chapter 5. Future work in this area is suggested.

6.2 Conclusions

The following conclusions can be drawn from the results in the previous chapter:

1. A recent continuous measurement technique has been adapted for use in ballistic impact experiments, and has been successfully used in the ballistic impact of textiles. From the UBC Enhanced Laser Velocity System (ELVS), displacement, velocity, energy and force histories of the impact event are obtained, as well as force- and energy-displacement curves. This technique offers an important advantage over conventional measurement techniques in that it provides information *during* the impact event.

2. More detailed information about the ballistic response of textiles has been obtained by combining results from the ELVS and high speed video images of the fabric deformation. This combination has lead to the following observations:

    - in non-perforating tests, the majority of the impact energy is absorbed by the target within the first 25 mm of displacement. Substantial growth of the deformation pyramid beyond this occurs as a result of the absorbed energy being re-distributed within the fabric.

- the strain in the deformation pyramid can reasonably be assumed to be proportional to the pyramid depth.

- initially in the formation of the deformation pyramid, most of the projectile energy is absorbed by the target in the form of kinetic energy. This, however, reaches a peak value and then decreases to zero as the projectile comes to a stop. The energy absorbed in the form of strain energy increases slowly in the initial stages of pyramid formation, and as the pyramid depth increases, the strain energy increases more quickly.

3. The ballistic impact response of textile materials appears to involve both a local and a global deformation mechanism. The global mechanism is seen in the formation of the deformation pyramid and the local mechanism is seen in the local deformation of the material directly in contact with the projectile. It is the local mechanism which dictates when failure of the material will occur. The bulk of the energy absorbed by the target appears to be equal to the energy absorbed in global deformation, however, the *maximum* value of the energy absorbed by the global mechanism is a function of the local response.

6.3 Future Work

The experimental results indicate that obtaining information about the ballistic impact of textile materials during the impact event is key to developing a greater understanding of the ballistic response of these materials. The results and conclusions presented in this thesis have just begun to "scratch the surface" of this largely investigated, yet poorly understood, area. As a result of the work presented here, the following future work is suggested:

1. Experiments should be performed in which an additional ELVS is used to measure back face deformation. This would provide a continuous displacement history of the back face deformation, and would provide increased knowledge of the ballistic response of textiles. Experiments could also be performed using the additional ELVS to quantify the effects of boundary conditions and to investigate their influence on back face deformation and blunt trauma.

2. A more detailed, multi-axis photographic investigation of the impact event should be performed with an effort to determine the strain history in the deformation pyramid. This could be performed by placing a grid system on the back face of a target and photographically recording the displacement of the grid during the impact event. This would offer significant information and would help determine how the energy is absorbed in a textile. This knowledge would aid in the optimization of textile materials for ballistic applications.

3. Quasi-static characterization tests should be performed in an attempt to quantify global deformation phenomena.

4. Further investigation of the effect of the projectile nose shape on the ballistic response of textiles should be performed in an attempt to gain a better understanding of the local deformation response.

5. The results of the experiments performed for the present research and the investigations suggested for future consideration could be used in the development and validation of increasingly accurate analytical and numerical models to predict the ballistic response of textile materials.

References

Briscoe, B. J. and Motamedi, F., "**The Ballistic Impact Characteristics of Aramid Fabrics: the Influence of Interface Friction**", *Wear*, Volume 158, No. 1-2, October 1992, p.p. 229 - 247.

Cunniff, P. M., "**A Semiempirical Model for the Ballistic Impact Performance of Textile-Based Personnel Armor**", *Textile Research Journal*, Volume 66, Number 1, January 1996, p.p. 45 - 59.

Cunniff, P. M., "**An Analysis of the System Effects in Woven Fabrics Under Ballistic Impact**", *Textile Research Journal*, Volume 62, Number 9, September 1992, p.p. 495 - 509.

Dean, B., **Helmets and Body Armor in Modern Warfare**, New Haven: Yale University Press, 1920.

Delfosse D., Pageau G., Bennett R. and Poursartip A., **"Instrumented Impact Testing at High Velocities"**, *Journal of Composites Technology & Research*, JCTRER, Vol. 15 (1), 1993, pp. 38-45.

Department of Justice, "**Ballistic Resistance of Police Body Armor**", **NIJ Standard 0101.03**, April 1987.

Espinosa H.D., Lu H-C. and Xu Y., **"A Novel Technique for Penetrator Velocity Measurement in Ballistic Penetration Studies"**, MD-Vol. 75/AMD-Vol. 219, *Advances in Failure Mechanisms in Brittle Materials,* ASME, 1996, pp. 23-47.

Figucia, F., "**Energy Absorption of Kevlar Fabrics Under Ballistic Impact",** June 1980, p.p. 29 - 41.

Figucia, F., Weiner, L., and Laible, R., "**The Mechanical Properties of Textile Materials as Influenced by Complexity and Rate of Testing**", *Polymer Engineering and Science*, Volume 11, Number 4, July 1971, p.p. 289 - 294.

Freeston, Jr., W. D. and Claus, Jr., W. D., "**Strain-Wave Reflections During Ballistic Impact of Fabric Panels**", *Textile Research Journal*, Volume 43, Number 6, June 1973, p.p. 348 - 351.

Hsieh, C. Y., Mount, A., Jang, B. Z., and Zee, R. H., "**Response of Polymer Composites to High and Low Velocity Impact**", *Society for the Advancement of Material and Process Engineering*, Massachusetts, November 1990, p.p. 14 - 27.

Kraak, G. W., "**Gas Gun for Ballistic Testing of Body Armour to STANAG 2920**", PSE Letter Report 7019-57, Diemaco

Laible, R. C., et al, "**Laminates for Ballistic Protection**", February 1975.

Laible, R. C., Figucia, F., and Ferguson, W. J., "**The Application of High-Modulus Fibers to Ballistic Protection**", *J. Macromol. Sci.-Chem.*, A7(1), 1973, p.p. 295 - 322.

Laine, I. and Vahakangas, P., **"Energy Absorption Mechanisms of FSP in Aramide Fabric"**, *Proceedings of the Personal Armour Systems Symposium '96,* Colchester, U. K., September 3 - 6, 1996, p.p. 101 - 114.

Leech, C. M. and Adeyefa, B. A., "**Dynamics of Cloth Subject to Ballistic Impact Velocities**", *Computers and Structures*, Volume 15, Number 4, 1982, p.p. 423 - 432.

Leech, C., Hearle, J. W. S., and Mansell, J., "**A Variational Model for the Arrest of Projectiles by Woven Cloth and Nets**", *J. Text. Inst.*, Volume 43, Number 11, 1979, p.p. 469 - 478.

Lin, L. C. and Bhatnagar, A., "**Ballistic Energy Absorption of Composites. III**", *Advanced Materials: Meeting the Economic Challenge*, Toronto, October 1992, p.p. T291 - T306.

Lomov, S. V., "**Modelling of the High-Velocity Impact on the Textile Woven Targets**", *Clothing and Personal Equipment for the Combat Soldier Post 2000 Conference,* Science and Technology Division, Defence Clothing and Textiles Agency, Ministry of Defence, Colchester, October 1995, p.p. 212 - 221.

Lomov, S., "**Oblique High-Velocity Impact on a Textile Woven Target: Mathematical Simulation**", *Proceedings of the Personal Armour Systems Symposium '96,* Colchester, U. K., September 3 - 6, 1996, p.p. 145 - 156.

MIL-STD-662E, Military Standard, **Guidelines for the Ballistic Testing of Armor Against Small Arms Projectiles**, 1986

Montgomery, T. G., Grady, P. L., and Tomasino, C., "**The Effects of Projectile Geometry on the Performance of Ballistic Fabrics**", *Textile Research Journal*, Volume 52, Number 7, July 1982, p.p. 442 - 450.

NATO Standardization Agreement 2920, Ballistic Test Method for Personal Armour Materials and Combat Clothing, Part 1: Fragmentation-Protective Materials, Edition 2, March 1996.

NATO Standardization Agreement 2920, Ballistic Test Method for Personal Armour Materials and Combat Clothing, Part 2: Bullet-Protective Materials, Edition 2, March 1996.

Pageau, G., The Defence Research Establishment Valcartier (DREV), personal communication, 1997.

Parga-Landa, B. and Hernandez-Olivares, F., "**An Analytical Model to Predict Impact Behaviour of Soft Armours**", *International Journal of Impact Engineering*, Volume 16, Number 3, 1995, p.p. 455 - 466.

PPAA-STD-1989-05, **Testing Standards for Ballistic Resistance of Personal Body Armor**, Personal Protective Armor Association, June 22, 1989.

Prevorsek, D. C., Kwon, Y. D., and Chin, H. B., "**Analysis of the Temperature Rise in the Projectile and Extended Chain Polyethylene Fiber Composite Armor During Ballistic Impact and Penetration**", *Polymer Engineering and Science*, Volume 34, Number 2, January 1994, p.p. 141 - 152.

[a]Prosser, R. A., "**Penetration of Nylon Ballistic Panels by Fragment-Simulating Projectiles. Part I: A Linear Approximation to the Relationship Between the Square of the V_{50} or V_c Striking Velocity and the Number of Layers of Cloth in the Ballistic Panel**", *Textile Research Journal*, February 1988, p.p. 61 - 85.

[b]Prosser, R. A., "**Penetration of Nylon Ballistic Panels by Fragment-Simulating Projectiles. Part II: Mechanism of Penetration**", *Textile Research Journal*, March 1988, p.p. 161 - 165.

Ramesh, K.T. and Kelkar, N., "**Technique for the Continuous Measurement of Projectile Velocities in Plate Impact Experiments**", *Rev. Sci. Instrum.*, Vol. 66 (4), 1995, pp. 3034-3036.

Roylance, D. and Wang, S. S., "**Penetration Mechanics of Textile Structures. Ballistic Materials and Penetration Mechanics**", Elsevier Scientific Publishing Co. (1980), p.p. 273 - 292.

Roylance, D., "**Ballistics of Transversely Impacted Fibers**", October 1977.

Roylance, D., "**Stress Wave Propagation in Fibres: Effect of Crossovers**", *Fibre Science and Technology*, Volume 13, 1980, p.p. 385 - 395.

Roylance, D., Wilde, A., and Tocci, G., "**Ballistic Impact of Textile Structures**", *Textile Research Journal*, Volume 43, Number 1, January 1973, p.p. 34 - 41.

Sanders, T. A., "**Penetration of Composite Laminates by Conical Indenters and Projectiles**", Masters Thesis, Department of Civil Engineering, University of British Columbia, July, 1997.

Segal, C. L., "**High-Performance Organic Fibers, Fabrics, and Composites for Soft and Hard Armor Applications**", *Advanced Materials/Affordable Processes*, Volume 23, New York, October 1991, p.p. 651 - 660.

Shim, V. P. W., Tan, V. B. C., and Tay, T. E., "**Modelling Deformation and Damage Characteristics of Woven Fabric Under Small Projectile Impact**", *International Journal of Impact Engineering*, Volume 16, Number 4, 1995, p.p. 585 - 605.

Smith, J. C., Blandford, J. M., and Schiefer, H. F., "**Stress-Strain Relationships in Yarns Subjected to Rapid Impact Loading. Part VI: Velocities of Strain Waves Resulting from Impact**", *Textile Research Journal*, October 1960, p.p. 752 - 760.

Smith, J. C., Fenstermaker, C. A., and Shouse, P. J., "**Stress-Strain Relationships in Yarns Subjected to Rapid Impact Loading. Part X: Stress-Strain Curves Obtained by Impacts with Rifle Bullets**", *Textile Research Journal*, November 1963, p.p. 919 - 934.

Smith, J. C., McCrackin, F. L., and Schiefer, H. F., "**Stress-Strain Relationships in Yarns Subjected to Rapid Impact Loading. Part V: Wave Propagation in Long Textile Yarns Impacted Transversely**", *Textile Research Journal*, April 1958, p.p. 288 - 302.

Smith, J. C., McCrackin, F. L., Schiefer, H. F., Stone, W. K., and Towne, K. M., "**Stress-Strain Relationships in Yarns Subjected to Rapid Impact Loading. Part IV: Transverse Impact Tests**", *Textile Research Journal*, November 1956, p.p. 821 - 828.

Taylor, Jr., W. J. and Vinson, J. R., "**Modeling Ballistic Impact into Flexible Materials**", *AIAA Journal*, Volume 28, Number 12, December 1990, p.p. 2098 - 2103.

Ting, J., Roylance, D., Chi, C. H., and Chitrangad, B., "**Numerical Modeling of Fabric Panel Response to Ballistic Impact**", *25th International SAMPE Technical Conference*, October 1993, p.p. 384 - 392.

Vinson, J. R. and Zukas, J. A., "**On the Ballistic Impact of Textile Body Armor**", *Journal of Applied Mechanics*, June 1975, p.p. 263 - 268.

Walsh, T. F., Lee, B. L., and Song, J. W., **"Penetration Failure Mechanisms of Woven Textile Composites"**, Eleventh Technical Conference of the American Society for Composites, October 7 - 9, 1996, p.p. 979 - 988.

White, F. M., **Fluid Mechanics**, Third Edition, Toronto: McGraw-Hill Inc., 1994.

Wilde, A. F., "**Photographic Investigation of High-Speed Missile Impact upon Nylon Fabric. Part II: Retarding Force on Missile and Transverse Critical Velocity**", *Textile Research Journal*, October 1974, p.p. 772 - 778.

Wilde, A. F., Roylance, D. K., and Rogers, J. M., "**Photographic Investigation of High-Speed Missile Impact upon Nylon Fabric, Part 1: Energy Absorption and Cone Radial Velocity in Fabric**", *Textile Research Journal*, Volume 43, Number 12, December 1973, p.p. 753 - 761.

Wu E., Sheen H-J., Chen Y-C., and Chang L-C., **"Penetration Force Measurements of Thin Plates by Laser Doppler Anemometry"**, *Experimental Mechanics*, Vol. 34 (2), 1994, pp. 93-99.

Zee, R. H., Jang, B. Z., Mount, A., and Wang, C. J., "**Microvelocity Sensor for Instantaneous Velocity Determination**", *Rev. Sci. Instrum.*, Volume 60, Number 12, December 1989, p.p. 3692 - 3697.

Appendix A : Air Drag Calculations

To determine the effect of air drag on the projectiles in the video camera ballistic impact experiments, the following equation (White [1994]) was used to determine the acceleration, a, of the projectile:

$$a = -\frac{1}{2}\frac{C_D \rho_{air} v_{os}^{\ 2} A}{m_p} \tag{A.1}$$

where C_D is the coefficient of drag for a cylinder, ρ_{air} is the density of air (at standard temperature and pressure), v_{os} is the velocity given by the optical sensors, A and m_p are the cross-sectional area and mass of the projectile, respectively. This value of acceleration was then used to determine the velocity of the projectile at the point of impact, v_s, using the following equation (White [1994]):

$$v_s = \sqrt{v_{os}^{\ 2} + 2aL_{offset}} \tag{A.2}$$

where v_s is the impact velocity and L_{offset} is the distance between the optical sensors (end of gun barrel) and the target. The values used for all constants are given in Table A-1. In order to find the appropriate value of C_D, the Reynolds number had to be determined using (White [1994]):

$$\textbf{Reynolds \#} = \frac{\rho_{air} v_{os} d_p}{\mu_{air}} \tag{A.3}$$

where d_p is the diameter of the projectile and μ_{air} is the viscosity of air (at standard temperature and pressure). The value of C_D shown in Table A-1 is valid for a Reynolds number greater than 1×10^4. The results from the above equations are given in Table A-2.

Table A-1: Values used in the calculation of the effect of air drag on the 2.8 g (43 grain) blunt projectiles. (White [1994])

Constant	Value
C_D	0.99
ρ_{air}	1.2 kg/m^3
A	2.27 x 10^{-5} m^2
m_p	0.0028 kg
d_p	0.00538 m
μ_{air}	1.78 x 10^{-5} kg/ms

Table A-2: Results from air drag calculation

Test #	v_{os} (m/s)	L_{offset} (m)	Reynolds #	a (m/s^2)	v_s (m/s)
L1	278	0.127	1.01 x 10^5	-372.44	278
L2	341	0.127	1.23 x 10^5	-559.46	340
L3	341	0.127	1.24 x 10^5	-562.10	341
L4	343	0.127	1.24 x 10^5	-568.04	343
L5	303	0.127	1.10 x 10^5	-441.59	302
L11	406	0.178	1.47 x 10^5	-796.51	406
L12	401	0.178	1.45 x 10^5	-775.87	401
L13	404	0.178	1.46 x 10^5	-787.13	404
L14	397	0.178	1.44 x 10^5	-759.71	397
L15	431	0.178	1.56 x 10^5	-893.78	430
L16	459	0.178	1.66 x 10^5	-1013.82	458

Appendix B : UBC Enhanced Laser Velocity System (ELVS)

Introduction

This appendix describes the UBC Enhanced Laser Velocity System (ELVS) in detail. The system components are discussed, and the calibration and data analysis procedures used with the technique are explained. The capabilities and limitations of the system are presented.

ELVS Components

A detailed description of the ELVS components, including the part numbers, is given in Table B-1.

Calibration

The calibration data was obtained by performing a number of "no-target" ballistic tests. The projectiles used for these calibration tests were 2.8 g blunt aluminum cylinders, 46 mm in length. The ELVS was used to measure the motion of the projectile. A voltage-time curve for one of the "no-target" calibration tests is shown in Figure B.1. The data obtained from the calibration test is normalised for displacement by multiplying each time step on the x-axis by the impact velocity of the projectile, v_s. This value is found by dividing the projectile length by t_{AC} (the time between points A and C in Figure B.1). In this manner, a voltage-displacement data set with the same number of data points as a ballistic impact test is obtained. This calibration data, in the form of a look-up table, is then used with data from a ballistic impact test to derive the projectile displacement history. If a test value falls between two calibration points the appropriate value is found through linear interpolation between existing points. This method ensures that the test displacement-time results always reflect the original calibration data.

A problem sometimes encountered when performing impact experiments with the system is that the maximum laser intensity, and hence the maximum voltage, is not always the same for each test. The Lexan sheets protecting the lenses may get dirty or scratched or the laser itself may get dirty, and thus the intensity of the sheet diminishes resulting in a drop in the maximum voltage. It is therefore useful to normalise the calibration so that if the maximum voltage changes, the calibration is adjusted accordingly.

Data Analysis

The flow chart in Figure B.2 describes the process of data reduction from the initial input of raw test data to the final output of results. The raw data points acquired from the oscilloscope are first read into the analysis program and then converted into voltages. The voltage-time curve is converted into displacement-time values using the calibration look-up table described in the previous section. The displacement-time curve is then differentiated to determine velocity values. The acceleration values are calculated by a second differentiation, and from these, force values are determined. Energy absorption values are obtained by taking the difference between the incident projectile energy ($\frac{1}{2}m_p v_s^2$) and the projectile energy at any time during the impact event ($\frac{1}{2}m_p v_p^2$), where m_p is the projectile mass, v_s is the projectile impact velocity, and v_p is the projectile velocity at any time during the impact event.

To ensure that the ELVS works properly during the test and to ensure that data obtained from the test is valid, a set of two "data checks" can be performed on the voltage-time data. These checks include a calculation of the projectile length and a check of the ratio between the impact and residual velocities. The first data check, that of the projectile length, is obtained by using appropriate values from a voltage-time curve of a ballistic impact test, an example of which is

shown in Figure B.3. The target in this test was an 18.5 mm thick, glass-fibre reinforced composite laminate, impacted by a projectile 38 mm in length. For a projectile that is shorter than or equal to the width of the laser sheet, w_{ls}, the projectile length, l_p, is calculated from:

$$l_p = \frac{w_{ls}}{V_{full} - V_{blocked}} \cdot (V_A - V_B) \tag{B.1}$$

where V_{full} is the voltage at 100 % intensity, $V_{blocked}$ is the voltage at 0 % intensity, V_A and V_B are the voltages at points A and B in Figure B.3, respectively. For a projectile that is longer than w_{ls}, the projectile length is calculated from:

$$l_p = \frac{w_{ls}}{V_{full} - V_{blocked}} \cdot (V_A - V_B) + \frac{w_{ls}}{t_{AB}} \cdot t_{BC} \tag{B.2}$$

where t_{AB} is the time duration between points A and B, and t_{BC} is the time duration between points B and C. The calculated value for the projectile length is then compared to the actual projectile length measured prior to testing.

The second check is that of the ratio between the slope of line AB and the slope of either line DE, in the case of a target test, or line CE for a no-target test. The ratio between these slopes will be 1 when there is no target or when the target fails to slow the projectile down, and will be less than 1 when the target is successful in slowing the projectile down.

System capabilities and limitations

Displacement Measurement Resolution

The vertical resolution of the oscilloscope used is 255 bits. With a laser sheet width of 25.4 mm, the maximum vertical resolution of the system is 0.1 mm. However, the observed noise

bandwidth of a typical impact test is 2 bits, resulting in a displacement measurement tolerance of ± 0.1 mm.

Maximum Velocity

The ELVS is capable of continuously measuring projectile motion during a ballistic impact event. Based on limitations of the photodetector sampling frequency (50 MHz) and the displacement measurement tolerance (± 0.1 mm), the maximum velocity our system is 10,000 m/s. This value is based on using only two data points to determine the velocity. In order to obtain enough data for a complete analysis, however, the effective maximum working velocities are on the order of 5000 m/s. Typically, 5000 data points are acquired during a ballistic impact experiment, however, half this amount will give accurate results. Hence, velocities of 1000 m/s (ordinance range) can be easily measured using the system.

Repeatability

A number of "no-target" ballistic tests at different velocities were performed, with the resulting voltage-time curves shown in Figure B.4(a). The impact velocities ranged from 204 to 460 m/s. All tests were performed using a blunt-tipped projectile, 46 mm in length. The time axes on all curves were then multiplied by the projectile impact velocity, v_s, to produce the voltage-displacement curves shown in Figure B.4(b). These curves clearly show the repeatability of the ELVS.

Limitations

There are a few limitations with the system. When used in impact tests with materials that deform significantly during impact, such as the textile materials used in body armour applications, the projectile often leaves the laser sheet before the impact event is over. As a

result, some information about the impact event is lost. If the projectile is too short, again there is the possibility that the projectile will leave the sheet before the impact event is over, resulting in lost information about the impact event. Another limitation to the system involves the data analysis. The data reduction program has been developed with the assumption that the projectile is rigid, i.e., the projectile does not deform during the impact event. If the projectile were to deform significantly during an impact test, the information determined by the data reduction program concerning the energy absorbed by the target will not be accurate.

Table B-1: Description of ELVS components (Item #'s correspond to Figure 4.7).

ITEM #	COMPONENT	SPECIFICS	PART NUMBER	COMPANY
1	Diode laser	• 670 nm wavelength • produces 1 mW of power • classified as a Class II, eye safe laser by The United States Center for Devices & Radiological Health (CDRH).	SNF-501L-670-1-10°	Lasiris Inc.
2	First cylindrical lens	• 250 mm focal length • 60 x 50 mm	01LCP017	Melles Griot
3	Aperture	• 25.4 x 10.0 mm	---	made in-house
4	Neutral Density Filter	• 50 mm square	03FNG007	Melles Griot
5	Second cylindrical lens	• 40 mm focal length • 60 x 15 mm	01LCP001	Melles Griot
6	Collector lens	• bi-convex lens • 100 mm focal length • 50 mm diameter	01LDX002	Melles Griot
7	Photodetector	• silicon PIN photodetector • rise/fall time of ≤7 ns • sensitive up to a bandwidth of 50 MHz	PDA 150	Thorlabs Inc.
---	Mounting equipment	• optical rail, rail carriers, post holders, lens holders	---	Melles Griot

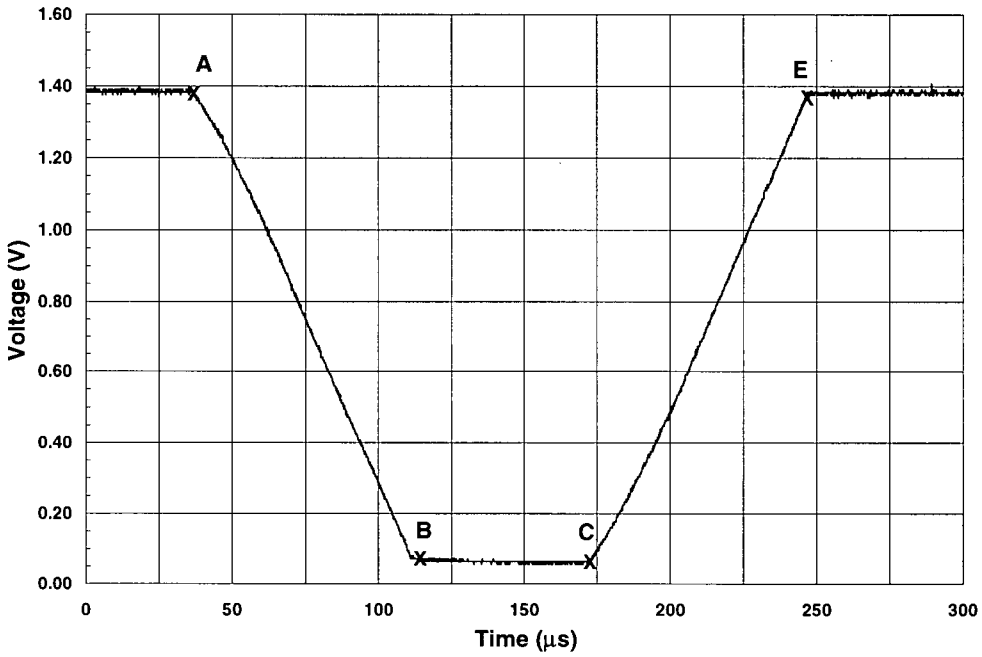

Figure B.1: Voltage versus time curve for a "no-target" test.

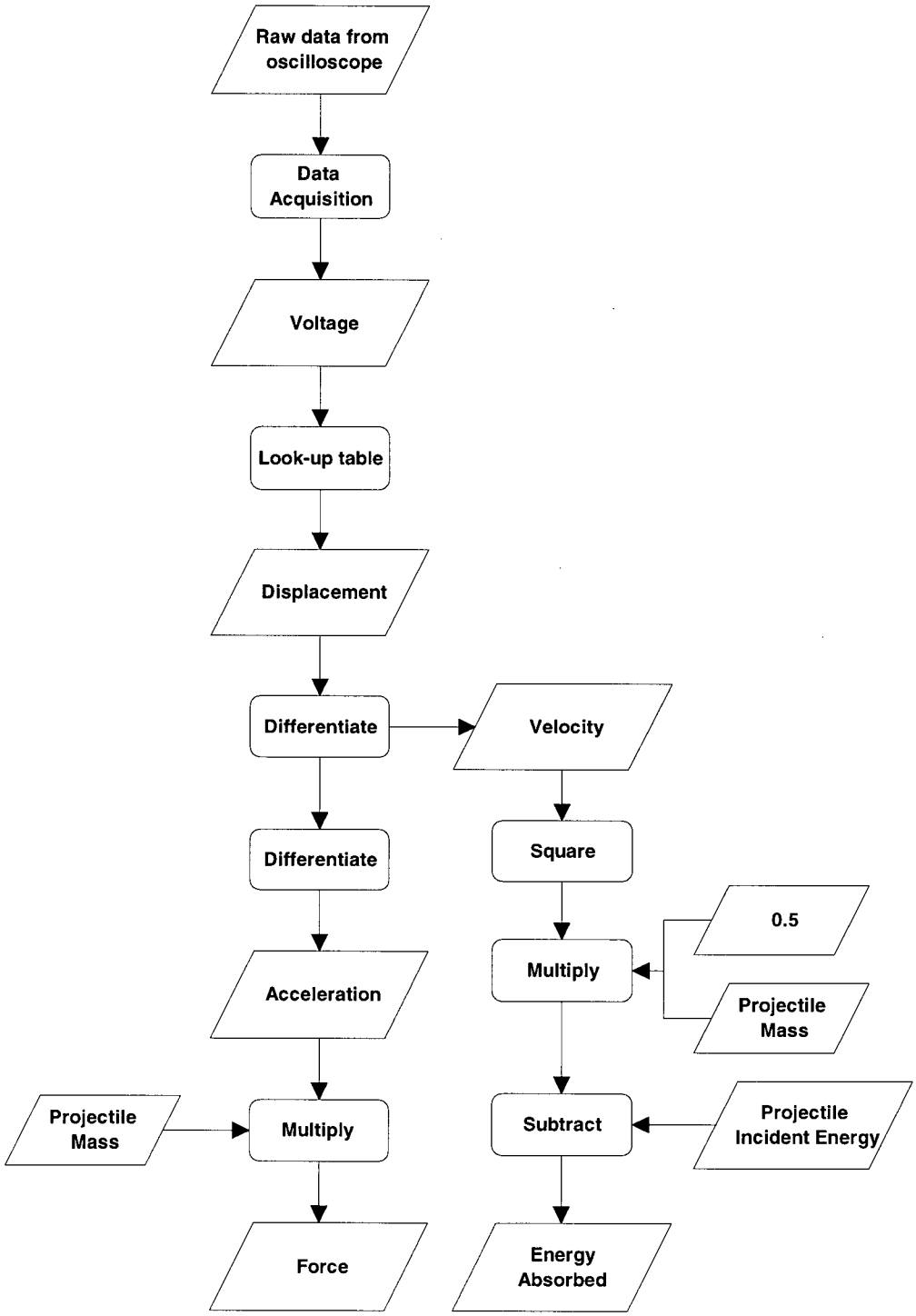

Figure B.2: Flow diagram showing the data analysis technique used with the ELVS.

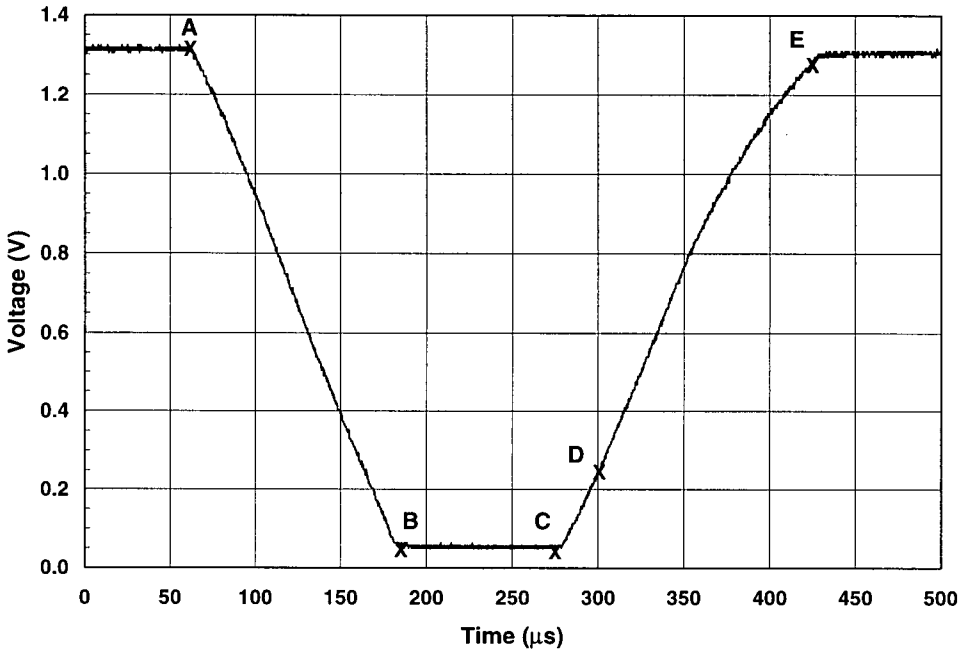

Figure B.3: Voltage versus time curve for a ballistic impact test.

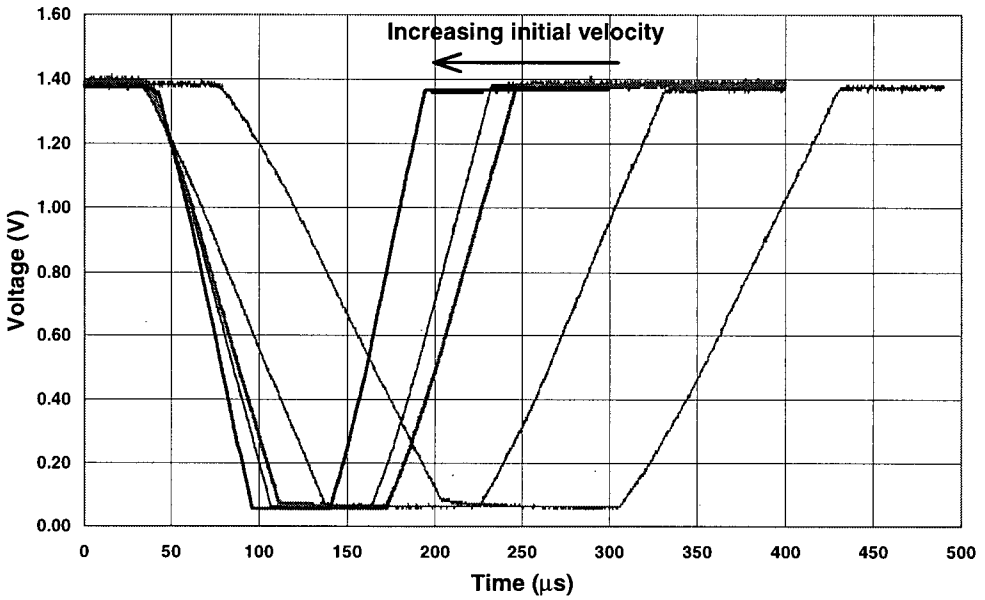

(a)

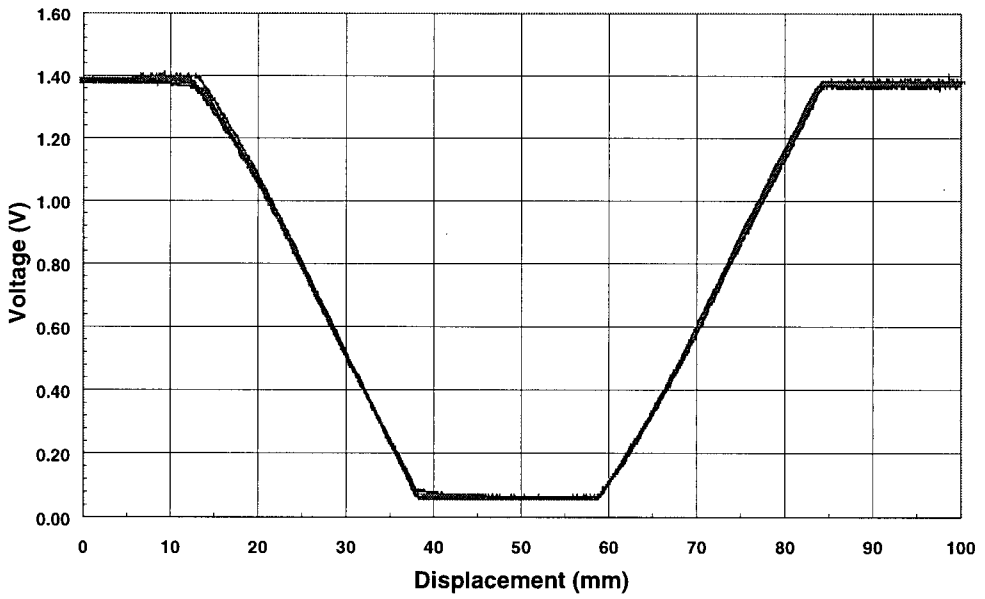

(b)

Figure B.4: Curves representing the repeatability of the ELVS, where (a) shows the voltage versus time curves for a series of "no-target" impact tests and (b) shows these curves with the time axis multiplied by the impact velocity to give voltage versus displacement curves.

Appendix C : Video Images

The video images obtained for the ballistic impact tests performed at DREV using the high speed video camera are presented here. Figures C.1 to C.2 show the images for tests performed on 8-ply Kevlar® targets and Figures C.3 to C.4 show the images for tests performed on 16-ply Kevlar® targets, both using the 2.8 g (43 grain) blunt aluminum projectiles. Figure C.5 shows the images for tests using the 1.1 g (17 grain) hemispherical projectiles. Figure C.6(a) shows the images for a 1.1 g (17 grain) 120° conical projectile test. Figures C.6(b) and C.7 show the images for the 1.1 g (17 grain) blunt projectile tests. All of the 1.1 g projectile tests were performed using 8-ply Kevlar® targets. The time values for each image and the measurements taken from each image can be found in Tables 5-1 and 5-2, for the 2.8 g projectile tests and the 1.1 g projectile tests, respectively.

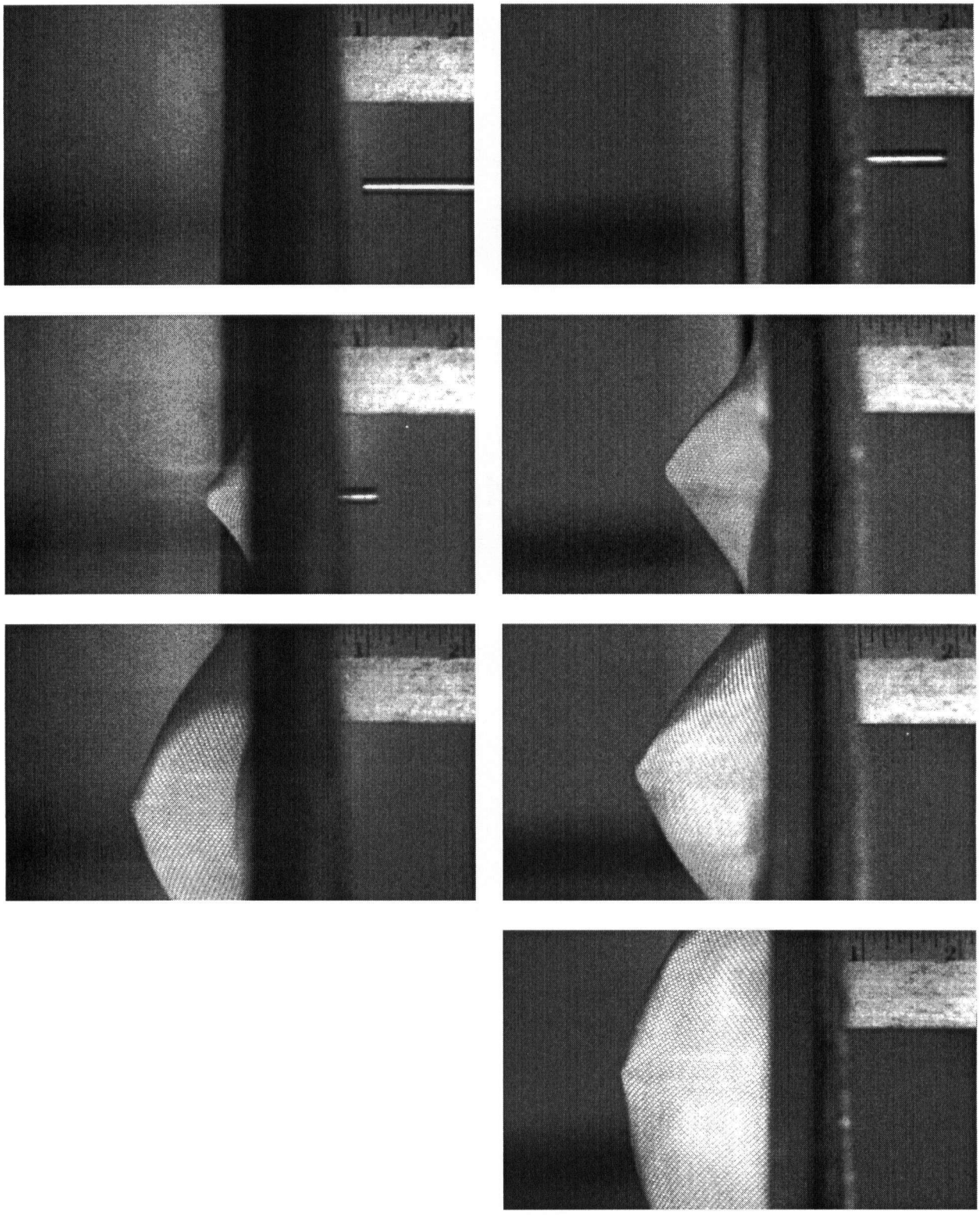

(a) (b)

Figure C.1: Video images for test #L1 (a) and #L3 (b).

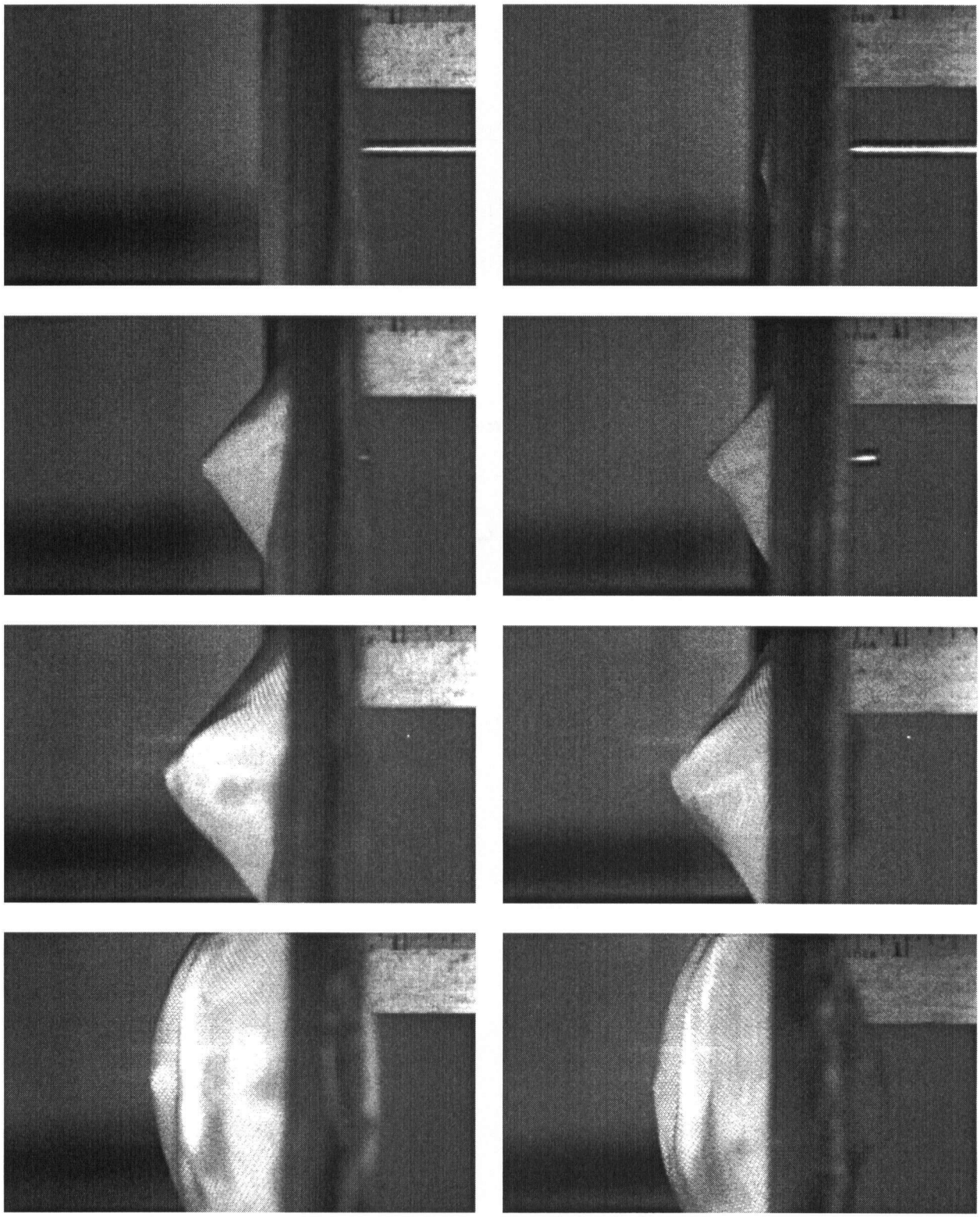

(a) (b)

Figure C.2: Video images for test #L4 (a) and #L5 (b).

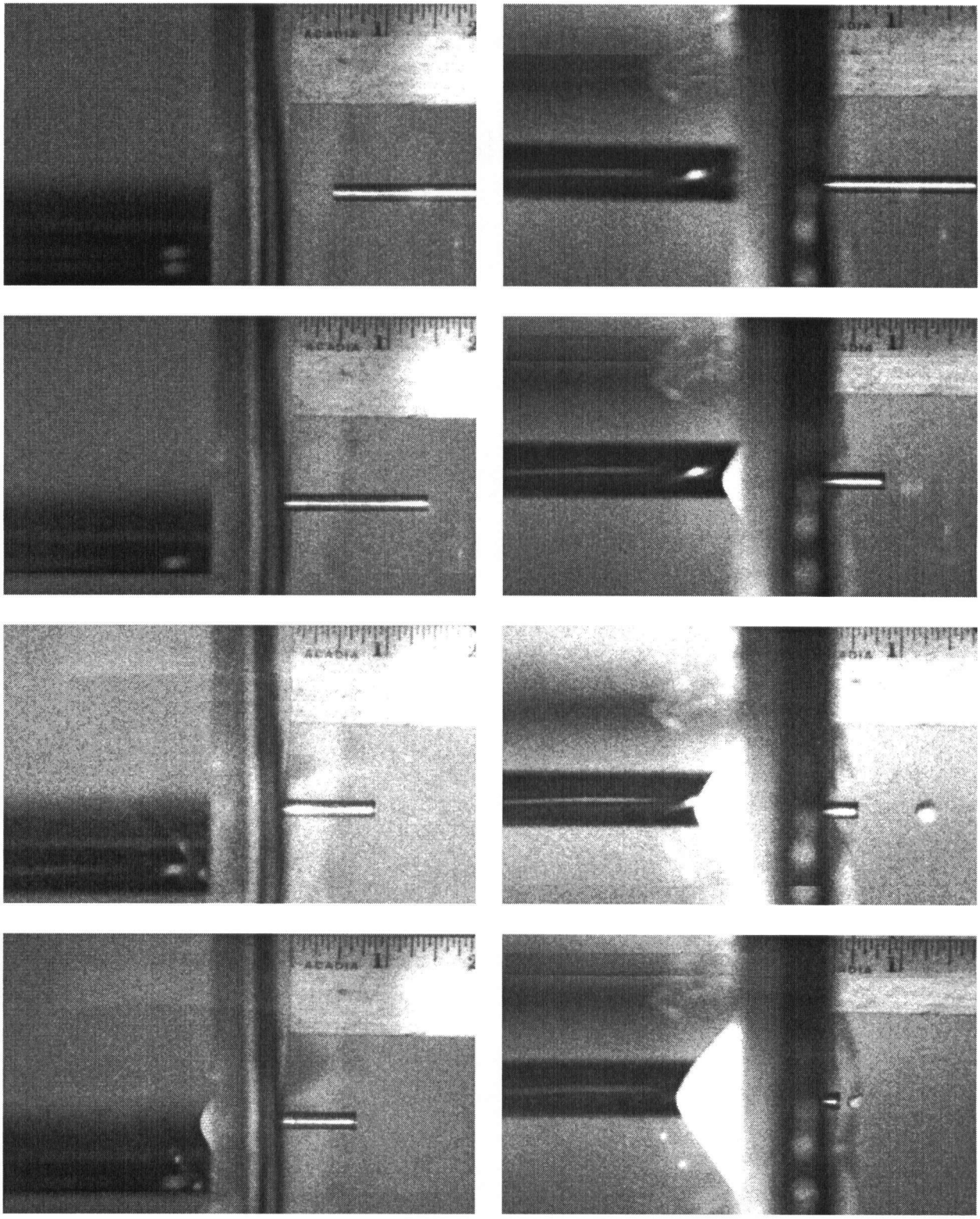

(a) (b)

Figure C.3: Video images for test #L12 (a) and #L14 (b).

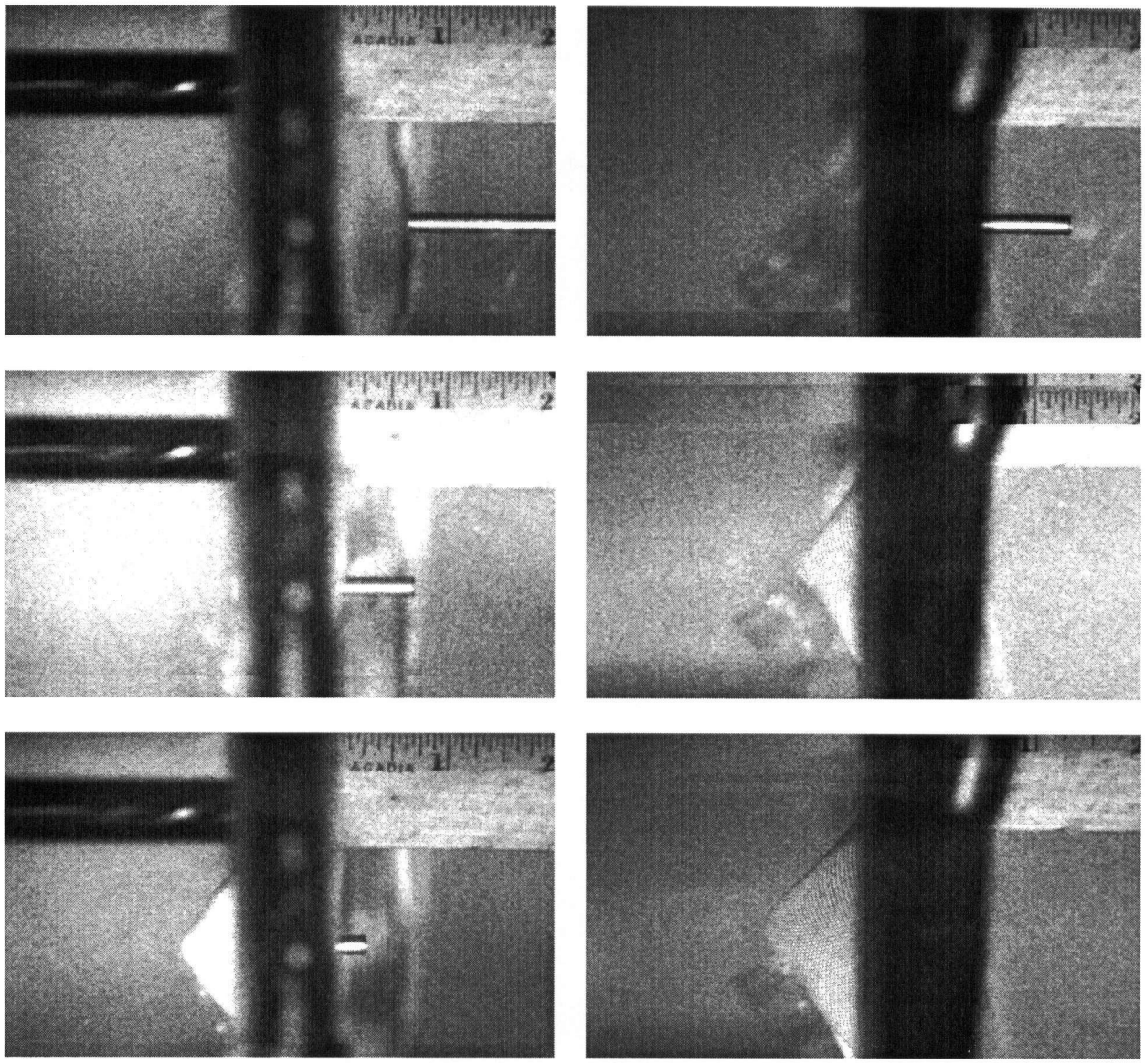

(a) (b)

Figure C.4: Video images for test #L15 (a) and #L16 (b).

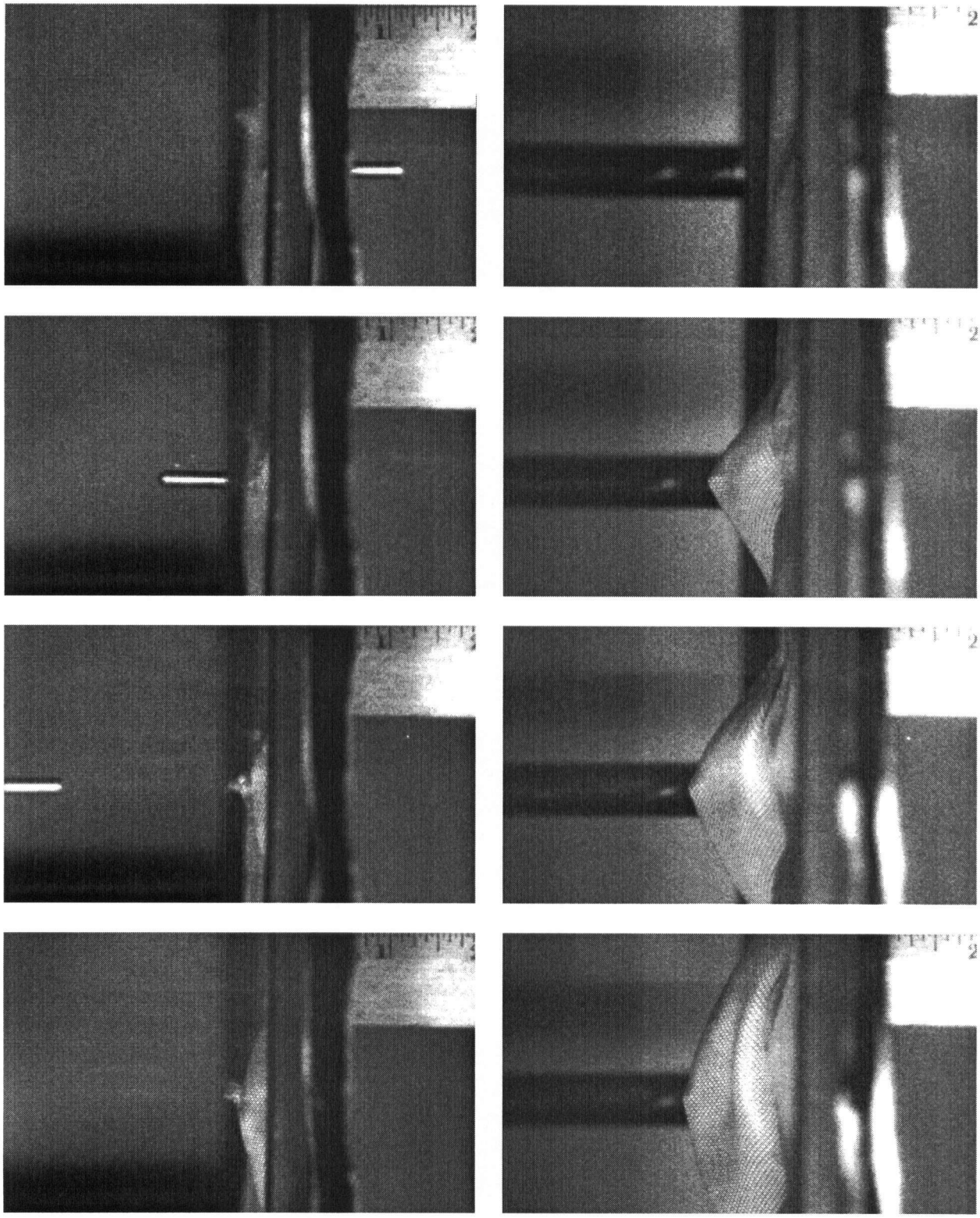

(a) (b)

Figure C.5: Video images for test #H23 (a) and #H26 (b).

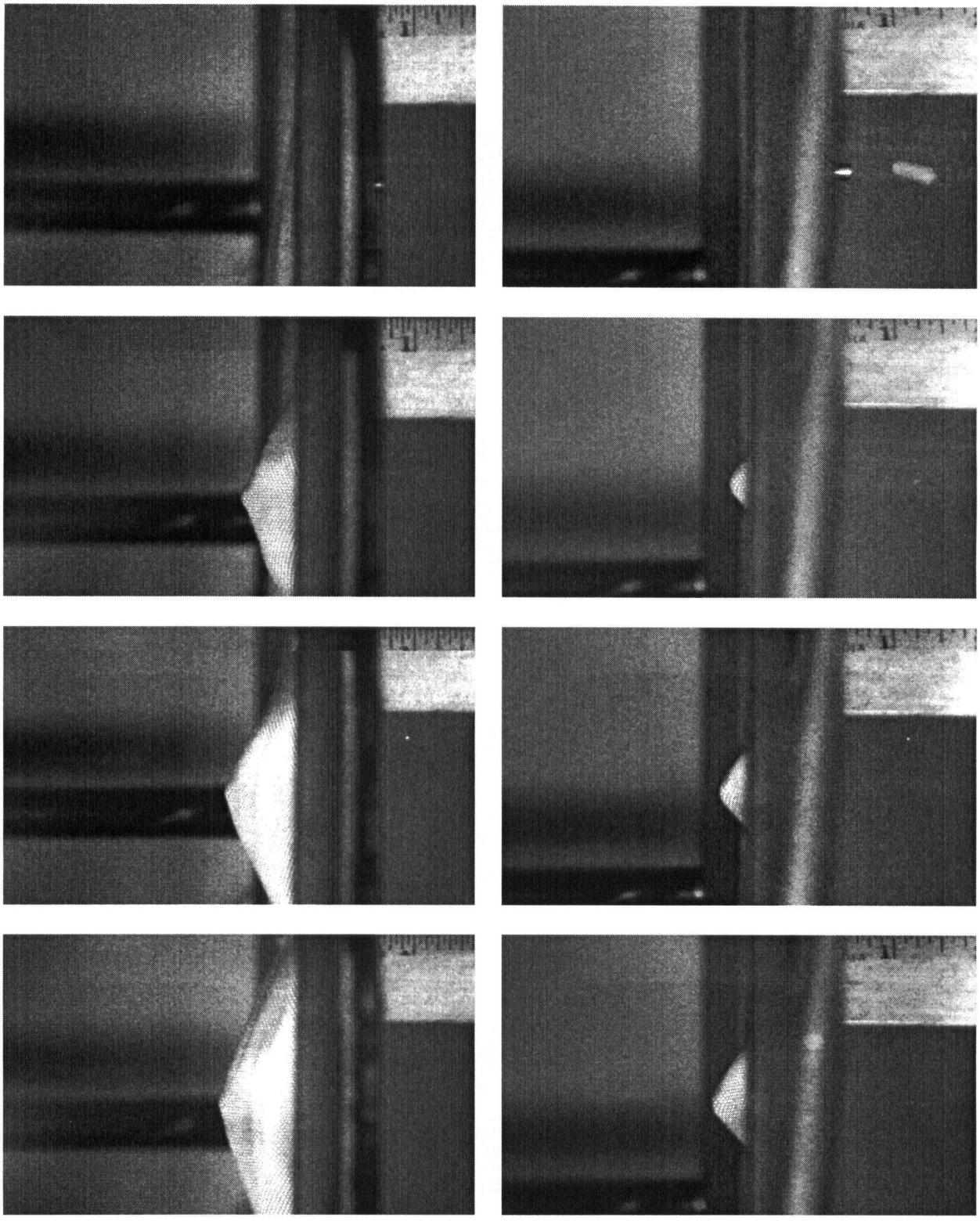

(a) (b)

Figure C.6: Video images for test #C19(a) and #S28 (b).

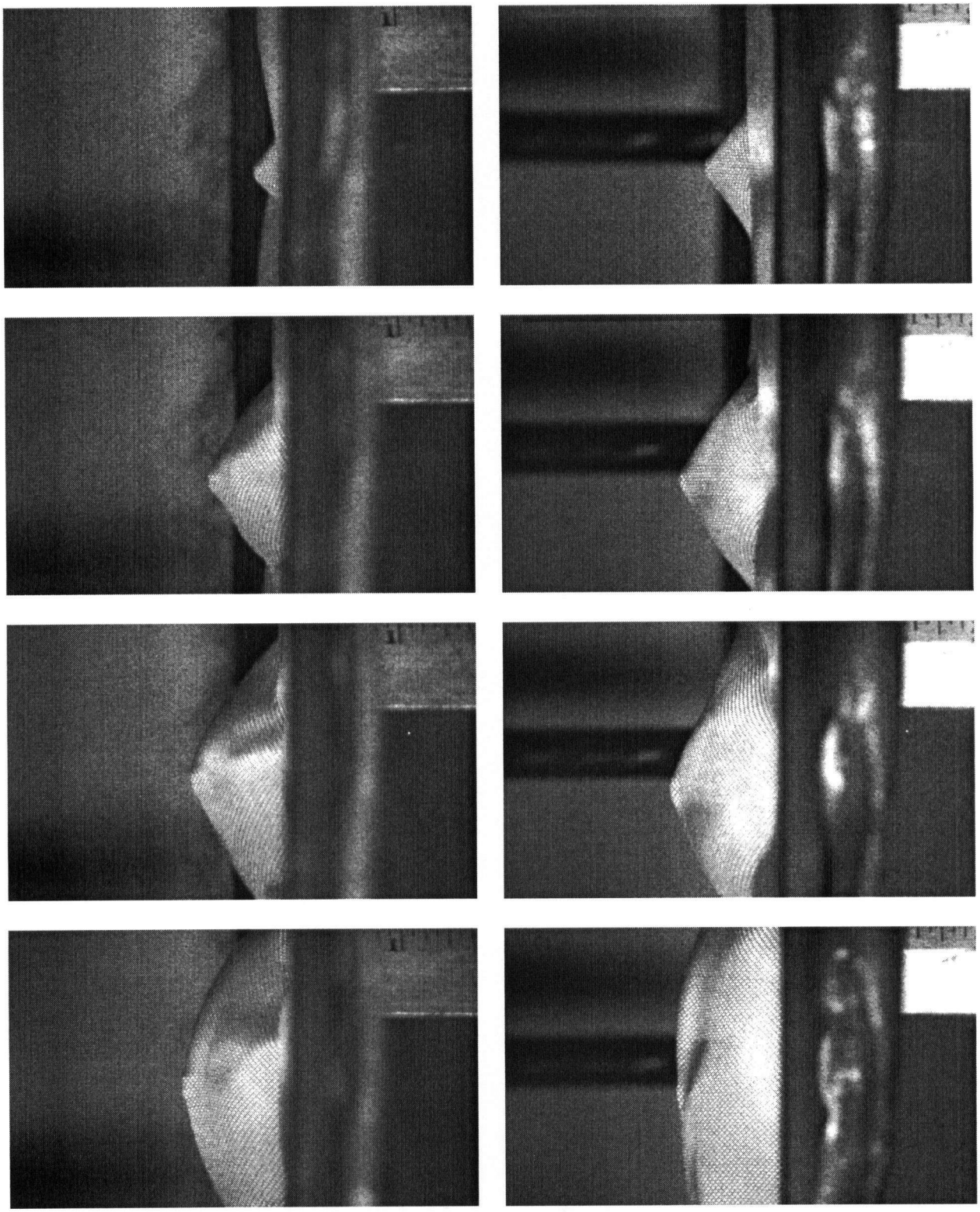

(a) (b)

Figure C.7: Video images for test #S29 (a) and #S32 (b).

Appendix D : ELVS Results

The ELVS results obtained for the ballistic impact tests performed at UBC are presented. The projectile displacement-time, velocity-time, force-time, force-projectile displacement, and energy absorbed-projectile displacement curves are shown for the remaining 8-ply Kevlar® tests. In all tests, the 2.8 g (43 grain) blunt aluminum projectile was used.

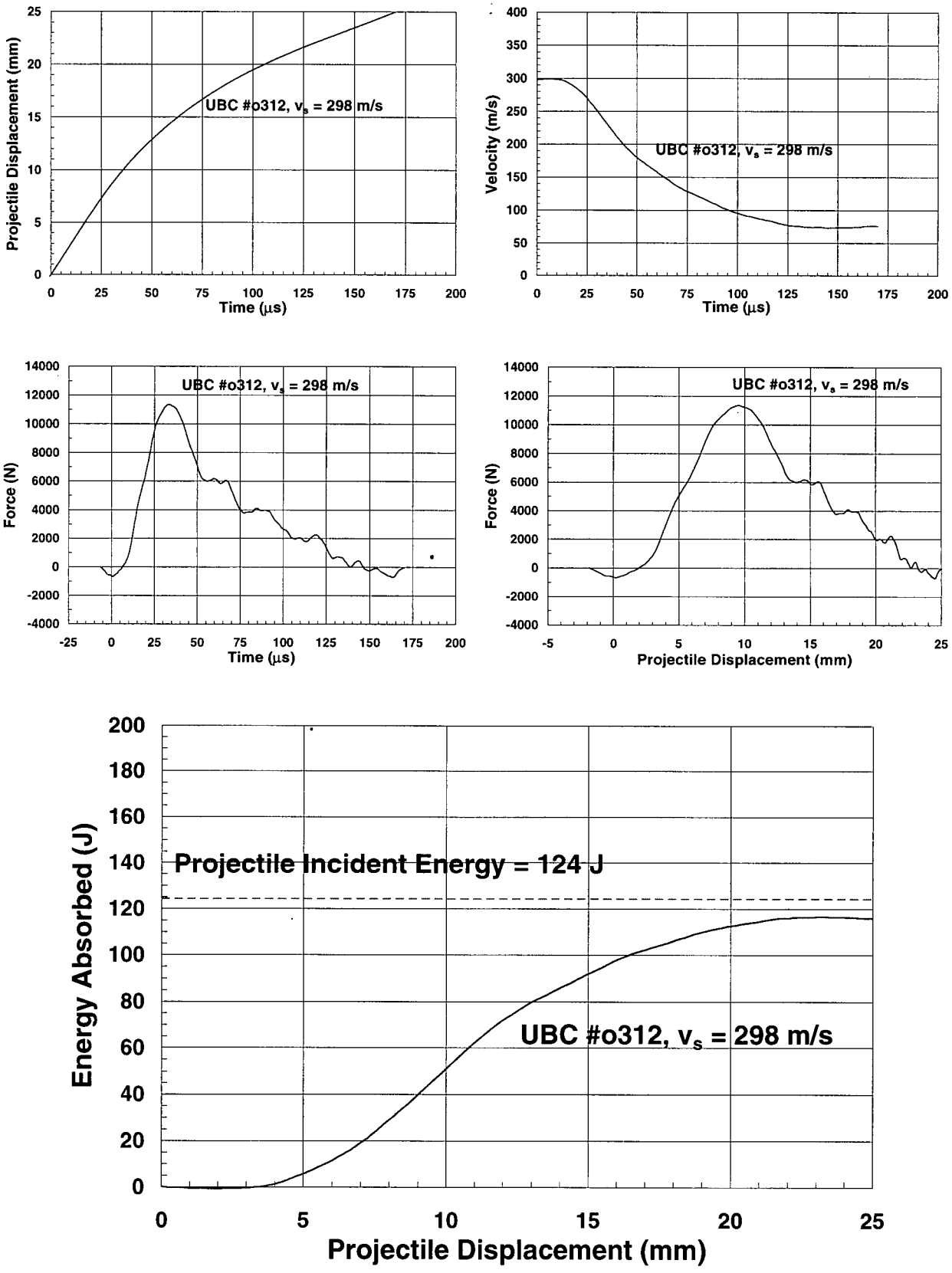

Figure D.1: ELVS results for test UBC #o312, where v_s is 298 m/s.

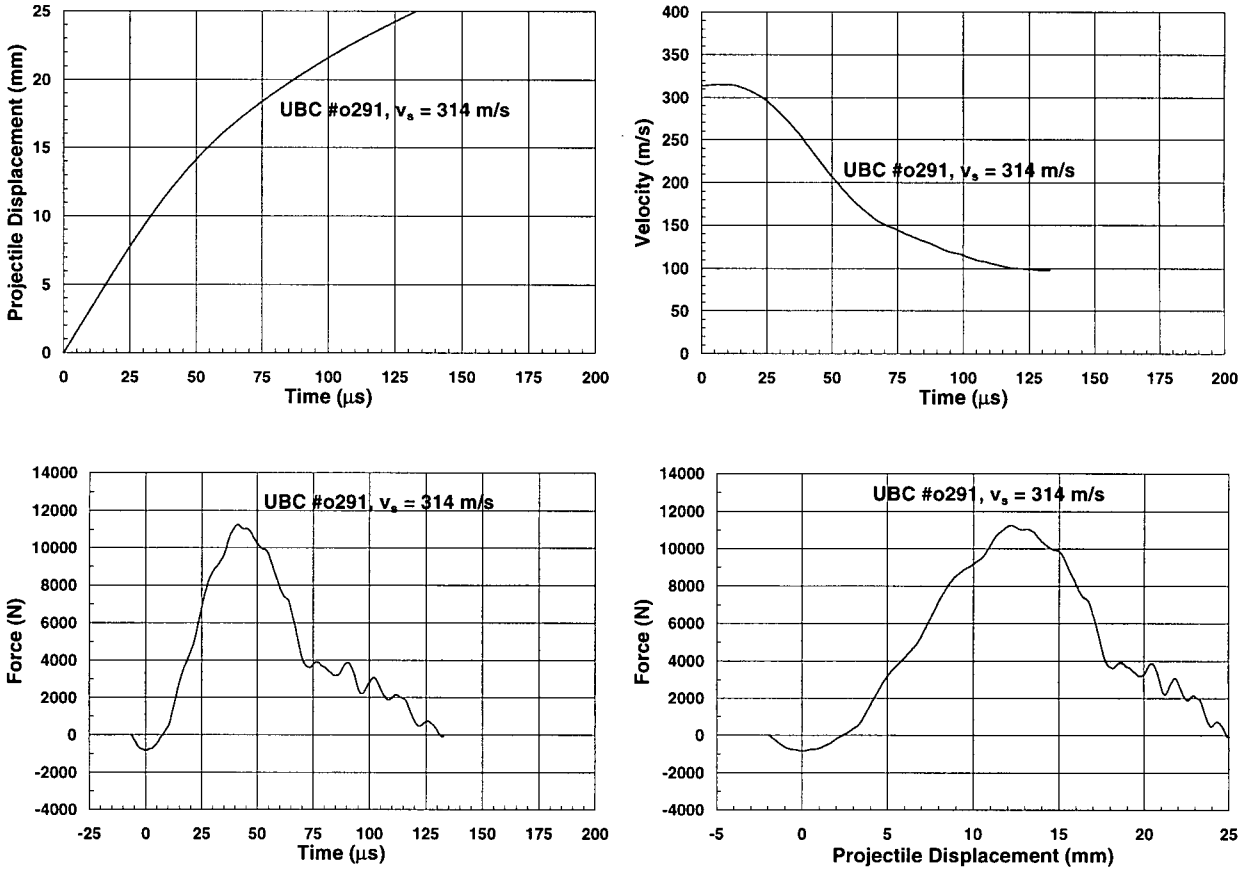

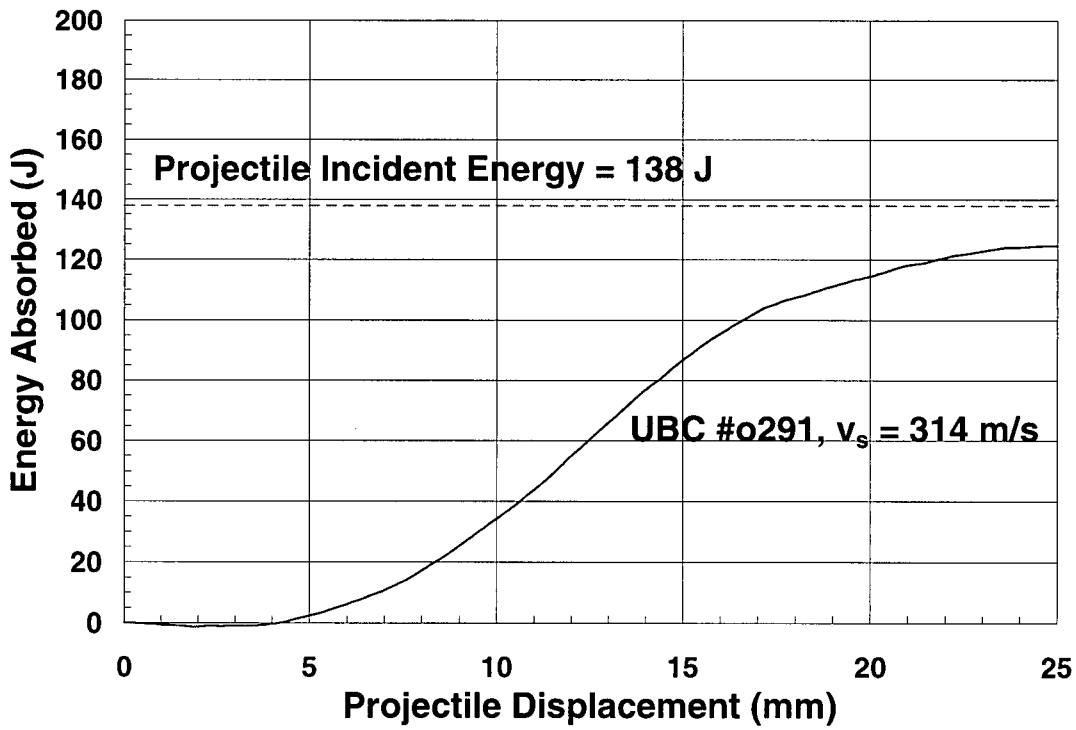

Figure D.2: ELVS results for test UBC #o291, where v_s is 314 m/s.

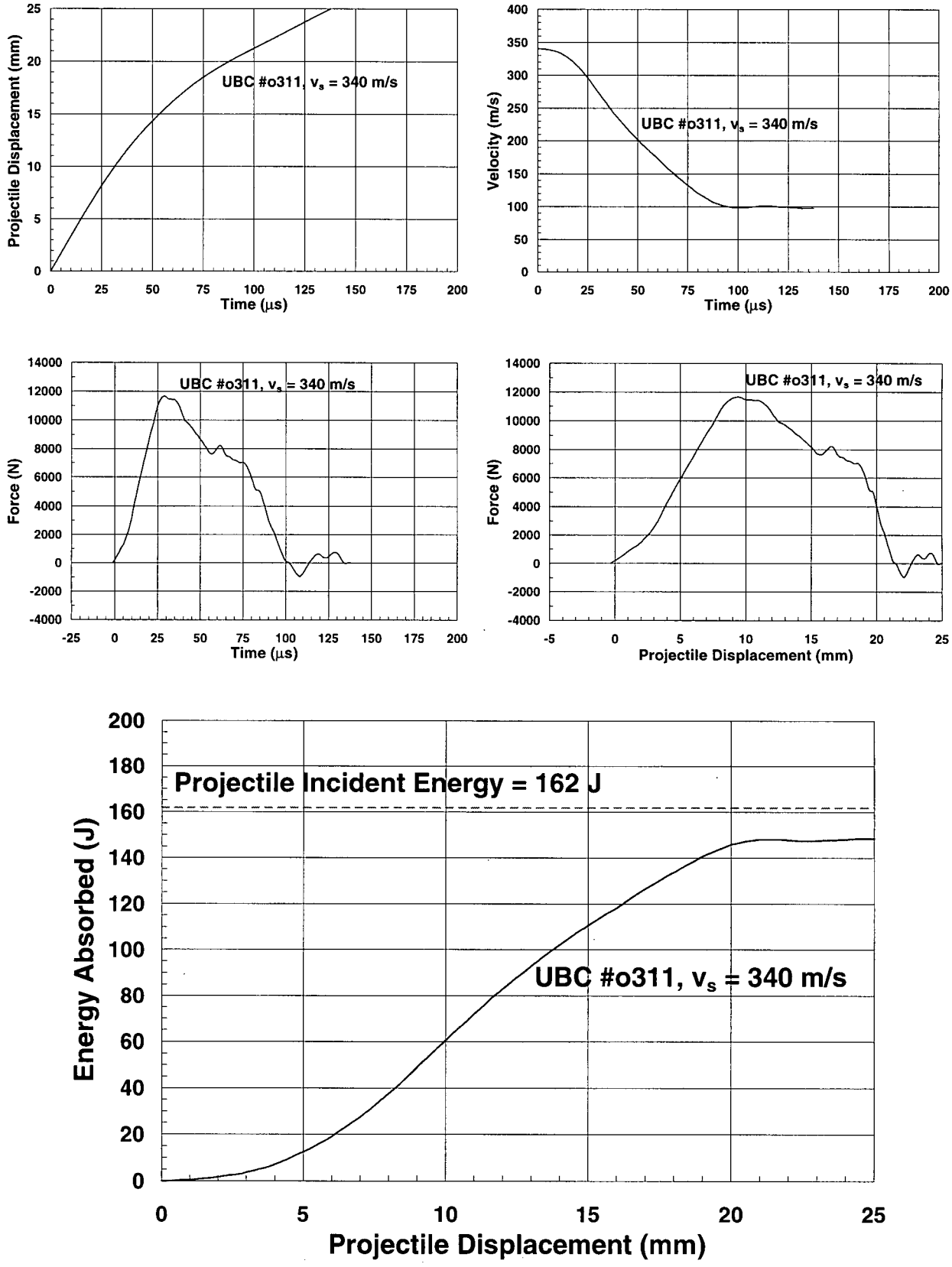

Figure D.3: ELVS results for test UBC #o311, where v_s is 340 m/s.

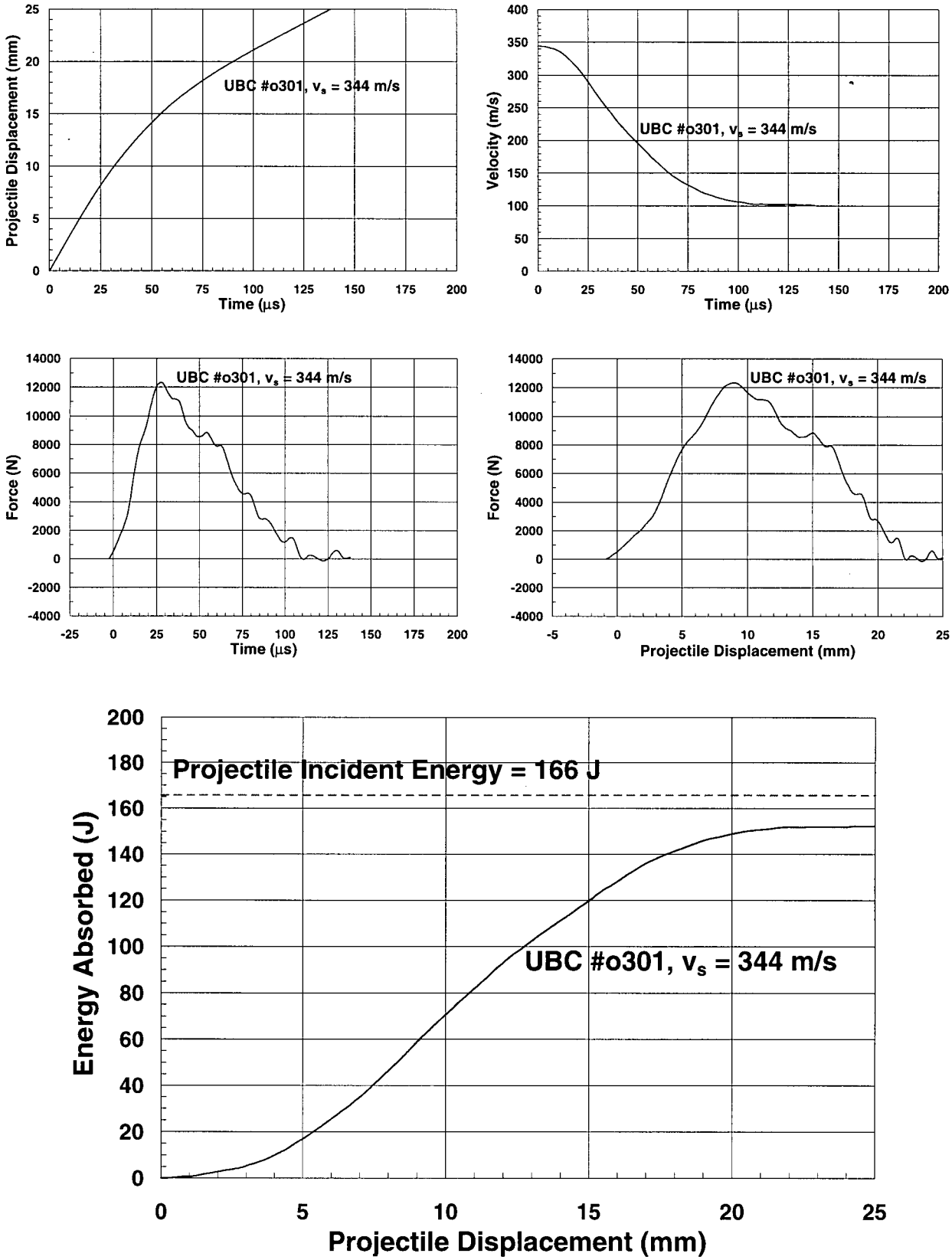

Figure D.4: ELVS results for test UBC #o301, where v_s is 344 m/s.

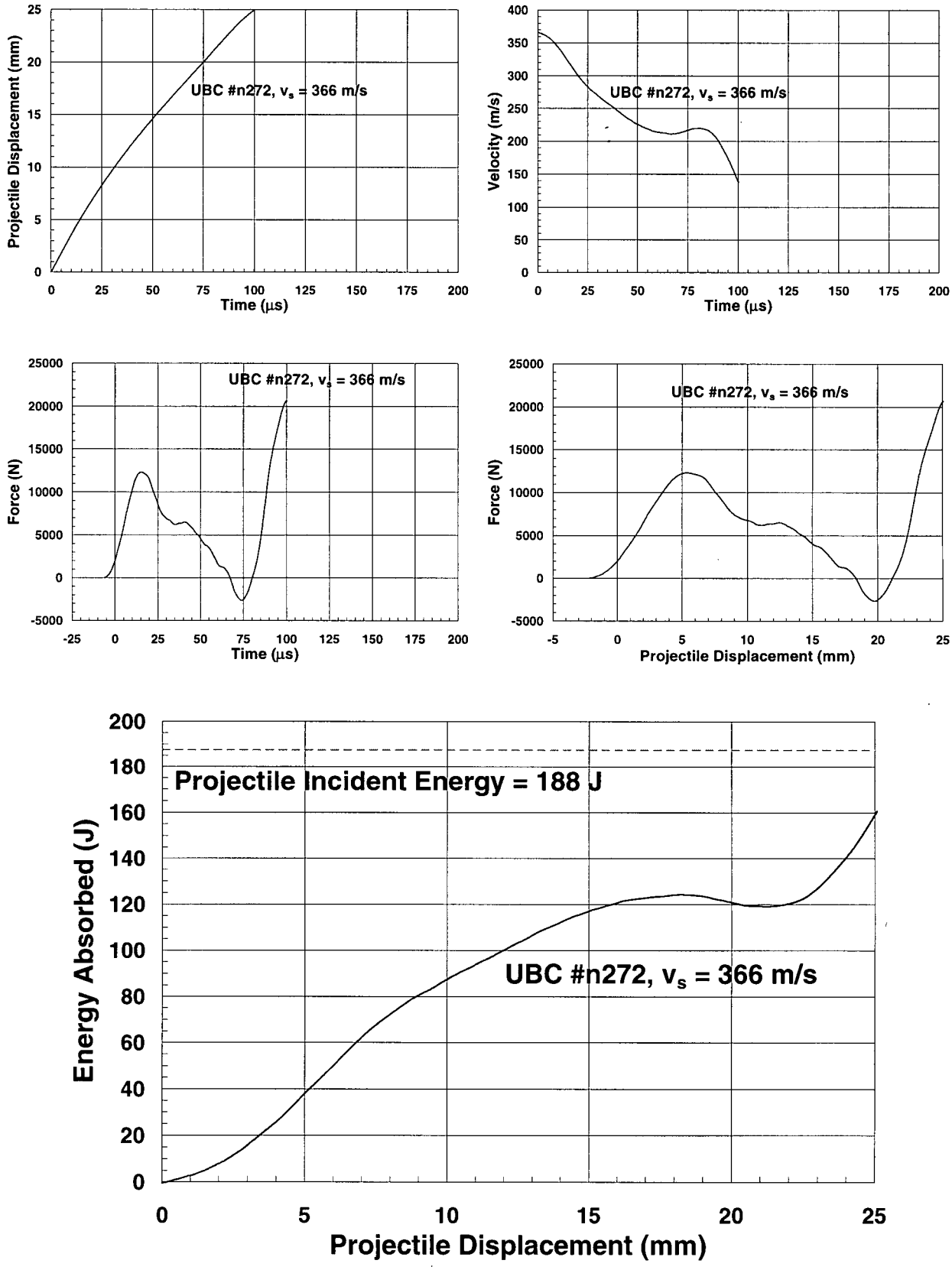

Figure D.5: ELVS results for test UBC #n272, where v_s is 366 m/s.